DLP HYPERSPECTRAL IMAGING FOR SURGICAL AND CLINICAL UTILITY

by

ROBERT PAUL FRANCIS

Presented to the Faculty of the Graduate School of

The University of Texas at Arlington in Partial Fulfillment

of the Requirements

for the Degree of

MASTER OF SCIENCE IN BIOENGINEERING

THE UNIVERSITY OF TEXAS AT ARLINGTON

MAY 2009

ACKNOWLEDGEMENTS

Throughout my research, Dr. Karel Zuzak and Jack Smith have been instrumental in getting external support, organizing project goals, and ensuring project success. I have learned much about business, engineering, and life from both of them.

Without the following engineering and medical support, this thesis could not have been written. I hereby acknowledge my colleagues in the Laboratory of Biomedical Imaging at UTA: Santosh Hariharan and Tinsy Perumanoor for easing my transition into the lab; Swetha Suresh, Umesh Agarwal and Abhas Thapa for helping collect and analyze clinical data; Preston Powell and Mihir Mehta for helping transport the system across the metroplex; and Eleanor Wehner for editing my writing. I also acknowledge my colleagues at UTSW Medical Center: Van Jackson for navigating the bureaucracy, capturing surgical data, and being a helping hand; Drs. Chad Tracy and Jeffrey Caddedu for allowing us to image their surgeries; and Dr. Edward Livingston for presenting the medical need and making hyperspectral imaging relevant to surgery.

I thank my collaborators at NIST: Dr. Maritoni Litorja and David Allen for guiding my lab experiments. I thank the engineers at Optronic Labs, Princeton Instruments, and AAVA Technology for their assistance in making the prototype operational. In addition to appreciating their funding, I must thank Texas Instruments for the technical and strategic advice from Leigh Files, Dennis Doane, Paul Barker, Rajeev Ramanath, and Shekar Rao.

On a personal note, I would like to thank my son Wesley for taking long naps so that I could finish my research and write this thesis. I could not have completed it without his aunts and grandmothers helping take care of him. Nor could I have survived the long nights of research without the respite of my wife at home. Thank you, Stephanie, for loving and supporting me in all my endeavors.

April 13, 2009

ABSTRACT

DLP HYPERSPECTRAL IMAGING FOR

SURGICAL AND CLINICAL UTILITY

Robert Paul Francis, M.S.

The University of Texas at Arlington, 2009

Supervising Professor: Karel J. Zuzak

Surgeons want technology to help them see differences in tissue chemistry. If they know how oxygenated tissues and organs are during medical procedures, they are more able to eliminate dangerous tissues and maintain viable organs. Hyperspectral imaging non-invasively measures the optical absorbance spectrum of each pixel in a spatial field of view and, with chemometric image processing, can visualize the spatial distribution of tissue oxygenation. Current hyperspectral imaging systems are too slow to monitor real-time physiological changes in live tissue. Therefore, a novel DLP Hyperspectral Imaging (DLP HSI) system is developed for real-time, non-invasive, *in vivo* imaging of tissue chemistry in surgical and clinical applications.

The cornerstone of the new hyperspectral imaging system is an OL 490 spectral light engine created with Texas Instruments' "Digital Light Processor" (DLP®) technology. In the OL 490, polychromatic visible light is dispersed onto the micromirror array of a DLP chip so that each column of micromirrors corresponds to a narrow band of monochromatic light. Programming the mirrors individually allows the user to precisely define the intensity of each

wavelength in the light engine's optical output spectrum. The OL 490 can illuminate with narrow bandpasses of light as in traditional hyperspectral imaging, but the novelty of the DLP HSI is using the OL 490 to illuminate with complex broadband illumination spectra. Regardless of the illumination scheme, the light from the OL 490 is reflected from a tissue sample of interest and detected by a scientific grade CCD focal plane array.

The spectral light engine and the camera detector are fully characterized as individual components, synchronized by software, and integrated into a robust system prototype that is transported throughout surgical and clinical suites. To visualize the spatial distribution of oxygenation, a Spectral Sweep mode mimics traditional hyperspectral imaging, explicitly measures the absorbance spectrum of each image pixel, and compares each spectrum to reference spectra of tissue chromophores. Spectral Sweep mode requires 20 seconds to generate a single image chemically-encoded for relative oxygenation. In contrast, a 3 Shot mode illuminates tissue with three complex broadband spectra derived from the reference spectra of tissue chromophores, measures the relative absorbance of the complex illuminations, and directly outputs an image also chemically-encoded for relative oxygenation. The 3 Shot mode can generate 3 chemically-encoded images every second.

After calibrating and optimizing the performance of the DLP Hyperspectral Imaging system, the principle of visualizing oxygenation is proven by following the reactive hyperemia in an occluded finger example. The imaging system is then applied to partial nephrectomy, lower limb neuropathy, brain surgery, reactive hyperemia in the foot, and diabetic retinopathy. Representative images show that the system is useful for visualizing relative tissue oxygenation, but the absolute values are not yet calibrated. Overall, the DLP HSI is widely accepted by urologists, neurosurgeons, and clinicians.

TABLE OF CONTENTS

LIST OF ILLUSTRATIONS

Figure Page

LIST OF TABLES

CHAPTER 1

INTRODUCTION

Colors of living things represent more than just aesthetics. Yellow bananas are good to eat, but every baker knows that when the peel turns black it is time to make banana bread. In the same way, green grass is living, but a brown lawn means it is time to fertilize or turn on the sprinkler.

Color changes occur because chemical changes in living objects cause the objects to reflect and absorb different wavelengths of light. Obvious changes like yellow to black are easy to identify with the naked eye because yellow corresponds to the reflection of mid-wavelength light and black corresponds to the absorption of all light. However, photoreceptive rods and cones in the human retina only respond to four broadband sections of the visible light spectrum.[4] If two colors are within the same broadband section, it is improbable that a human can distinguish between the colors.

In medicine, surgeons have traditionally noted the color of tissues as they operate. Red tissue generally corresponds to oxygenated, viable tissue. When the tissue turns pink, it is losing oxygen. If the tissue turns purple or blue, it is nearly dead. Even William Shakespeare's Romeo knew that Juliet still seemed alive by "the crimson in thy lips and in thy cheeks" (Romeo and Juliet, Act V, Scene 3). However, color observations by the human eye are subjective and some color differences cannot be detected.

Advancements in silicon photodetectors and prismatic optics have led to the development of visible reflectance spectroscopy for distinguishing between two objects that appear to be the same color. Light reflected from an object is filtered into its constituent wavelengths and the number of reflected photons for each wavelength is detected by a point or array detector. Filtering the broadband light into each wavelength component allows a spectrum of

reflectedintensity versus wavelength to be plotted. Comparing or contrasting an object's reflectance spectrum to spectral signatures of known reflectance materials enables unique identification of the object. Thus, visible reflectance spectroscopy is used to identify objects with unique optical characteristics and contrast objects with differing optical characteristics.

1.1 Hyperspectral Imaging

Hyperspectral imaging is the equivalent of reflectance spectroscopy at many discrete points arranged in a spatial pixel array. Reflectance spectroscopy involves collecting the reflectance of light at each wavelength, in the spectral dimension. Projecting the spectral dimensions to each pixel in an image results in a 3D data cube that contains the intensity spectrum for each pixel in a 2D spatial array (see Figure 1.1). A hyperspectral data cube can be acquired in two fundamental ways: scanning a point spectrometer over a spatial area, or sweeping the wavelengths of light incident on an array detector. With the 2-dimensional array detectors available today, the reflectance of light can be collected in two spatial and one spectral dimension.

The first way to capture a hyperspectral image cube is by moving a sample on a mechanical stage to raster-scan a point spectrometer through the image field of view (FOV).[5] A point spectrometer couples a very small area of broadband light into a prismatic grating. The grating spatially disperses polychromatic light into its monochromatic components, which are then uniquely detected to quantify the intensity spectrum as a function of wavelength. The spectrum measured by a point spectrometer is a measurement of all the light coupled into the spectrometer. To generate a 3D hyperspectral image cube, the point spectrometer must capture an intensity spectrum at each spatial pixel in the image FOV.

The second fundamental method of hyperspectral imaging is acquiring all spatial information at a wavelength of interest and scanning through a spectral range using optical or electro-optical filters. A liquid crystal tunable filter (LCTF) or acousto-optic tunable filter (AOTF)

is used to cut off all broadband light except for a precisely tuned narrow bandpass.[5] A scientific grade camera captures an image of a full 2D scene (e.g. tissue sample) at each narrow bandpass through a sweep of contiguous wavelengths, resulting in a 3D hyperspectral image cube.

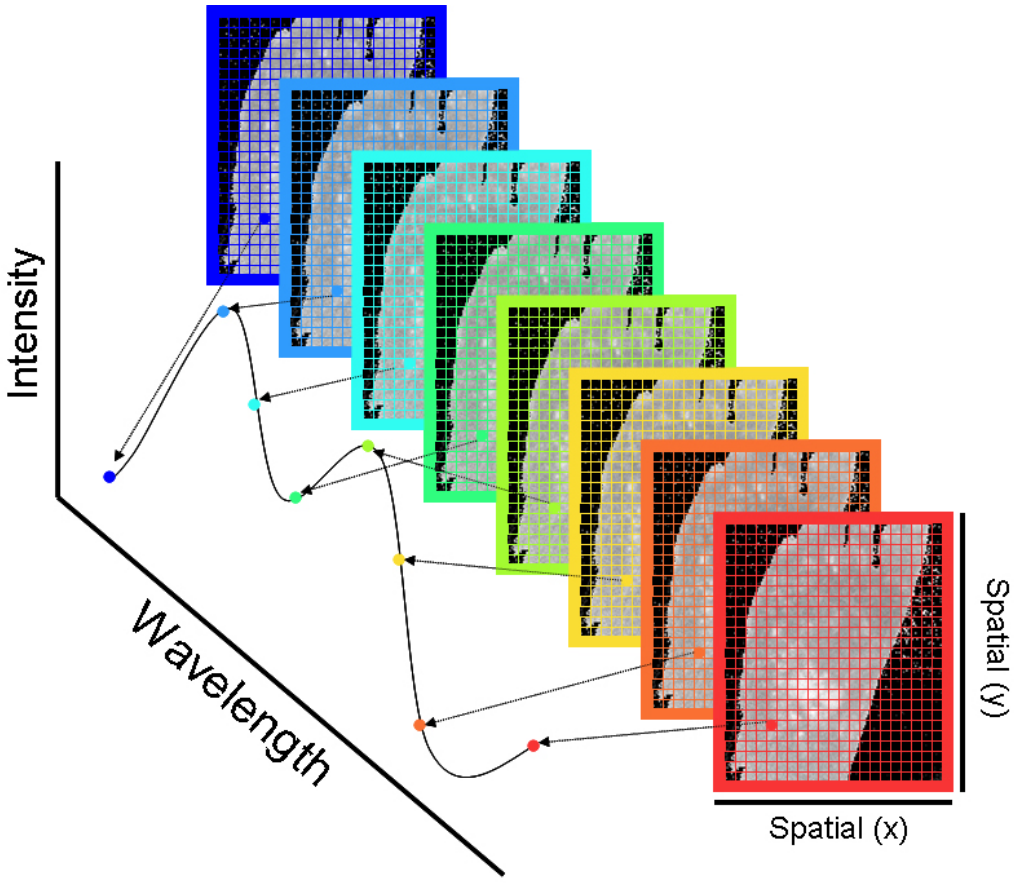

Figure 1.1 Illustration of a hyperspectral image cube with two spatial and one wavelength dimension. Each spatial pixel corresponds to a single intensity versus wavelength spectrum.

1.2 Medical need for real-time, non-invasive, *in vivo* imaging

According to surgeons, there is a vast medical need for increasing the contrast between different tissue types and visualizing changes in tissue chemistry as they are happening. A

real-time medical imaging device to remotely detect tissue chemistry in live human subjects without damaging any tissue would satisfy this need.

In a cholecystectomy, a surgeon must cut between the gallbladder and the biliary tree to remove a poorly functioning gallbladder. There are 750,000 cholecystectomies performed each year in the United States, with 5,000 resulting in bile duct injury because the surgeon cannot identify exactly where to cut. The reflectance spectrum of gallbladder tissue is different than that of bile duct tissue, so hyperspectral imaging is a non-invasive way to distinguish between the two organs.[6,7] A real-time hyperspectral imaging system would help surgeons visually contrast biliary structures to determine exactly where to cut during cholecystectomy.

Almost all of the 65,000 amputations performed annually are due to inadequate blood flow in the lower extremity. The foot or leg exhibiting this decreased blood flow must be removed, but portions of the lower extremity with normal blood flow should remain. If too much of the lower extremity is removed, the amputee may not rehabilitate as quickly. On the other hand, if too little of the lower extremity is removed, the wound may not heal because it is in a tissue bed with inadequate blood flow. A real-time hyperspectral imaging system would help surgeons determine the appropriate level at which to amputate by visualizing the spatial profile of blood flow in the entire leg.

In a partial nephrectomy, a surgeon must clamp the renal vasculature to prevent hemorrhage when removing part of the kidney. It is important to adequately occlude blood flow to the kidney without inflicting long-term damage due to prolonged ischemia. Current oxygen probes to monitor the extent of ischemia only measure oxygenation at a single point.[8] A real-time imaging system to non-invasively monitor the ischemia caused by renal clamping would improve surgical clamping methods for the 5,000 partial nephrectomies performed annually in the United States and countless others worldwide.

There are many other applications for real-time, non-invasive imaging of *in vivo* tissue chemistry such as monitoring retinal vasculature for over 15,000,000 diabetic patients,

determining limits of resection in skin wounds and burns, and monitoring the blood flow of the cerebral cortex to prevent stroke in brain surgery. A real-time hyperspectral imaging system would be a platform for visualizing tissue chemistry in a myriad of surgical and clinical applications.

1.3 Hypothesis

Current hyperspectral imaging can remotely visualize tissue chemistry and increase contrast between tissue types in live human subjects without damaging any tissue.[6,9-12] The limitation is that current hyperspectral image cubes take 20 to 30 seconds to acquire and process which is too slow for widespread surgical and clinical use. Spectral light engines based on “Digital Light Processor” (DLP®, Texas Instruments, Plano, TX) technology have been developed that can precisely shape the spectral profile of narrow and broadband illumination.[1,13] Using a DLP-based spectral light engine to revolutionize the illumination methodology of hyperspectral imaging, the hypothesis is that a novel hyperspectral imaging system can be developed for real-time, non-invasive, *in vivo* imaging of tissue chemistry in surgical and clinical applications.

CHAPTER 2

SPECTRAL LIGHT ENGINE

A spectral light engine is defined as a light source with projection optics and filters that allow the user to precisely shape the spectral and temporal illumination profiles.[13]. Digital programming of the light engine effectively modulates the light source spectrum at each individual wavelength to produce a desired optical output spectrum. The programmed spectrum can be adjusted in time to create temporal sequences of multiple illumination spectra. Spectral light engines have only become available in the last four years, and their utility in fluorescence and hyperspectral imaging is of great interest.[1]

2.1 Overview and beam path

Developed and produced by Optronic Laboratories (Orlando, FL), the OL 490 Agile Light Source is comprised of a power supply, lamp source assembly, and optics head. The power supply features a cooling fan, AC input power, and a circular connector for cabling power to the lamp assembly. Four status LEDs on the face of the power supply indicate when the power supply is plugged into external AC power, when the cable between the power supply and the lamp source are correctly connected, when the lamp and power supply temperatures are within operating limits, and when the lamp is turned on. All four LEDs must be solid green in order for the OL 490 to operate correctly. The lamp assembly consists of a pressurized 500 W Xenon lamp, igniter electronics, a cooling module, and an output connector with room to place one of four slits. The output connector of the lamp source assembly can be directly coupled to the optics head and secured by tightening three set screws. Inside the optics head, broadband light from the Xenon lamp is focused by collimating optics onto a diffraction grating as in Figure 2.1. The diffraction grating breaks the broadband light into its constituent wavelengths, which are

then reflected from a digital micromirror device (DMD) and refocused into a uniform spectral output. A user can program the spectral output by interfacing the DMD control electronics within the optics head via a USB 2.0 connection. Light is output from the OL 490 through a liquid light guide probe that can be coupled directly to the optics head encasement.

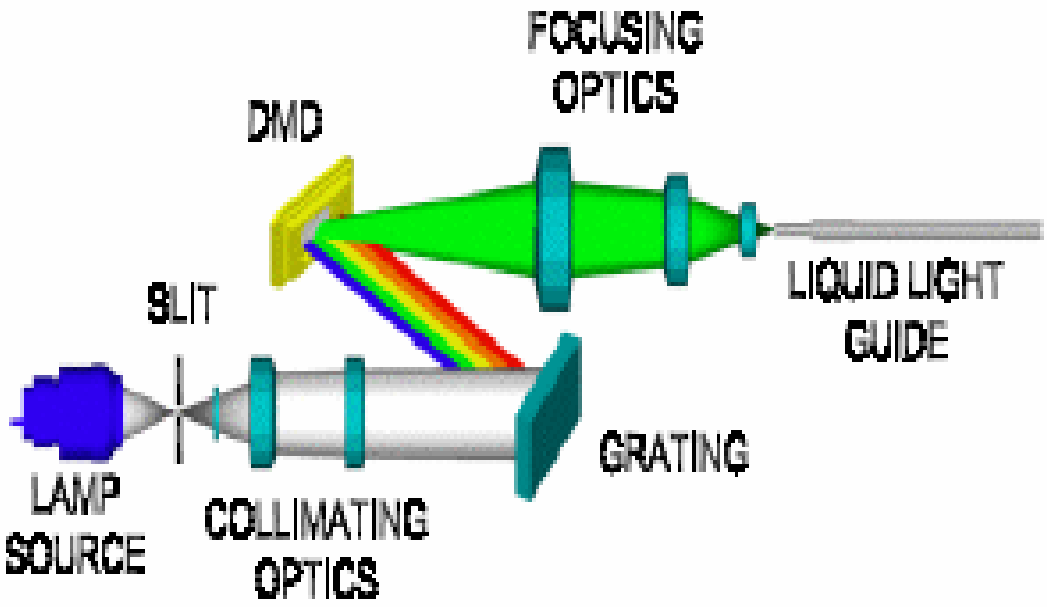

Figure 2.1 Light path of the OL 490 Agile Light Source from Xe lamp source to LLG output. [Copied from [1]]

2.1.1 DMD operation

The DMD was integrated into a DLP® chip as a spatial light modulator by Larry Hornbeck of Texas Instruments, Inc. (Plano, TX) in 1987.[14] In its most basic form, a DMD is an m x n array of square mirrors which can be controlled individually to switch between an 'on' and 'off' state. Each aluminum mirror sits on it own underlying memory cell on a CMOS substrate and hinges about its diagonal axis (see Figure 2.2). By controlling the voltage bias that creates an electrostatic attraction between the mirror and an address electrode and an opposite force between the yoke and an address electrode, each mirror can be switched from 'on' to 'off' very quickly.[3] The positive and negative deflection angle of the mirror is determined by the mechanical design of the DMD; the electrostatic forces cause the mirror to hinge all the way in

one direction, and the mirror angle is therefore constrained by the physical distance it is allowed to rotate.

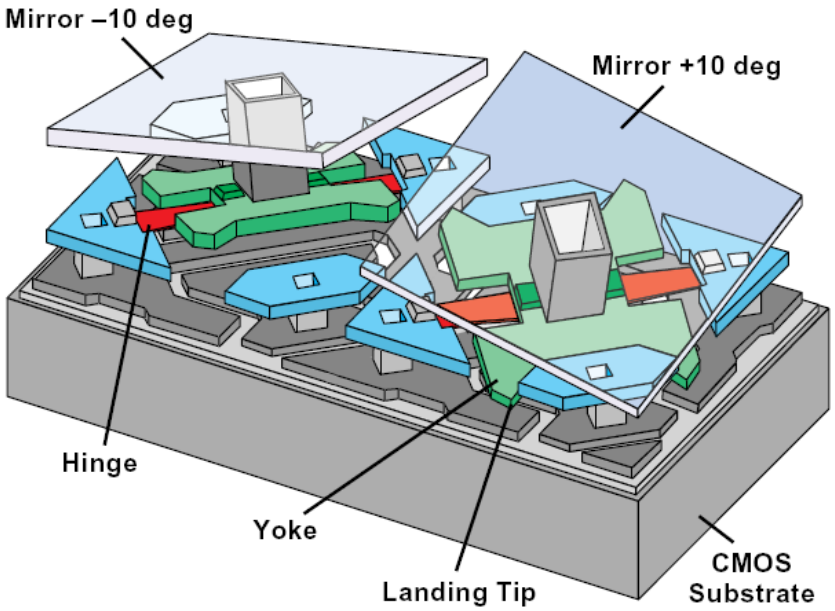

Figure 2.2 Two DMD pixels (mirrors are shown as transparent). [Copied from [2]]. The mirrors are in different states shown at +/-10 deg, as in the original DMD design. The mirrors in the DMD of the OL 490 hinge between +/-12 deg.

In spatial light modulation, the DMD array reflects light through optics such as a projection lens onto an area of interest. The angle and distance between the optics and DMD are designed so that when all of the mirrors are 'on' the entire area is illuminated, and when all of the mirrors are 'off' none of the area is illuminated. If only one section of the area should be illuminated, then only the mirrors corresponding to that section are 'on' and all other mirrors are 'off'. To further modulate the light reflected from each individual mirror, pulse width modulation increases the number of grayscale levels possible for illumination (see Figure 2.3).

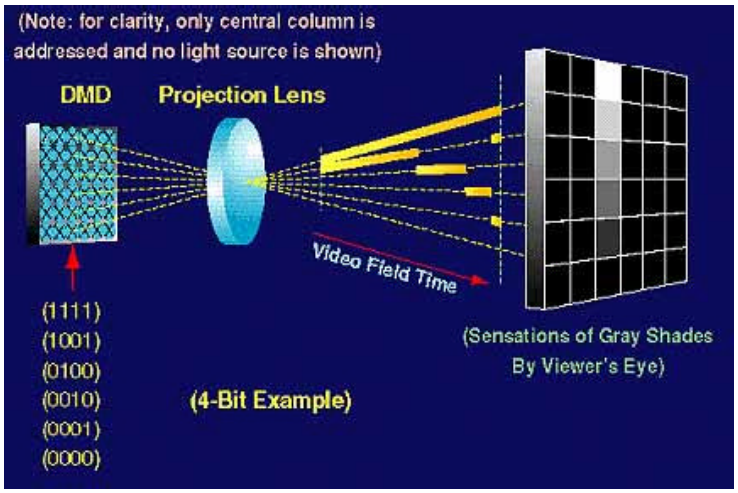

Figure 2.3 Example of DMD array projecting variable gray levels. [Copied from [3]].

Inside the OL 490, the DMD Discovery 3000 chip (Texas Instruments) is integrated as a spatial light modulator for spectral filtering. This DMD is a 768 x 1024 array of micro-mechanical mirrors, which can each be rotated by +/- 12 deg on its own 3.68 μm pitch.[14] When a mirror is 'on', the light incident on that mirror is reflected to collection optics for illumination, and when a mirror is 'off', the light incident on that mirror is reflected to an internal heat sink.

2.1.2 Spectral filtering with the DMD

The basis of spectroscopy is determining the differential effects of light on an object along the frequency or wavelength axis. To measure these effects, broadband light passed through a thin diffraction grating or prism is angularly dispersed into different wavelength components.[15] Spectral spatial analysis is the physical basis of a common point spectrometer, in which a point sample of light is dispersed through a grating and detected by a line array of photodetectors, each detector in the array corresponding to a narrow band component of the original broadband sample. Similarly, in the OL 490, broadband light from the Xe lamp is angularly dispersed onto the DMD array, and each column of the array corresponds to a unique narrow band component of the broadband light. To illuminate with one of the narrow bands of light at maximum intensity, all 768 of the mirrors in the corresponding DMD column are switched 'on' and all of the mirrors

in every other column are ‘off’. To reduce the intensity to half of maximum, only 384 mirrors are switched ‘on’. Therefore, by turning ‘on’ a variable number of mirrors in each column, the user can precisely determine the spectrum of light illuminated by the OL 490 (see Figure 2.4(a)).

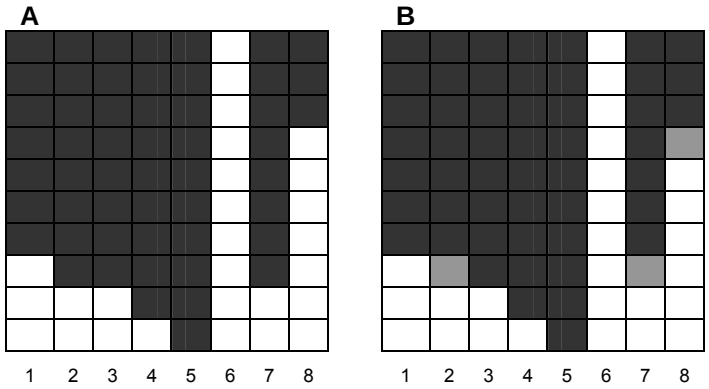

Figure 2.4 Scaled down example of DMD in (a) 1-bit operation and (b) 2-bit operation. White squares represent mirrors ‘on’, black squares represent mirrors ‘off’, and gray squares represent half ‘on’ and half ‘off’ by PWM. In (a) column 1 reflects at 30% intensity, column 2 at 20%, column 3 at 20%, etc. In (b) column 1 reflects at 30%, column 2 at 25% (by PWM), column 3 at 30%, etc.

In 1-bit operation, where the only possible mirror states are ‘on’ and ‘off’, the number of intensity levels equals the number of mirror rows, 768. In this mode of operation, the only time that a mirror may change state is when a new illumination spectrum is programmed, so the illumination spectrum can be changed as fast as the mirror state can be switched. In 2-bit operation, where a half ‘on’ and half ‘off’ mirror state is possible by pulse width modulation (PWM), the number of intensity levels equals the number of mirror rows times two, 1,536. In this mode of operation, the final mirror in any column may require switching twice before the illumination spectrum can be changed, so the speed of switching between spectra is cut in half. However, the resulting spectrum has better intensity resolution (see Figure 2.4(b)). The OL 490 is capable of modulating 64 grayscale levels (6-bit operation) per mirror for a total of 49,152 intensity levels. PWM requires more time to switch between spectra and the imaging of the illumination spectrum is not as stable if the integration time of the detector is less than the time to switch between spectra. 768 intensity levels should be adequate for the prototype hyperspectral imaging system, so for the remainder of this thesis the OL 490 is always operated in 1-bit mode.

2.1.3 Software control of the OL 490

When the OL 490 Agile light source is shipped to its end user, it comes with OL 490 Application Software (AS) and a software development kit (SDK). The SDK contains sample applications written in C# programming language and the dynamic link libraries (DLLs) necessary to write programs to control the OL 490 hardware. The OL 490 AS features a graphical user interface (GUI) in which the user may program a single illumination spectrum or a list of spectra to be emitted from the optics head (see Figure 2.5). Prior to starting the OL 490 AS, the OL 490 optics head is connected to a PC via USB 2.0 and turned on. The user must then click the cogwheel button on the toolbar to adjust the settings of the optics head. In the settings window, the user selects which slit is between the Xe lamp and the entrance port to the optics head so that the appropriate calibration profile may be loaded in software. The calibration profile indicates which columns of mirrors correspond to which wavelengths.

After the appropriate calibration profile is loaded, the user may close the settings window and program desired illumination spectra. An illumination spectrum can be created by rendering sliders or by loading a tab-delimited text file. The “Render Sliders” option allows the user to select a center wavelength between 380 nm and 780 nm, a desired bandwidth from 5 nm to 200 nm, and an intensity percentage from 0 to 100. If more than one band is desired, the user can save the constraints for one band, select three parameters for a second band, add both bands to a list, and save the list as a frame. Rendering sliders is quick and easy when the desired illumination spectrum is simple (one or two bands), but writing a tab-delimited text file is better suited for creating complex illumination spectra with variable intensities at many wavelengths.

In a tab-delimited Gwectra file (extension *.GXT), two columns of text precisely define which mirrors of the DMD are turned on. Specifically, the first column of text is a list of 1024 discrete wavelengths that cover the wavelength range of the OL 490 in even increments and the second column of text is a fixed-point value having 2 decimal places ranging from 0.00 to

100.00. Each value in the second text column defines the percentage of mirrors turned on corresponding to the wavelength in the first text column. Five header lines describe with which software version the Gwectra file is compatible and when the file was created.

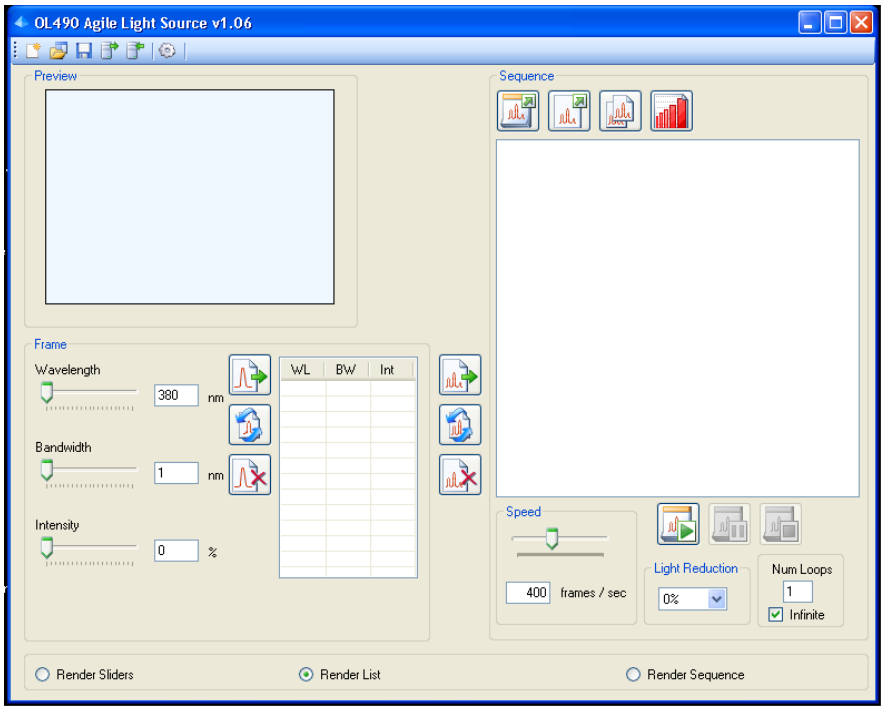

Figure 2.5 Screen shot of OL 490 Application Software on startup.

To alternate between illumination spectra, the desired frames or Gwectra files must be loaded into the "Sequence" area on the right of the OL 490 AS window. Below the "Sequence" area, the user can control the speed of switching between illumination spectra from 1 frame per sec to 12,500 frames per sec, the percentage of light reduction, and how many times to loop the sequence. Percentage of light reduction in this selection window is applied to all wavelengths equally. If the user wishes to reduce the amount of light to the maximum of a specific wavelength in order to flatten the spectral profile of illumination, linear light reduction is adjusted in the settings window. Be aware that linear light reduction is arbitrary and does not flatten the spectral response of the Xenon lamp to the same degree as modulation of Gwectra files described in section 6.1.1.1.

To program the OL 490 to sweep through illuminations of contiguous bandpasses with constant intensity and bandwidth, the user can select the “Create Sweeps” button on the far right above the sequence area. The user then defines a sweep by selecting the start and end center wavelengths, the wavelength increment, a single intensity value applied to each bandpass, and a single bandwidth applied to each bandpass. The “Create Sweeps” option is very useful for quickly generating a sweep of contiguous bandpasses as required by traditional hyperspectral imaging.

2.2 Characterization of the OL 490

Before implementing the spectral light engine into our hyperspectral imaging system, the manufacturer specifications in Table 2.1 for the OL 490 are verified in the laboratory. In addition to these manufacturer specifications, the stability of the light source is verified to ensure reliable and reproducible measurements in clinical and surgical imaging. The manufacturer also publishes timing and electrical specifications. The most important of those are minimum exposure time of 80 μs (corresponding to a spectral scan rate of 12,500 spectra per sec) and external power input of 100 VAC to 260 VAC (47 Hz to 63 Hz). The following sections describe experiments and results that fully characterize the optical performance of the OL 490.

Table 2.1 Optical output specifications from the manufacturer of the OL 490.

Spectral Range	380 nm to 780 nm
Spectral Accuracy	1 nm
Out of Band Rejection (@550 nm, output 450 nm)	~1000:1
Wavelength Resolution	0.39 nm
Intensity Control Levels	768 to 49,152 levels
Output Intensity (350 μm slit, all mirrors on)	~200 mW
Half-Bandwidths	
150 μm slit	~5 nm
350 μm slit	≤10 nm
500 μm slit	≤15 nm
750 μm slit	≤20 nm

2.2.1 Photodiode stability

Three questions are answered by calibrated photodiode tests. How long does it take the OL 490 to warm up once the lamp has been switched on? How stable is the output over time? And how does the OL 490 stability compare to a QTH lamp used in previous hyperspectral imaging systems?

2.2.1.1 Methods

To answer these questions, the output of the OL 490 LLG is coupled to an aspherical lens and the output beam intensity is measured by a photodiode. The aspherical lens encasement is abutted to a 2.4 cm inner diameter baffle (Thor Labs, Newton, NJ), which has a 15^{o} light shaping diffuser 3.5 cm from the inlet end and a National Institute of Standards and Technology (NIST) calibrated photodiode 9.1 cm from the inlet end to measure all incident light. The photodiode is connected with a BNC cable to a DLPCA-200 amplifier (FEMTO Messtechnik GmbH, Berlin) which is set to amplify with respect to ground at 10^{3} V/A amplification and 10 Hz noise filtering. From the amplifier output, a DC voltage signal is sent to the analog input of an NI USB-6216 DAQ (National Instruments, Austin, TX) to transfer the analog signal into a digital readout in LabView (National Instruments, Austin, TX). A LabView VI is written to sample the input voltage once every 5 sec, and record the voltage, between 0 V and 10 V, as a function of time.

Photodiode tests are performed with the OL 490 (350 μm slit) programmed to output a bandpass centered at 580 nm, with bandwidth of 10 nm, and 33% intensity. This illumination bandpass is selected because the photodiode's response is good and the OL 490 is planned to be used between 520 nm and 645 nm for initial applications. The intensity has to be reduced to 33% so that the maximum amplified photodiode voltage response will be near 9 V but will not overload the amplifier.

In all tests, recording in LabView is started simultaneous to switching on the lamp for the OL 490. Tests are performed on two separate days to verify results. Each day, four tests are

run. Prior to the first run, the OL 490 optics head is turned on and programmed to illuminate with the bandpass described above. In each run, the lamp source remains on for a period of 30 min, and then is off for a period of 20 min before the next run. Since the lamp is cold at the beginning of the day, the first run is labeled “From Cold” and subsequent runs are labeled “From Warm.”

2.2.1.2 Results and Conclusions

Figure 2.6 shows the results of “From Cold” for each day, and Figure 2.7 shows the average results of the three “From Warm” runs for each day. The plots show that there is little variance from day to day, and qualitatively it appears that the OL 490 requires about 15 min to reach steady state “From Cold” and about 5 min to 10 min to reach steady state “From Warm”.

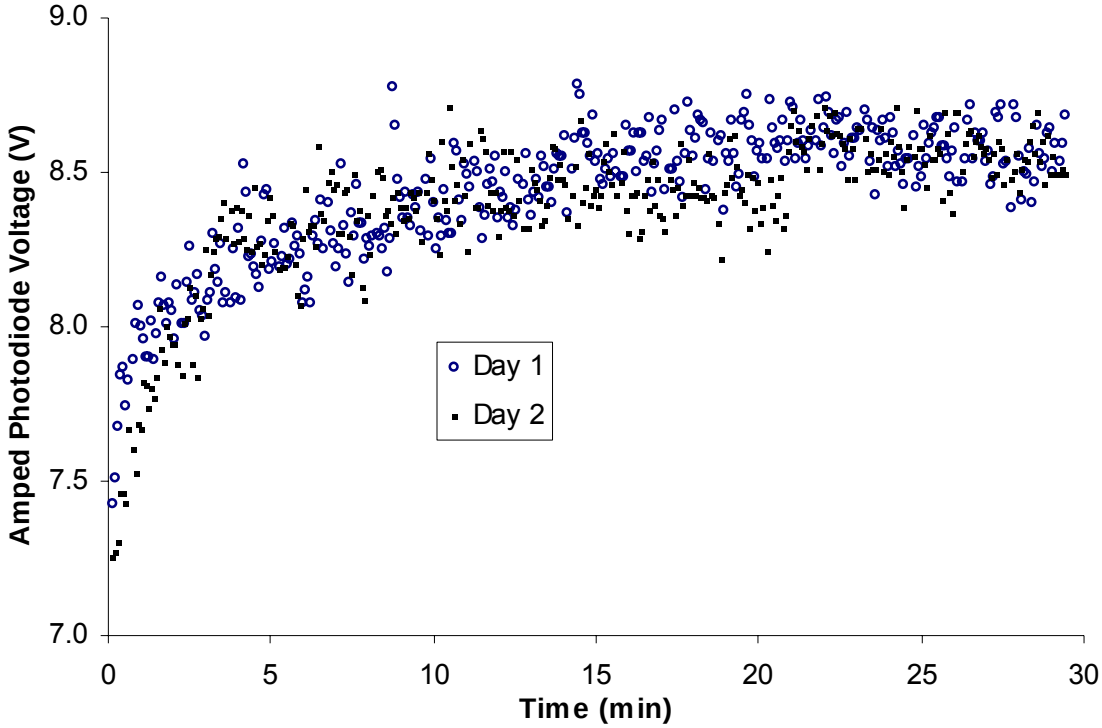

Figure 2.6 Amped photodiode voltage measured “From Cold” as OL 490 lamp source is switched on and left illuminating 580 nm, 10 nm bandwidth, at 33% for 30 minutes.

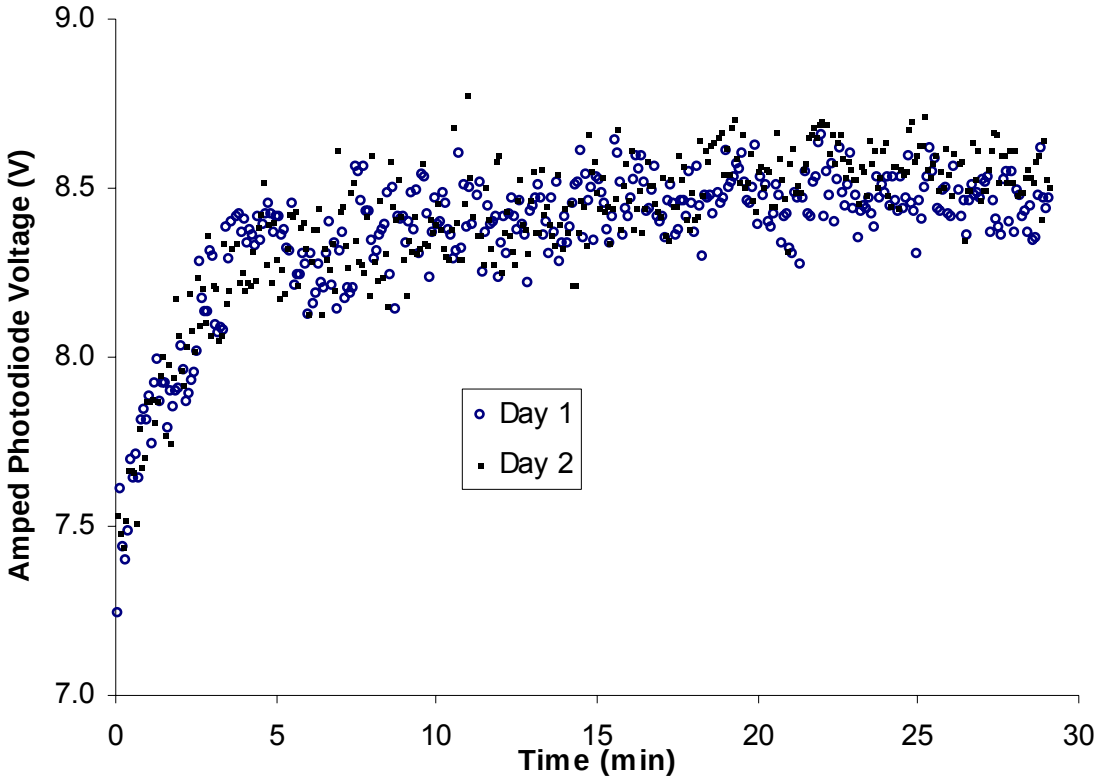

Figure 2.7 Amped photodiode voltage measured "From Warm" (average of 3 runs) as OL 490 lamp source is switched on and left illuminating 580 nm, 10 nm bandwidth, at 33% for 30 minutes.

Quantitatively, the rise time and standard deviation once at steady state for each case is calculated to answer the questions at the beginning of this section. Taking a 3 min moving average "From Cold" and "From Warm" data, the final steady state value is 8.56 V "From Cold" and 8.50 V "From Warm." The steady state standard deviation is 0.08 V (< 1%) in both cases. By the first 5 sec time point, the "From Cold" curve is already at 6.45 V (75%) of steady state, and the "From Warm" curve is at 7.39 V (86%) of steady state. In the next 25 sec, both curves reach 90% of steady state, which indicates that starting the lamp "From Warm" is most beneficial in the first 5 sec, and according to Table 2.2 there is a 1% advantage to having the lamp already warmed up until about 15 min (900 sec) of operation.

Based on the photodiode calibration curve, the Xe lamp should be turned on for 15 min (900 sec) the first time each day it is operated prior to collecting hyperspectral images. Every

time thereafter, the lamp should be given at least 10 min (600 sec) of warming up before collecting hyperspectral images. There is less than 1% deviation from steady state after that time. Since the experiments were repeated over two days with similar results, the OL 490 day-to-day stability is verified.

Table 2.2 Percent of steady state after turning the lamp on for certain time “From Cold” and “From Warm”

	Percent of Steady State	
Time (s)	"From Cold"	"From Warm"
5	75.4%	86.9%
10	85.7%	88.8%
30	89.5%	90.3%
60	91.5%	92.2%
120	93.4%	93.9%
180	94.7%	96.3%
300	97.0%	98.3%
600	98.2%	99.2%
900	99.2%	99.6%
1200	99.5%	99.6%

To verify long term operational stability, the “From Cold” test above is repeated for a period of two hours, recording photodiode voltage in 1 sec increments. The plateau in Figure 2.8 demonstrates that the OL 490 optical output is extremely stable when the lamp is left on for long periods of operation. Over many hours of lamp use, the optical output will likely decline, so it is recommended that the light source undergo photodiode calibration at least once a year.

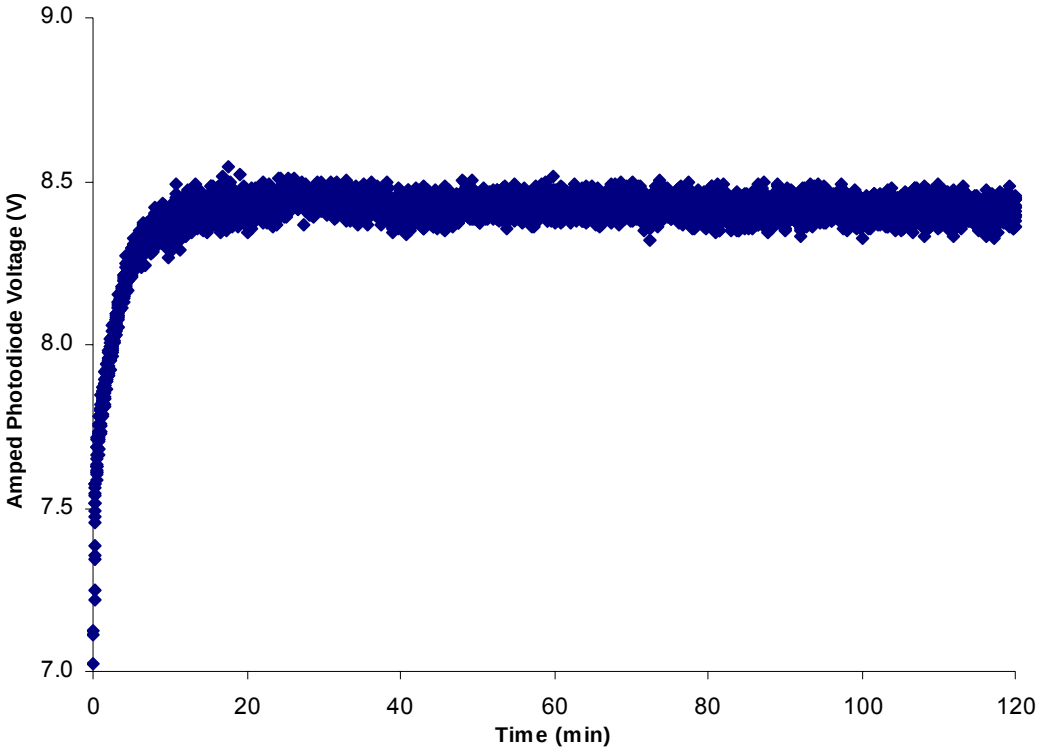

Figure 2.8 Amped photodiode voltage response of the OL 490 measured "From Cold" in 1 sec increments for a period of 2 hrs.

Finally, the photodiode voltage response to broadband illumination from a QTH lamp source is compared to the OL 490 response in Figure 2.9. It is important to note that the QTH overshoots its steady state voltage in the first minute and then gradually drops to an eventual steady state, whereas the OL 490 gradually rises to attain its steady state. It is also of note that there is no random variation in the QTH response relative to the widespread variation of the OL 490 response. This indicates that the OL 490 is less stable than the QTH light source. The reason for this instability is unknown, but may be due to the Xenon lamp, the entrance slit, the collection optics, the DMD filtering, or the collimating optics. It is most likely a combination of two or more of those factors, and compensating for the intensity fluctuation may be necessary to produce repeatable spectral illuminations.

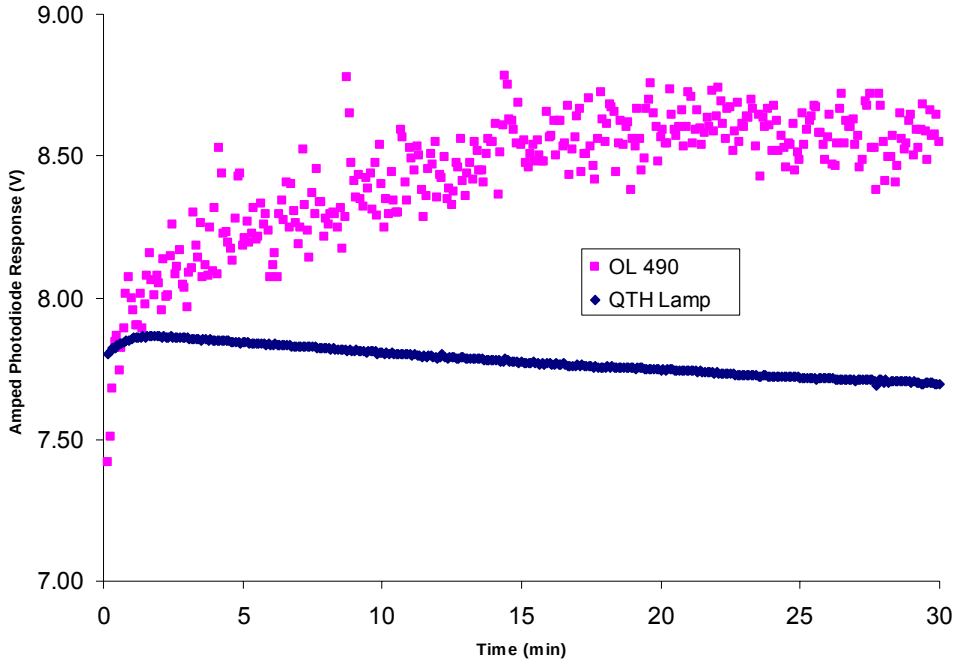

Figure 2.9 Comparison of photodiode stability between OL 490 and a QTH lamp in 5 sec increments for a period of 30 min

2.2.2 Selecting a slit width

According to Optronic Laboratories, the slit between the lamp and optics head is necessary to direct and define the path geometry of the source to be dispersed, i.e. the Xe lamp. Wide slits allow for greater optical power output than narrow slits, but narrow slits allow for tighter bandpasses and better spectral resolution than wide slits. To determine which slit should be used in the DLP HSI, the exact effects of slit width on output intensity, spectral accuracy, and minimum bandwidth must be considered.

2.2.2.1 Output intensity

The output of the OL 490 LLG is made spatially uniform in a 50 mm integrating sphere before reaching an Ocean Optics USB2000+ visible (350 nm to 1000 nm) spectrometer (Ocean Optics, Dunedin, FL) via a 50 μm UV/VIS Premium Fiber in order to measure irradiance. The

Ocean Optics spectrometer and accompanying SpectraSuite software is used to record the illuminated spectrum produced by the OL 490. To eliminate differential spectrometer responses due to changing parameters, the SpectraSuite parameters are constant even when slits are changed.

For each of the four slits (150 μm, 350 μm, 500 μm, and 750 μm) the illumination spectrum created by turning on 80% of the mirrors in every column is measured. This illumination spectrum is generated by the Gwectra file 'AllOn.gxt' which sets the magnitude to 80 for each of the 1024 wavelengths. Originally, 'AllOn.gxt' set the magnitude to 100, so that all of the mirrors on the DMD array would be on, but this causes the spectrometer to saturate, so the intensity is reduced to 80. The 750 μm slit is inserted into the Xe lamp output slot first. After allowing 15 min for the lamp to warm up, the spectrometer response is saved. The lamp is switched off and cools down for several minutes before switching to the next slit. The recorded spectrum for each slit is plotted in Figure 2.10.

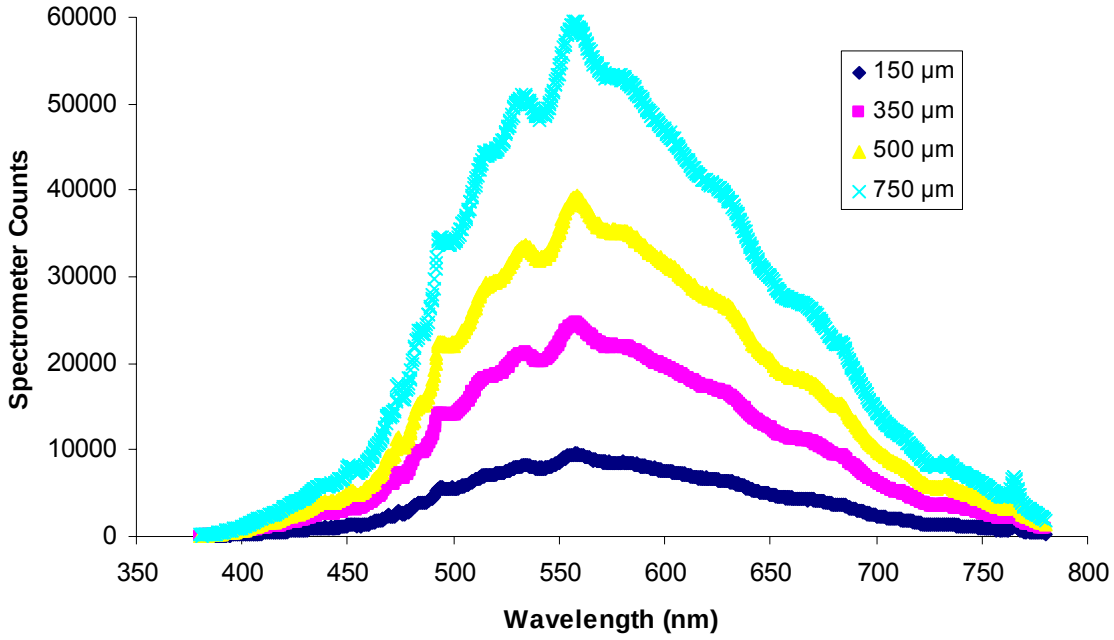

Figure 2.10 Spectrometer responses of illumination spectrum output with all mirrors on for each slit.

To quantify the differences in output intensity between the slits, a ratio of the spectrometer response for each slit compared to the narrowest slit is calculated at each recorded wavelength between 380 nm and 780 nm. The spectrometer resolution of ~0.37 nm means that 1,130 values are detected in the wavelength range, so 1,130 ratios are calculated for each slit. The means and standard deviations of these 1,130 ratios are shown in Figure 2.11 and Table 2.3. The 350 µm slit allows 2.5 times more light through the optics head than the 150 µm slit, the 500 µm slit allows 4 times more light through, and the 750 µm slit allows 6 times more light through. Rather large deviations can be attributed to low spectrometer response in the tails of all the recorded spectra. Even though the specifications denote a wavelength range of 380 nm to 780 nm, the low responses suggest that the useable wavelength range may be narrower.

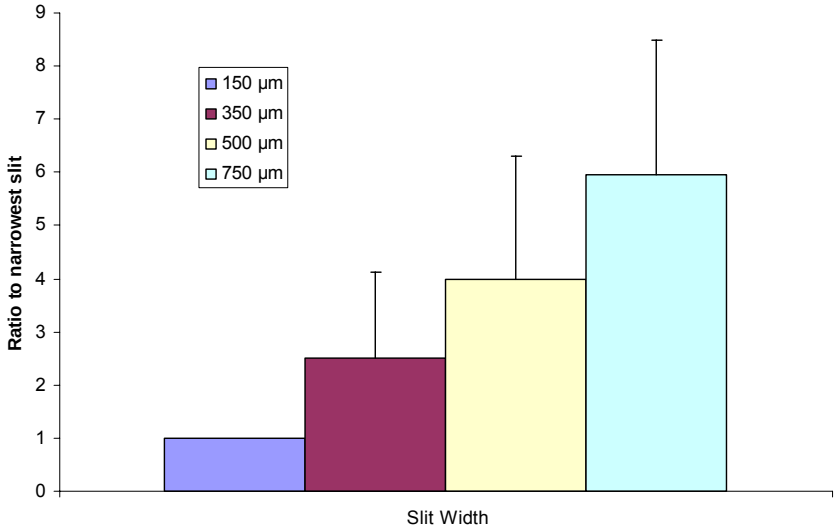

Figure 2.11 Ratio of spectrometer response to OL 490 illumination spectrum 'AllOn.gxt' between each slit and the narrowest slit (150 µm).

Table 2.3 Ratio of spectrometer response to OL 490 illumination spectrum 'AllOn.gxt' between each slit and the narrowest slit (150 µm).

	Slit Width			
	150 µm	350 µm	500 µm	750 µm
Mean	1.00	2.50	3.99	5.95
St. Dev.	0.00	1.61	2.32	2.55

In order to prove that the spectral profile of the OL 490 does not vary between slits, the recorded spectra are normalized and plotted on the same axes in Figure 2.12. Although there is some deviation at certain wavelengths, the normalized spectra generally overlap. A paired Student's T-test for two-tailed distributions is performed for the four normalized spectra, with the results showing no statistically significant difference ($p<0.05$) between any of the distributions (see Table 2.4). In fact, the smallest p-value is 0.56 for comparison of the 150 μm slit normalized spectrum and the 750 μm slit normalized spectrum.

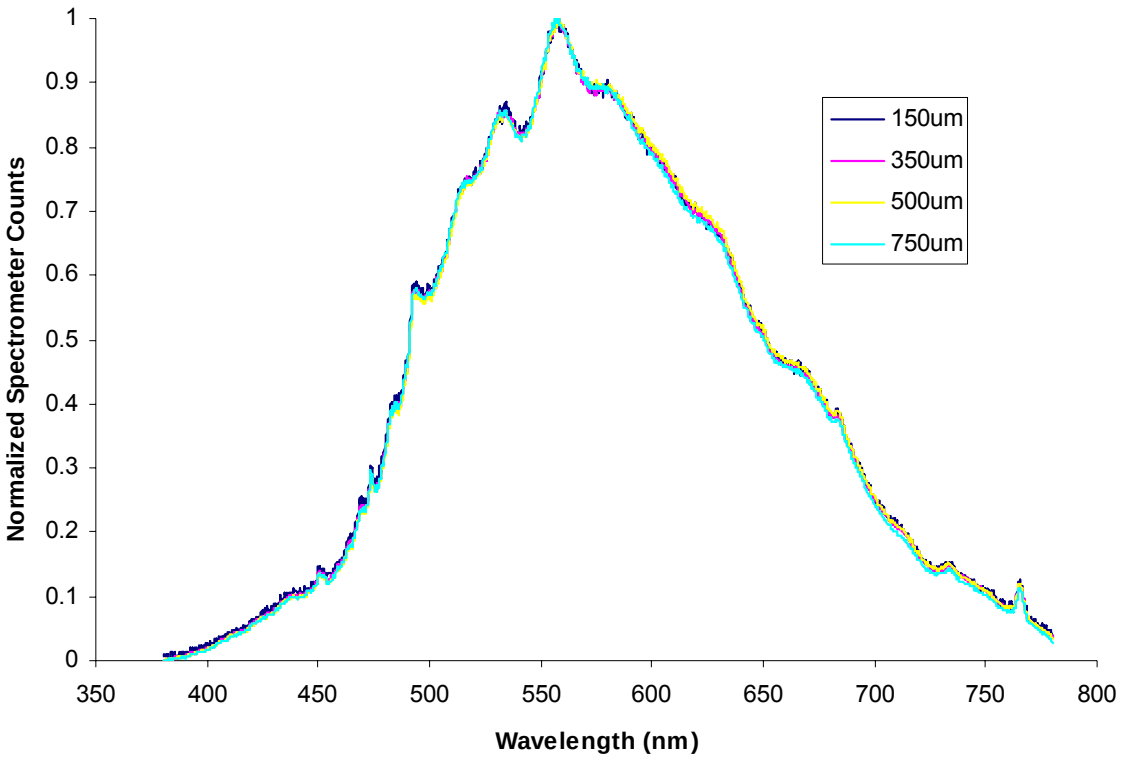

Figure 2.12 Normalized spectra from spectrometer responses in Figure 2.10.

Table 2.4 P-values resulting from paired Student's T-test between the normalized spectra in Figure 2.12.

	150 μm	350 μm	500 μm	750 μm
150 μm	1	0.74	0.83	0.56
350 μm	0.74	1	0.91	0.80
500 μm	0.83	0.91	1	0.71
750 μm	0.56	0.80	0.71	1

2.2.2.2 Center wavelength calibration

To verify its wavelength accuracy and minimum bandwidth specifications, the OL 490 is programmed in OL 490 AS to sweep from 380 nm to 780 nm at 10 nm increments with the minimum programmable bandwidth for the 350 μm slit (9 nm), the 500 μm slit (13 nm), and the 750 μm slit (19 nm). Since the minimum programmable bandwidth for the 150 μm slit is 5 nm, the OL 490 is programmed to sweep at 5 nm increments for that slit. The LLG output is measured by a spectrometer as described in section 2.2.2.1. One spectrum is measured for each bandpass in the sweep, resulting in 41 or 81 measured spectra for each slit (see Figure 2.13).

From each measured spectrum, the measured center wavelength (λ_M) is calculated according to the equation:

$$\lambda_M = \frac{1}{2}(\lambda_1 + \lambda_2) \qquad \text{eq 2.1}$$

where λ_1 and λ_2 are the wavelengths that correspond to half of the maximum intensity measured by the spectrometer. The measured center wavelength is then plotted as a function of the OL 490 programmed center wavelength (λ_P) to determine the center wavelength accuracy of the spectral light engine (see Figure 2.14). From the plotted data, a linear fit calibration curve is calculated in the form of eq 2.2 to quantify wavelength accuracy and compensate for any inaccuracy.

$$\lambda_M = m \cdot \lambda_P + b \qquad \text{eq 2.2}$$

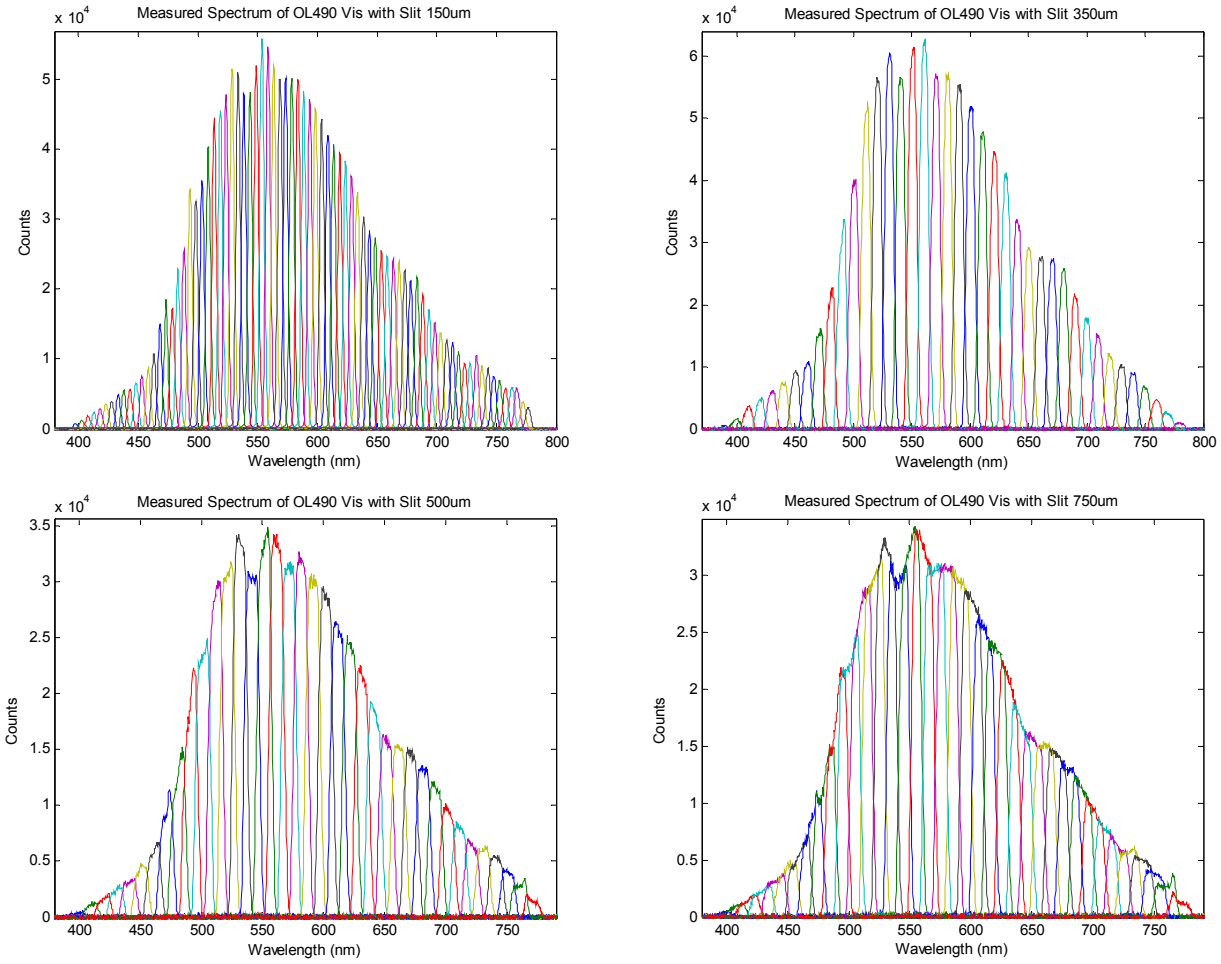

Figure 2.13 Spectrometer responses to bandpass illumination sweeps from the OL 490 with each bandpass in a different color. The top left set of axes includes 81 measured bandpasses, and the other sets of axes each include 41 measured bandpasses.

The relationship between measured and programmed center wavelength is linear with high correlation (R^2 = 0.999) regardless of the slit. For all of the slits, the slope of the calibration curve (m) is essentially equal to 1, which means that the y-intercept value (b) represents the wavelength accuracy offset. Following this metric, the wavelength accuracy is < 1 nm for all of the slits except for the 500 µm slit, in which b = 2.335. However, m = 0.998 for the 500 µm slit, which means that at a center wavelength in the OL 490's wavelength range (i.e. λ_P = 680 nm), the measured wavelength is still within 1 nm of the programmed wavelength (λ_M = 680.975 nm). Therefore, the manufacturer's accuracy specification can be validated. However, the desired

wavelengths of complex spectra programmed by Gwectra files should first be adjusted by the appropriate calibration curve before being sent to the OL 490 to refine its spectral accuracy.

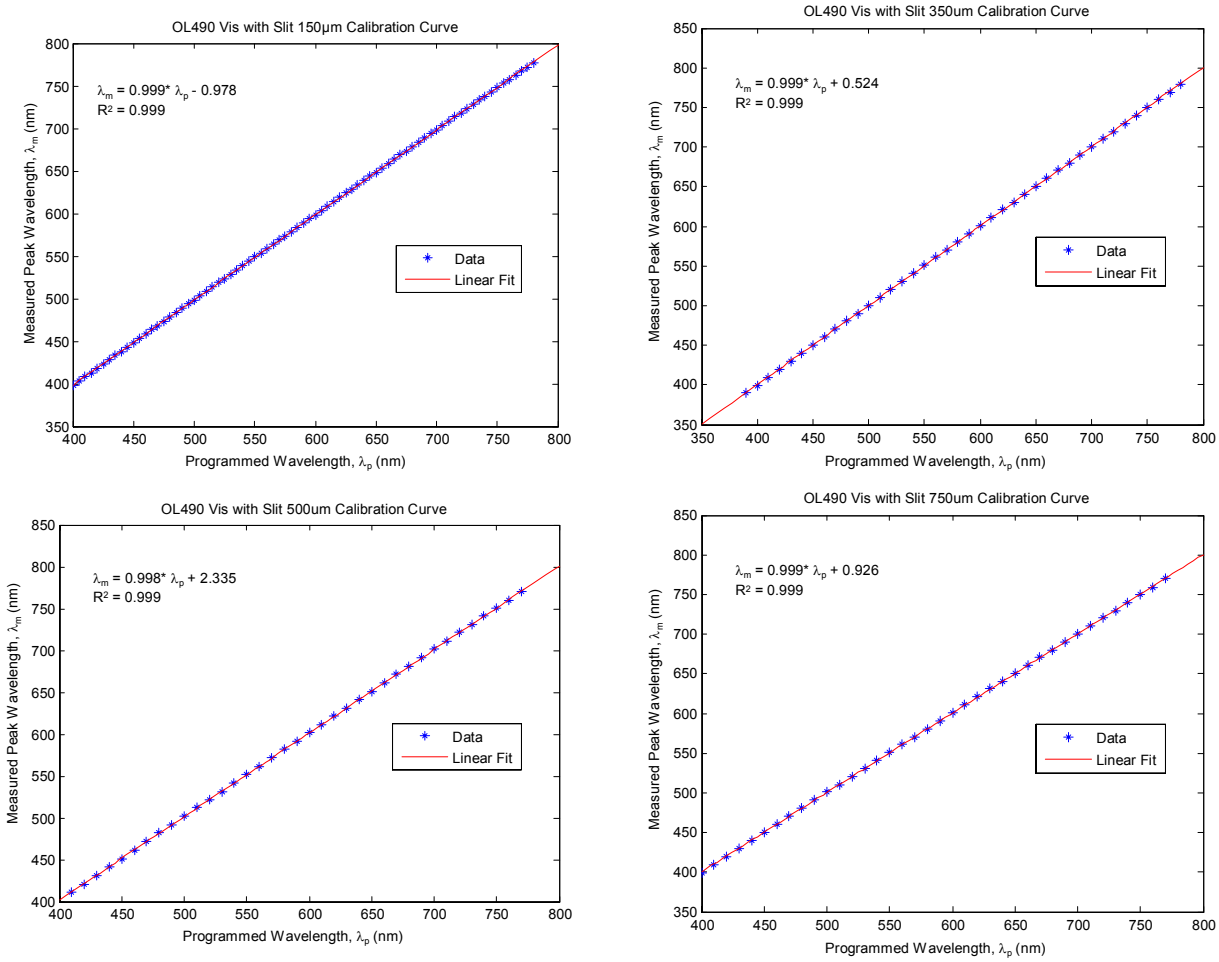

Figure 2.14 Center wavelength calibration curves for each slit. Measured center wavelength, λ_M, as a function of programmed center wavelength, λ_P, is plotted, and the linear fit is of the data with a slope near 1 and low y-intercept indicates wavelength accuracy.

2.2.2.3 Minimum bandwidth

From the same spectrometer data used for center wavelength calibration, the full-width half maximum (FWHM) bandwidth for each measured bandpass spectrum is calculated according to

$$FWHM = \left|\lambda_2 - \lambda_1\right| \qquad \text{eq 2.3}$$

where λ_1 and λ_2 are still the wavelengths that correspond to half of the maximum intensity measured by the spectrometer. For all bandpasses below 420 nm and above 760 nm, the

spectrometer response is too low to get an accurate measure of FWHM bandwidth, so only the values from 420 nm to 760 nm are calculated. Figure 2.15 shows that the measured bandwidth is constant for each slit as wavelength varies. The plot also shows that the measured minimum bandwidths are lower the manufacturer specifications. The output optical intensity at these minimum bandwidths is very low, so for practical use the minimum bandwidth should be greater than the minimum programmable bandwidth in the OL 490 AS.

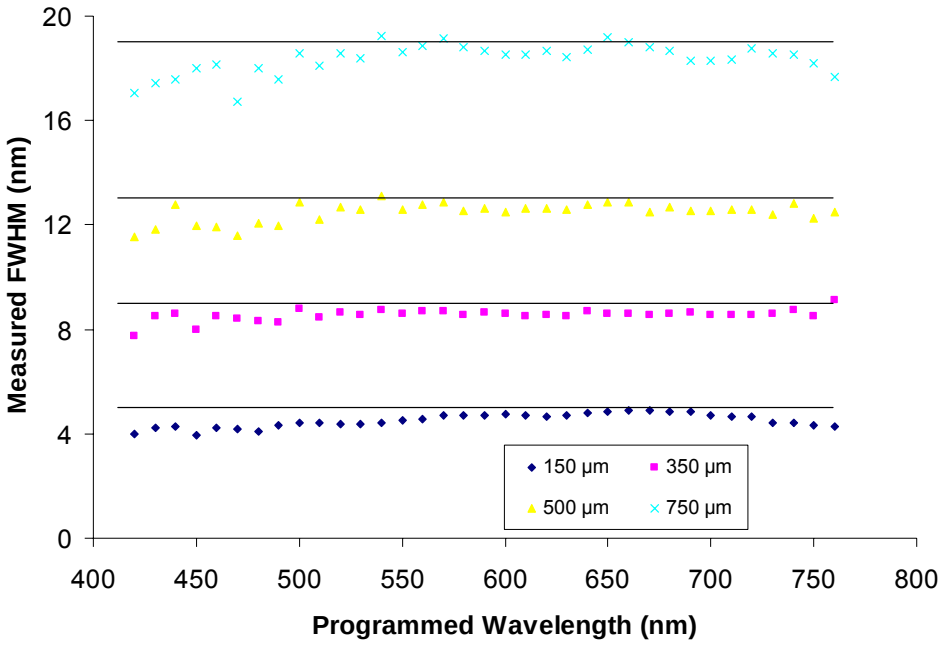

Figure 2.15 Measured FWHM bandwidths for OL 490 AS programmed center wavelength bandpasses from 420 nm to 760 nm in 10 nm increments. The programmed bandwidths (5 nm, 9 nm, 13 nm and 19 nm) are shown as horizontal line segments.

To further understand the minimum bandwidth constraints of the OL 490 and the effect of bandwidth on intensity, two narrow bandpasses of light are generated by turning on a single column of mirrors corresponding to 551.8762 nm in one Gwectra file and turning on 17 columns of mirrors centered at 551.8762 nm in a second Gwectra file. Additionally, two frames are rendered in OL 490 AS to output a 9 nm and 10 nm bandpass at 552 nm center wavelength. The SpectraSuite parameters for the spectrometer are an integration time of 27 ms, 10 scans to

average, and no boxcar filtering, so that the spectrometer does not saturate in the highest intensity illumination. Figure 2.16 shows the bandpass spectra measured when the 350 μm slit is inserted. From the results, an increase of 1 nm in programmable bandwidth causes a 16.2 fold increase in maximum output intensity and the measured FWHM bandwidth only increases from 8.4 nm to 9.4 nm. This indicates that the minimum useable bandwidth is 9.4 nm, which can be programmed in OL 490 AS by selecting a bandwidth of 10 nm or in Gwectra files by turning on 17 columns of mirrors.

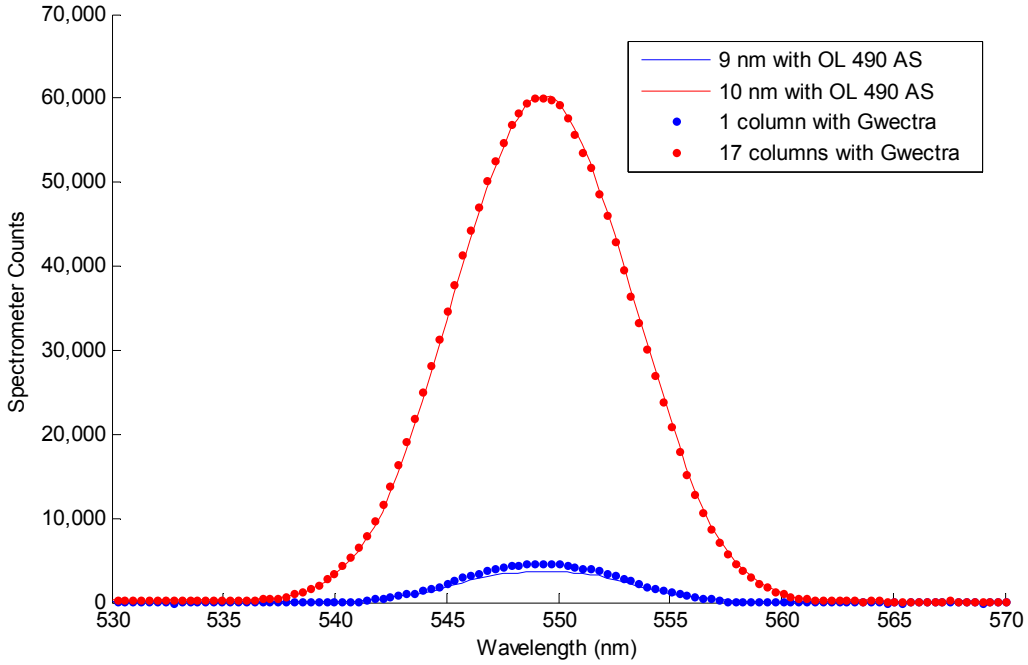

Figure 2.16 Spectrometer response of 9 nm and 10 nm illumination bandpasses created by the OL 490 AS and with Gwectra files.

2.2.2.4 Final slit selection

Understanding the effect that slit width has on output intensity and spectral resolution, the most practical slit for the DLP HSI prototype design can be selected. Prior LCTF-based hyperspectral imaging systems have a spectral resolution of 10 nm and have been optimized over a period of ten years.[6,9-12] Since the DLP HSI prototype will initially be compared to the LCTF systems, the 350 μm slit is selected to create the same spectral resolution. A

comparison of the output intensity at each wavelength (see Figure 2.17) indicates that the OL 490 with the 350 µm slit has more intense optical output in wavelengths shorter than 630 nm, but the LCTF system is more intense in longer wavelengths. When the DLP HSI is fully integrated, it may be necessary to use a broader slit to get adequate intensity in long wavelengths. Also, to compare spectra with fine spectral resolution, the 150 µm slit can be used, but the detector will have to integrate for a longer period of time, because the output intensity will be lower.

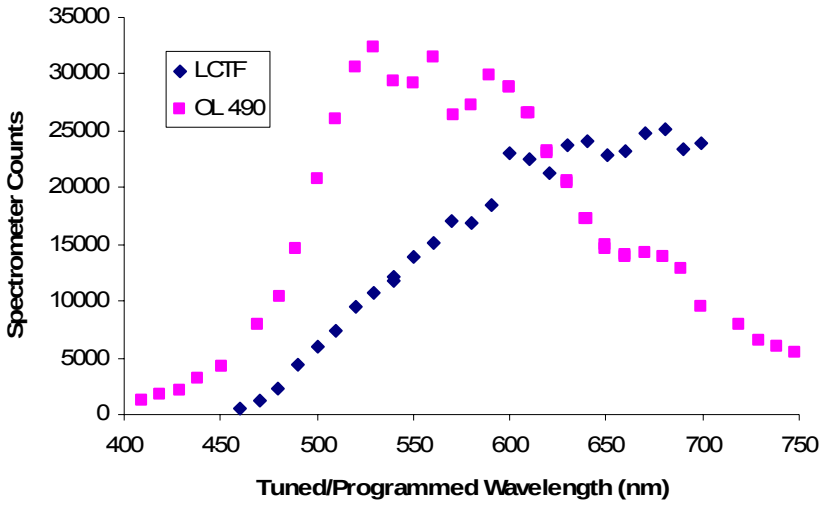

Figure 2.17 Comparison of bandpass intensity from LCTF-QTH system and OL 490 with 350 µm slit. Both illuminators were tuned or programmed to sweep in 10 nm increments with 10 nm bandpasses, and their peak output intensities as measured by a spectrometer with constant parameters are plotted.

CHAPTER 3

IMAGING DETECTOR

3.1 Selecting a camera

Prior to integrating the DLP Hyperspectral Imaging system, two scientific grade focal plane array (FPA) cameras are identified as possible detectors: the CoolSNAP HQ2 and the PIXIS 1024BR (Princeton Instruments, Princeton, NJ). Both cameras feature greater than 1 megapixel charge coupled device (CCD) arrays and are easily interfaced to a laptop via USB 2.0 (PIXIS) or Firewire (HQ2). As seen in Table 3.1, the HQ2 has a smaller pixel size which should allow for greater spatial resolution and higher A/D transfer rate which should allow for faster imaging. However, as seen in Figure 3.1 the quantum efficiency (QE) of the PIXIS is greater than the HQ2 at 500 nm and above, which is where most of the endogenous tissue chromophores exhibit absorption peaks. After much deliberation of the advantages and disadvantages of each imaging detector, it is determined that both cameras can successfully capture hyperspectral images in concert with the OL 490, so speed is the determining factor in selecting one over the other.

Table 3.1: Comparison of imaging specifications for detectors for integration into DLP HSI.

Model	PIXIS 1024BR	CoolSNAP HQ2
CCD Sensor	Back illuminated; deep depletion	Sony ICX285
Pixel Array	1024 x 1024	1392 x 1040
Pixel Size	20 x 20 μm	6.45 x 6.45 μm
Imaging Area	20.5 x 20.5 mm	8.98 x 6.71 mm
A/D Transfer	16 bits @ 2 MHz	14 bits @ 20 MHz

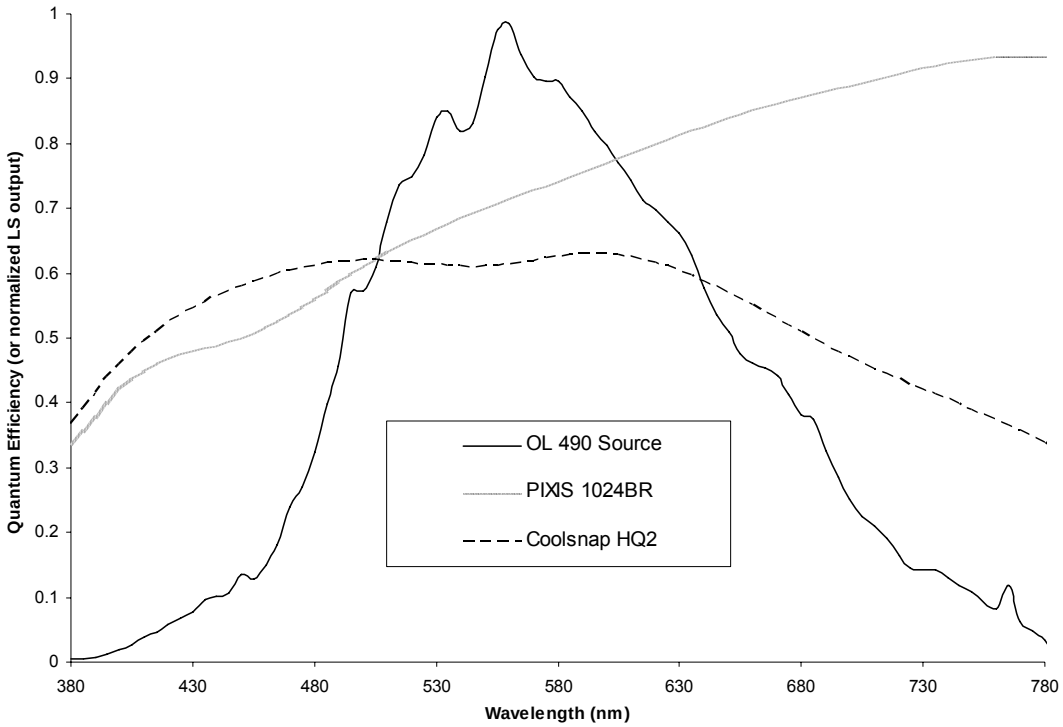

Figure 3.1 Quantum efficiency (QE) of each camera detector array over the wavelength range of the OL 490. The QE of the PIXIS is better than the HQ2 in the near IR, but the relationship is reversed in the near UV. [From Princeton Instruments' specification sheets]

3.1.1 Stopwatch Speed Tests

Speed has been one of the key limitations of hyperspectral imaging for medical applications. For a single hyperspectral image cube, multiple images must be captured, which means that the speed of a single image capture for the system's detector is multiplied by the number of images captured per cube. According to manufacturer specifications, the readout time for a single full-frame image binned 8 x 8 for the PIXIS is 0.14 sec, which corresponds to a frame rate (r) of 7.14 frames per second (fps) calculated with eq 3.1, where n is the number of frames.

$$r = \frac{n}{t_{readout}} \qquad \text{eq 3.1}$$

According to the specifications for the HQ2, r = 35 fps for a full-frame image binned 4 x 4 and r = 56 fps binned 8 x 8. Manufacturer specs are good for comparison prior to purchase, but

since both cameras had been purchased as part of previous hyperspectral imager designs, empirical laboratory tests are better for measuring true speed performance.

First, to determine the dependence of frame rate on exposure time in each camera, the time to collect and read out 100 full FPA frames with 4 x 4 binning is measured at various exposure times. A stopwatch with 0.01 sec resolution is started with the experimenter's left hand while acquisition is started by clicking the laptop mouse button with the right hand. The stopwatch is stopped with the left hand when the laptop display visually signals acquisition is complete. Four runs at each exposure time (1 ms to 13 ms in 1 ms increments) are timed, the frame rate for each run is calculated by eq 3.1, and the mean for each exposure time is plotted in Figure 3.2. From the figure, it is evident that the PIXIS frame rate is not dependent on detector exposure time, but the HQ2 frame rate decreases as exposure time increases. This is most likely due to the fast-acting electronic shutter in the HQ2 relative to the slow-acting mechanical shutter of the PIXIS, which means that much of the acquisition time in the PIXIS is consumed by opening and closing of the shutter.

Next, the exposure time was set to a constant 1 ms and the number of frames acquired (n) was varied to determine the static and dynamic constants associated with each camera. The static constant (S) refers to the time required to initialize capture and display on monitor that acquisition is complete. Readout time ($t_{readout}$) depends on the value of S only once, no matter the value of n. The dynamic constant (D) refers to the time required to open shutter, expose the CCD array, close shutter, and convert the analog signal array to a digital image. Since all of these actions occur once for every frame, $t_{readout}$ depends on the value of D times the value of n. The relationship should be linear according to eq 3.2.

$$t_{readout} = D \cdot n + S \qquad \text{eq 3.2}$$

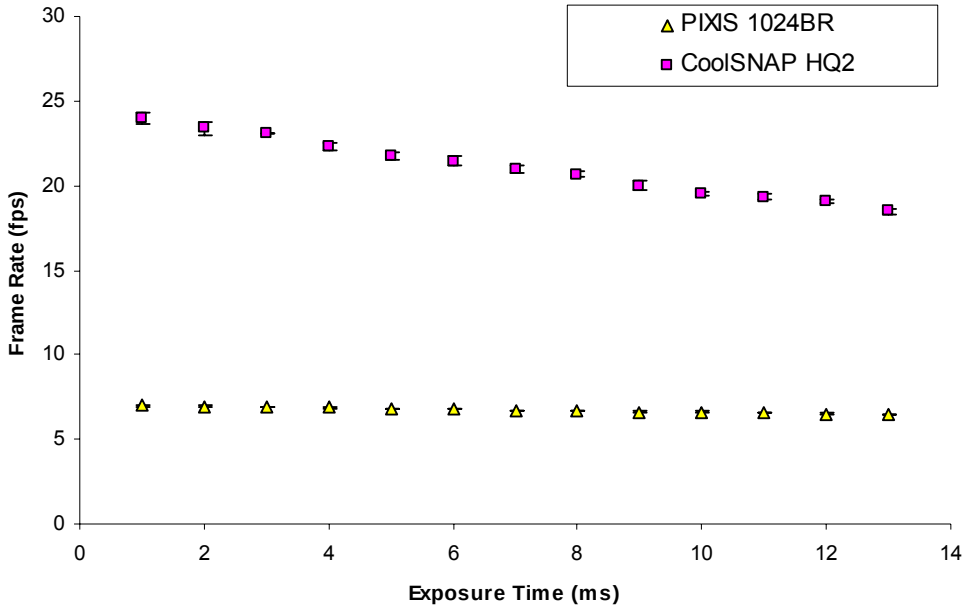

Figure 3.2 The dependence of camera frame rate on exposure time for the CoolSNAP HQ2 and PIXIS 1024BR as calculated by measuring with a stopwatch the time to acquire 100 frames.

A second set of stopwatch tests was run with the results shown in Figure 3.3. According to the highly correlated linear fit of each camera's dataset, the relationship is indeed linear. Assuming that the static constant is mostly a function of human response time with the stopwatch and the current software being used to acquire, S_{PIXIS} and S_{HQ2} have no effect on the respective camera's ideal maximum frame rate. By inverting the dynamic constant, D_{PIXIS} = 0.1369 and D_{HQ2} = 0.0369, the ideal frame rate is determined for each camera, r_{PIXIS} = 7.3 fps and r_{HQ2} = 27.1 fps.

Empirical results from the stopwatch speed tests indicate that the HQ2 is nearly four times faster than the PIXIS, which is slightly different than the manufacturer specs that indicate a five to eight fold advantage for the HQ2. Regardless, since speed is required for a clinical hyperspectral imaging system, the CoolSNAP HQ2 is selected over the PIXIS 1024BR.

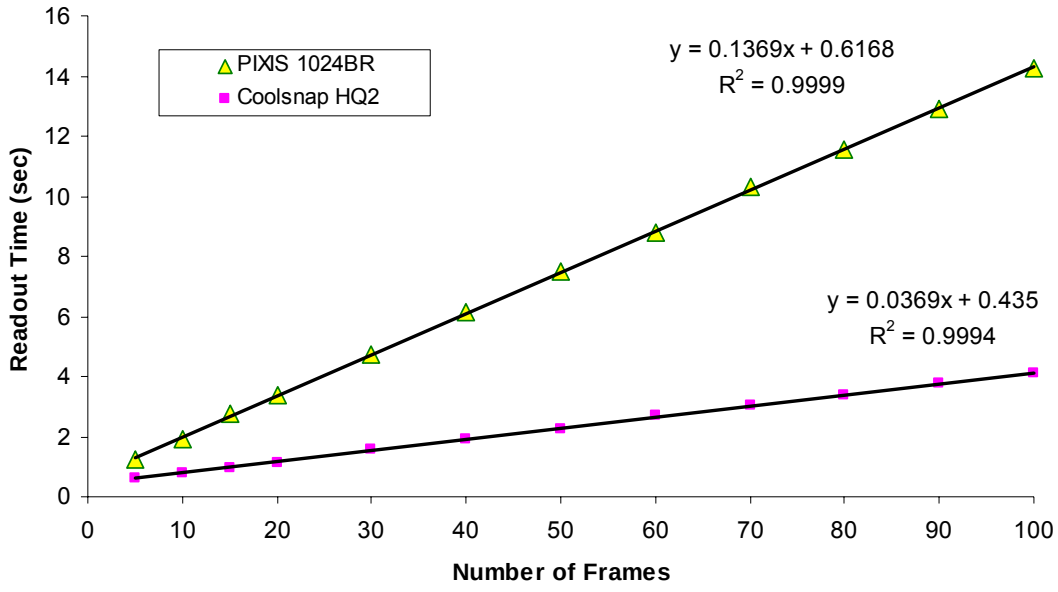

Figure 3.3 Results of second set of stopwatch speed tests, where exposure time remained constant and number of frames varied. The slope of each linear fit is used to calculate ideal frame rate of the camera.

3.2 Characterization of the CoolSNAP HQ2

3.2.1 Binning and Gain

The full 1392 x 1040 CCD array can be binned into square pixel bins of 1 x 1, 2 x 2, 3 x 3, 4 x 4, or 8 x 8. Binning effectively clusters pixels into a single superpixel. The analog photovoltaic response of all pixels in the bin is integrated into a single digital response for the superpixel. This means that when binning is set to 4 x 4, the analog response of 16 pixels is combined to a single digital count value. Table 3.2 enumerates the resulting digital image size when each binning option is selected. Because the individual response of several pixels is integrated into a single value, less exposure is required when larger binning parameters are selected. Also, with smaller image sizes, processing the hyperspectral image cube with chemometric and deconvolution algorithms is much faster. Therefore, larger bins are desired when speed is the number one priority. The cost of larger bins is decreased spatial resolution,

so the binning parameter must also be selected based on the size of the objects to be contrasted in an image.

Table 3.2 Binning options for CoolSNAP HQ2 and their effects on imaging

Binning	1 x 1	2 x 2	3 x 3	4 x 4	8 x 8
Image Size	1392 x 1040	696 x 520	464 x 346	348 x 260	174 x 130
Relative Response	1	4	9	16	64
Required Exposure	100	25	11	6	1

The HQ2 also offers three levels of adjustable analog gain. A camera gain of 1 means that each detector pixel outputs 1 digital count for every 2 incoming electrons, a gain of 2 means that each pixel outputs 1 count for every 1 incident electrons, and a gain of 3 means that each pixel outputs 4 counts for every 1 incident electron. Increasing the gain effectively lowers the required exposure time to reach counts near 12,000, which is an acceptable level just below saturation.

Saturation occurs when the electrons incident on any given pixel exceeds the full well limit for that pixel. Since the digitizer is 14 bits, saturation should occur when analog response dictates a digital count greater than or equal to 2^{14} = 16,384. As a precaution, any count above 14,300 is considered saturation for the DLP HSI.

3.2.2 Spatial resolution

One standard method of determining spatial resolution of an imaging system is to use a line pair gauge to create a modulation transfer function of the percent contrast visualized by the system versus frequency of line pairs.[16] Using the same method described in previous theses,[17,18] a USAF 1951 target (Edmund Optics, Barrington, NJ) is imaged to determine the minimum spatial resolution of the CoolSNAP HQ2 integrated with the OL 490. The line pair target is illuminated with broadband light from 527 nm to 638 nm from the OL 490, and the HQ2 is programmed with an exposure time of 800 μs, gain 1, and binning 4 x 4. A 50 mm Nikon lens

attached to the C-mount of the HQ2 focuses the image field of view (FOV) onto the FPA of the camera with an aperture of f/5.6. Grayscale images of a white background (Figure 3.4(a)) and the line pair target (Figure 3.4(b)) are captured at focal distances of 45 cm, 65 cm, and 85 cm. The purpose of acquiring the white background image is to calculate absorbance, which is explained in detail in section 4.4.

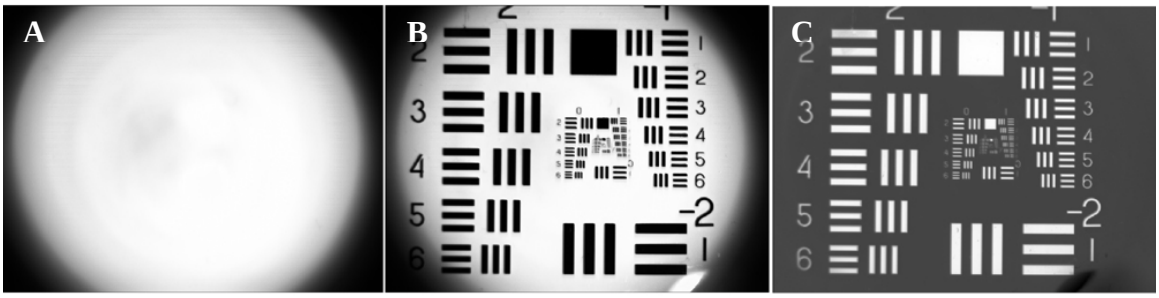

Figure 3.4 Grayscale images of (a) white background and (b) USAF 1951 target are ratioed to create an absorbance image (c). Images are captured at a 45 cm focal distance.

In MATLAB, the absorbance image (Figure 3.4(c)) is analyzed to determine the percent contrast between the vertical white bars and the dark background for each line pair. Specifically, the percent contrast is calculated according to eq 3.3, where I_{max} is the maximum pixel intensity from a white bar in the image and I_{min} is the minimum pixel intensity from the dark space in between the white bars.

$$\%C = \frac{I_{\max} - I_{\min}}{I_{\max} + I_{\min}} \times 100\% \qquad \text{eq 3.3}$$

Each line pair width is precisely defined on the quartz line pair target, so the result of eq 3.3 for each line pair is plotted as function of spatial resolution in Figure 3.5. As expected, the percent contrast drops off sharply as the line pair width decreases. Logarithmic fits of the data for each focal distance are calculated to extrapolate the minimum spatial resolution, defined as the size of an object which can be identified with at least 20% contrast. The minimum spatial resolution is 0.197 mm for 45 cm focus, 0.297 mm for 65 cm focus, and 0.505 mm for 85 cm focus, affirming that the minimum spatial resolution is proportional to the focal distance of the camera.

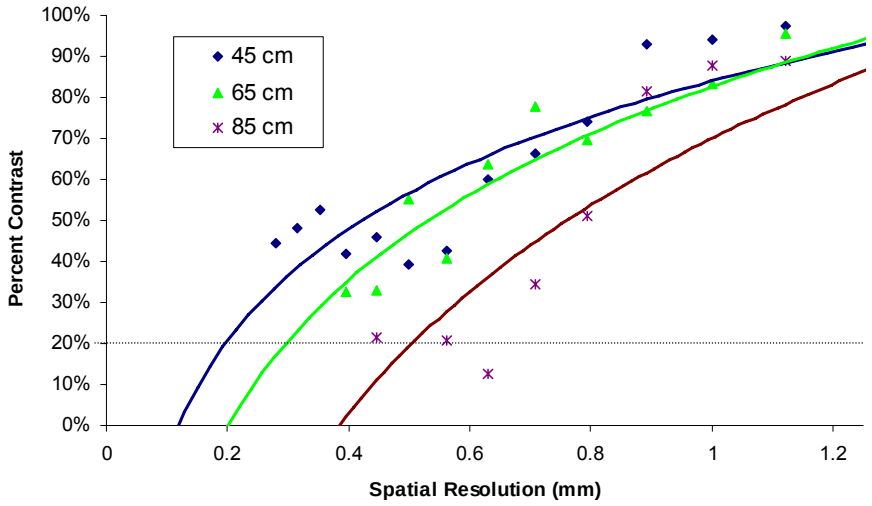

Figure 3.5 Percent contrast versus spatial resolution for 4 x 4 binning at different focal distances. Correlation of logarithmic fits are R^2 = 0.84 for 45 cm, R^2 = 0.91 for 65 cm, and R^2 = 0.85 for 85 cm.

3.2.3 Exposure time accuracy

Previous software used to control the CoolSNAP HQ2 limited the control of exposure time to 1 ms resolution. However, while trying to understand the speed limitations of the camera, new software was found which allows the user to set the detector's exposure time with 1 µs resolution. When the exposure time was increased from 1 µs to 2 µs to 3 µs and so on, the resulting raw images appeared unchanged and dark until 9 µs. The same phenomenon, this time with an brighter but still unchanged image, occurred while incrementing the exposure time by 1 µs from 9 µs up to 210 µs. To investigate the counterintuitive non-influence of exposure time on image intensity, images of an all white FOV were captured with varying exposure times from 10 µs to 2,500 µs in 10 µs increments. The mean of 2,601 pixels from the center of each image is plotted in Figure 3.6 as a function of the exposure time at which the image was captured. The resulting stair step profile with plateaus of 210 ± 10 µs indicates that the detector can actually only expose in increments near 0.2 ms even though the software allows inputs in increments of 1 µs. This observation is irrelevant when programming the detector in units of 'ms', but it is important to remember when programming in units of 'µs'.

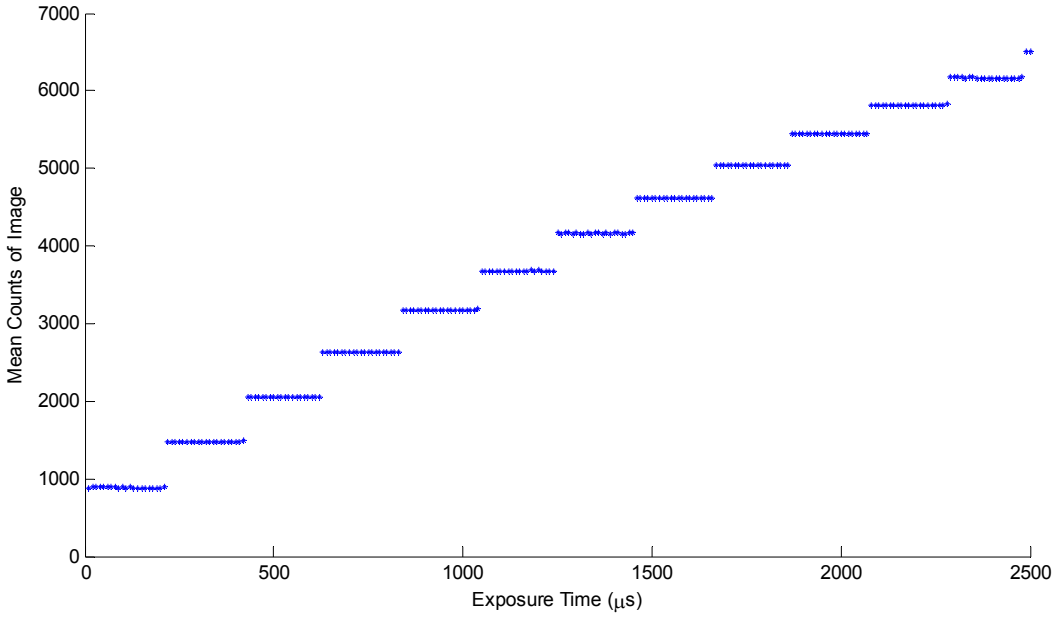

Figure 3.6 Stair step profile of average counts detected by CoolSNAP HQ2 as exposure time is incremented by 10 μs. This indicates that the minimum resolution of the detector's exposure time is 210±10 μs.

To verify the stair step profile in Figure 3.6 and determine what the actual time is that the detector integrates for in each plateau, the TTL pulse indicating the detector's exposure is measured and recorded in LabView. The time duration of each high pulse is calculated as several different exposure times are programmed to the HQ2. From these timing measurements, inputting any value between 430 μs and 630 μs results in a high voltage for a period of 620 μs, inputting values between 640 μs and 840 μs result in a high voltage for a period of 830 ± 10 μs, inputting 1,200 μs results in a high voltage for 1,240 μs, and inputting 2,640 μs results in a high voltage of 2,690 μs. These TTL pulse measurements verify the observation that the minimum exposure time resolution is 210 ± 10 μs and indicate that true exposure time for the detector is the highest exposure time in each plateau of Figure 3.6.

3.2.4 Limitations and opportunities for improvement

Even though the CoolSNAP HQ2 was selected because it is faster than the PIXIS camera discussed earlier, speed is still its largest limitation. A camera with an ideal frame rate of only 27.1 fps and minimum exposure time resolution of nearly 0.2 ms is insufficient for real-time hyperspectral imaging. The CCD detector array within the HQ2 is a standard Sony FPA that has great imaging qualities that make it suitable for medical imaging. Assuming that the fundamental limitations in speed of the HQ2 are not caused by the detector itself, but rather by the electronics controlling the detector, updates to the DLP hyperspectral imaging system might include a SonyICX285 with different control electronics and frame grabbing hardware and software.

CHAPTER 4

SYSTEM INTEGRATION AND SYNCHRONIZATION

4.1 System description

The DLP Hyperspectral Imaging system (DLP HSI) consists of a spectral light engine to illuminate the sample and a focal plane array (FPA) detector to capture reflected image information that are synchronized by a computer program. The image detector is a CoolSNAP HQ2 (Princeton Instruments, Trenton, NJ) with a Sony ICX285 CCD sensor, 1392 x 1040 array with 6.45 μm x 6.45 μm pixels, with a dual-speed 14 bit or 12 bit, 20 MHz or 10 MHz digitizer. The spectral illuminator is an OL-490 Agile Light Source (Optronic Laboratories, Orlando, FL) with a spectral range of 380 nm to 780 nm and a full width half maximum (FWHM) bandpass of 10 nm when using a 350 μm slit. Computer software developed by AAVA Technology (Plano, TX) manages the spectral illumination, data collection and image processing. Figure 4.1 shows the mechanically integrated system, in which the HQ2 image detector along with a standard 50 mm lens (Nikon, Melville, NY) and liquid light guide (LLG) beam shaping illumination optic are mounted side-by-side on a friction head atop a mobile Samson tripod (Quickset International, Northbrook, IL). The DLP® Agile light source along with battery backup systems and power supplies are placed on a standard Rubbermaid® cart (Winchester, VA) so the system can be easily transported within and between surgical and clinical suites.

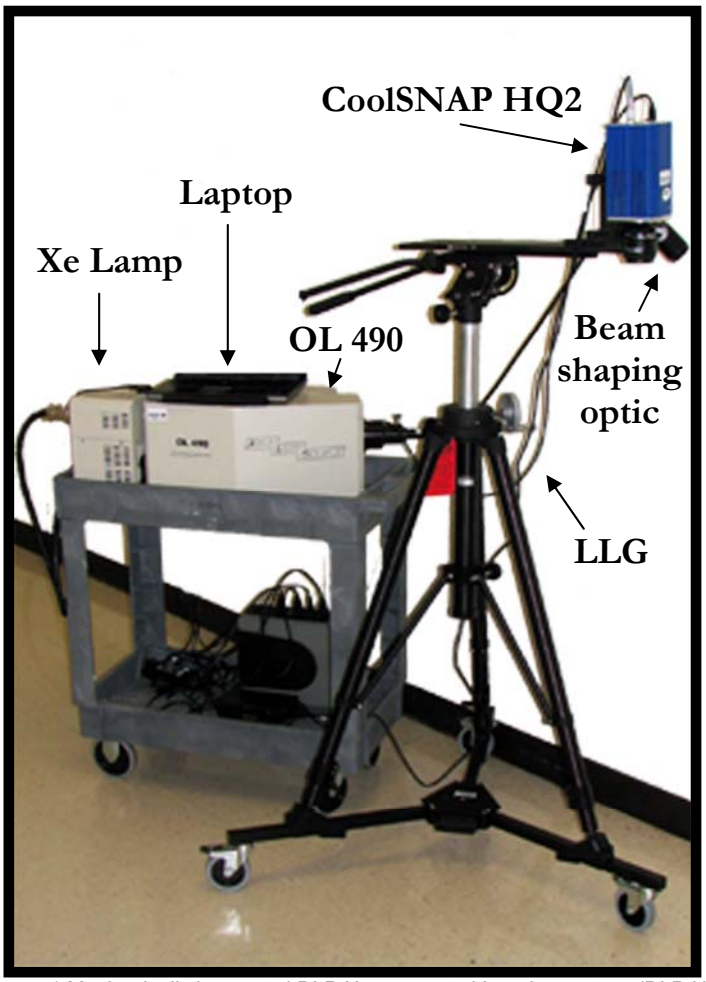

Figure 4.1 Mechanically integrated DLP Hyperspectral Imaging system (DLP HSI).

4.2 Software synchronization

A single Windows application written in C# programming language synchronizes the illumination and image capture, saves the hyperspectral image cube, and processes the cube with new and existing MATLAB algorithms. The centerpiece of the application written by AAVA Technology (Plano, TX) is a graphical user interface (GUI) that allows the user to set necessary illumination schemes, control the camera acquisition parameters, and select which processing algorithm to run (see Figure 4.2). The GUI also contains a window where a Windows bitmap image is displayed in one of two modes: “View Finder” or “Acquire”. When in “View Finder” mode, the displayed image is simply the most recent raw grayscale image acquired by the camera in free running mode with the light source illuminating broadband white light. When in

"Acquire" mode, the displayed image is the result of a processed hyperspectral image cube with the light source illuminating a programmed sequence of spectral illuminations.

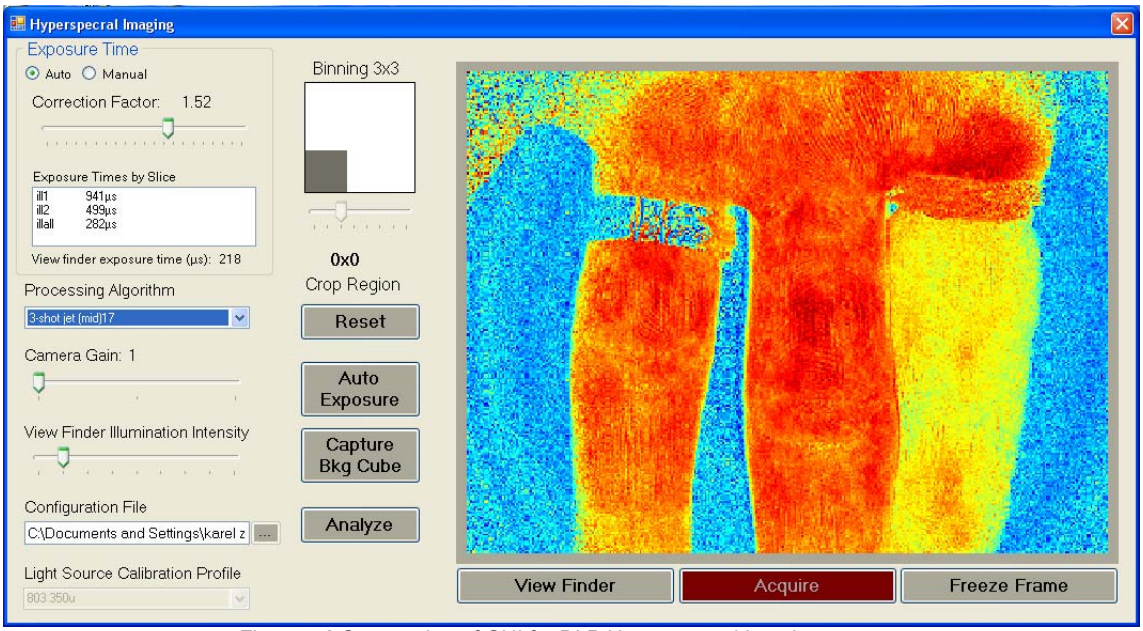

Figure 4.2 Screen shot of GUI for DLP Hyperspectral Imaging system.

OL 490 illumination schemes are programmed in the form of a configuration file (*.ini) which contains the following lines of text:

[Analyzer Parameters]
x=348
y=260
exptype=1
numframes=126
startwave=520.0
endwave=645.0
incwave=1.0
software version=1
bandwidth=10.0
SpectrumDefType=Parametric

'X' and 'y' initialize the horizontal and vertical pixel dimensions of the output image, 'numframes' describes the number of illumination spectra (and images) in a single sequence, and 'SpectrumDefType' can have a value of 'Parametric,' indicating a sweep of contiguous bandpasses, or 'Arbitrary,' indicating a sequence of complex broadband spectral illuminations.

If the value is ‘Parametric,’ then ‘startwave,’ ‘endwave,’ and ‘incwave’ indicate the wavelength range and increment of a sweep in nanometers, while ‘bandwidth’ describes the bandwidth of each bandpass. If the value for ‘SpectrumDefType’ is ‘Arbitrary,’ the other values have little meaning and an additional list of the *.gxt filenames must be appended to the lines of text in the configuration file.

Camera gain, binning and exposure time are controlled by their respective sliders in the Hyperspectral Imaging GUI. Exposure time has the most complex control because it can be variable by slice of the hyperspectral cube, or constant in all slices. If the radio button ‘Auto’ is selected in the ‘Exposure Time’ control box, the exposure time for each slice of the hyperspectral cube is defined by the list of illuminations and corresponding times in microseconds. This list can be augmented manually by opening up the currently loaded *.ini file in a text editor or automatically by clicking the ‘Auto Exposure’ button in the middle of the GUI. Clicking the ‘Auto Exposure’ button commands the system to acquire a hyperspectral image cube with the currently loaded illumination scheme and a constant 20 μs exposure time. The average intensity of each image in the cube is calculated, and a new list of variable exposure times is generated to correct for any variation in intensity values. Specifically, lower intensity image slices get increased exposure times, while saturated image slices get decreased exposure times. The theory behind the ‘Auto Exposure’ algorithm is valid, but it incorrectly assumes that exposure time can be incremented in 1 μs steps. Due to the stair step phenomenon shown in section 3.2.3, clicking ‘Auto Exposure’ often results in incorrect values for exposure time. If the radio button ‘Manual’ is selected in the ‘Exposure Time’ control box, the exposure time for each slice is constant.

Finally, the processing algorithm is selected from a pull down menu that is populated with a list of programmed MATLAB routines. New and augmented algorithms can be added to the list by creating a new ‘hsi.dll’ file in MATLAB and loading it into the Windows system path. Key processing algorithms are ‘Show 1st Raw Image’, which simply reads the hyperspectral cube

and displays the first slice with maximum contrast; ‘Show Absorbance’, which reads the hyperspectral cube and a previously acquired reference cube, calculates absorbance for each slice, and displays the average absorbance across the spectral dimension; ‘Oxyz Jet’, which processes a cube of contiguous bandpass images and results in an image color-coded for tissue oxygenation; and, ‘3shot Jet - *’, which processes a cube of three complex spectral illumination images and results in an image color-coded for tissue oxygenation.

4.3 Imaging procedure

Regardless of which illumination method is used, the following imaging procedure is standard. Prior to imaging, the OL 490 lamp must be turned on for a period of 10 minutes (longer for the first imaging session of the day, see section 2.2.1). In order for the synchronization software to recognize the drivers for the camera and light source, both the HQ2 and the OL 490 optics head must be switched on at least 20 seconds prior to starting the software in Windows. The software is slow to initialize the first time it is loaded. On startup, the GUI is always in ‘View Finder’ mode with camera parameters set by a saved startup file. The GUI will not open if it encounters errors associated with hardware and software DLLs or unrecognizable parameters in the startup file.

After all hardware components are running and the GUI window is visible on the screen, the first step is to focus the camera by adjusting the Nikon lens so that objects at the operating distance of the system are clear. It is important that this operating distance remains constant throughout the entire imaging session. If the image on the screen is dark or saturated, the exposure value of the detector can be augmented by adjusting the lens aperture, the camera binning or gain, and the ‘View Finder Exposure Time’ under the ‘Manual’ exposure setting. It is generally preferred to keep binning at 4 x 4 and gain at 1 to get noiseless images that do not overload the memory of the processor.

The next step is to load the configuration file for whichever illumination method is to be used. While loading the configuration file, a Spectralon 99.9% reflectance target is placed in the

FOV of the camera. The beam shaping optic that focuses the output illumination from the LLG is adjusted so that the beam spot on the reflectance target is in the center of the detector array. 'Capture Bkg Cube' is clicked and the OL 490 begins to sequence through programmed illumination spectra at the same time the camera begins to acquire one image per illumination spectrum. When the background cube has been completely captured, 'Processing Algorithm' is set to 'Show 1st Raw Image' and 'Acquire' is clicked to begin acquisition with the 99.9% reflectance target remaining in the FOV. After completion of one acquired cube, stand alone processing is initialized with the 'Analyze' button to check for saturation in each slice of the cube. If the maximum count measured is lower than 12,000, the exposure value should be increased to take advantage of the full well capacity of the detector, but if the maximum count measured is greater than or equal to 14,300, the exposure value must be decreased to avoid saturation. In 'Auto' exposure, the exposure time is adjusted by increasing or decreasing the correction factor so that all of the variable exposure times maintain correct proportion to each other. In 'Manual' exposure, the exposure time is adjusted by explicitly changing the exposure time of the detector. The process of acquisition and analysis of the Spectralon target is repeated until the ideal exposure time and lens aperture is determined. Finally, 'Capture Bkg Cube' is clicked again to overwrite the initial background cube with a background cube acquired using the ideal parameters.

Once the correct background cube has been captured, the Spectralon target is removed from the FOV and the system is redirected upon a sample area of interest (i.e. tissue). Acquisition is initialized, and the first output bitmap is a grayscale image representing the raw image acquired when the first illumination spectrum of the sequence is output from the OL 490. 'Processing Algorithm' may be changed at any moment during acquisition, as long as the new algorithm is appropriate for the illumination method in the current configuration file. Namely, 'Oxyz Jet' is only appropriate for an illumination method containing 126 contiguous bandpasses. Processed bitmap images are continuously displayed in the visualization area of the GUI until

'Freeze Frame' is clicked. 'Freeze Frame' freezes the current visualization bitmap and allows the user to probe the image by pressing 'Analyze' or switch to a new configuration file, saving the last five sample cubes acquired. Every bitmap that is displayed is also saved in the same parent directory as the configuration file.

4.4 Calculating Absorbance

According to the Beer-Lambert-Bouguer law, "Equal thickness of an absorbing material will absorb a constant fraction of the energy incident upon it." Specifically, it relates the radiant intensity leaving a sample, I, to the radiant intensity incident on a sample, I_0, by an absorbance factor, A, as in eq 4.1.[19]

$$A = \log\left(\frac{I_0}{I}\right) \qquad \text{eq 4.1}$$

Since the DLP HSI works on the principle of diffuse reflectance, a background cube of the Spectralon target mentioned above is considered to be I_0, or the reference path of light, and the sample cube of the area of interest is considered to be I.[10] The background cube is saved after initial acquisition and accessed for processing after every sample cube acquisition. To understand the enormity of this calculation, eq 4.2 is a reformation of eq 4.1in which R replaces I to indicate reflectance, the subscripts indicate each spatial pixel, and the lamda variable references the wavelength slice of the hyperspectral cube. This means that the logarithm of the ratio between background and sample is calculated for each pixel at each illumination. For example, a 348 x 260 x 3 data cube requires 271,440 operations of eq 4.1 and a 348 x 260 x 126 data cube requires 11.4 million operations just to calculate absorbance.

$$A_{xy}(\lambda_n) = \log(R_{xy}(\lambda_n)_0 / R_{xy}(\lambda_n)) \qquad \text{eq 4.2}$$

CHAPTER 5

ILLUMINATION METHODS

Currently there are three illumination methods implemented in the DLP HSI for hyperspectral imaging: Full Spectral Sweep, Spectral Sweep, and 3 Shot. These illumination methods will be discussed in the remaining sections; however, new illumination methods are easily created by programming the spectral light engine. In fact, one novelty in the system is the ability to change the illumination spectrum to any imaginable narrow or broadband spectrum in the wavelength range of the OL 490. This versatility means that the DLP HSI can be used for any number of imaging applications.

5.1 Full Spectral Sweep

To utilize the practical wavelength range of the system, the Full Spectral Sweep method sweeps bandpass illuminations with 10 nm bandwidth from 450 nm to 650 nm in 4 nm increments. A hyperspectral image cube acquired with this method consists of 51 slices and is generally used to explicitly measure the absorbance spectroscopy of an area of interest. Formally, the following series of illuminations is programmed into the OL 490:

$$\{L_{1,FullSweep} = L_{OL490}(\lambda_1),\ \ L_{2,FullSweep} = L_{OL490}(\lambda_2),\ \ \ldots\ \ L_{51,FullSweep} = L_{OL490}(\lambda_{51})\} \qquad \text{eq 5.1}$$

for,

$$\lambda_n = 450 + 4(n-1)\text{, n = \{1:51\}} \qquad \text{eq 5.2}$$

where, $L_{OL490}(\lambda_n)$ is the total radiant power emitted from the OL 490 at a center wavelength, λ_n, with 10 nm full width half maximum (FWHM) bandwidth.

After proportioning with the background, each slice in the cube represents the absorbance of the bandpass illumination at which the image is acquired. Thereby, each spatial pixel in the

processed cube represents a discrete absorbance spectrum of the tissue or other material in the physical position corresponding to that pixel. The wavelength limits of Full Spectral Sweep intentionally truncate the wavelength limits of the OL 490 since the output intensity of the OL 490 is very low near the extremes of its wavelength range (see Figure 2.10).

This illumination method is only used to help calibrate the system as a spectrophotometer, and no algorithms currently exist to process its image cubes for visualization of tissue chemistry. However, with the spectral information acquired using Full Spectral Sweep illumination, it is possible to search for spectral signatures of chemical chromophores and develop new processing algorithms.

5.2 Spectral Sweep

To mimic the illumination of LCTF-based Hyperspectral Imaging systems, the Spectral Sweep method sweeps bandpass illuminations with 10 nm bandwidth from 520 nm to 645 nm in 1 nm increments. A hyperspectral image cube acquired with this method consists of 126 slices and explicitly measures the absorbance spectroscopy of an area of interest. Formally, the following series of illuminations is programmed into the OL 490 by loading a configuration file with 'SpectrumDefType=Parametric':

$$\{L_{1,Sweep} = L_{OL490}(\lambda_1),\ \ L_{2,Sweep} = L_{OL490}(\lambda_2),\ \ \ldots\ \ L_{126,Sweep} = L_{OL490}(\lambda_{126})\} \qquad \text{eq 5.3}$$

for,

$$\lambda_n = 520 + (n-1),\ \text{n = \{1:126\}} \qquad \text{eq 5.4}$$

where, $L_{OL490}(\lambda n)$ is again the total radiant power emitted from the OL 490 at a center wavelength, λ_n, with 10 nm FWHM bandwidth.

After proportioning out the background, each slice in the cube represents the absorbance of the bandpass illumination at which the image is acquired. Thereby, each spatial pixel in the processed cube represents a discrete absorbance spectrum of the tissue or other material in

the physical position corresponding to that pixel: identical to the Full Spectral Sweep, but with better spectral resolution and narrower wavelength range. Each pixel absorbance spectrum is then compared to reference spectra for oxy- (HbO_2) and deoxy-hemoglobin (Hb) in Figure 5.1(a) by multivariate least squares analysis to calculate the percent HbO_2 for that pixel. The output bitmap after processing with 'Oxyz – Jet' is a color-coded two-dimensional image, where more intense pixels (red) signify that the pixel absorbance spectrum more closely resembles the HbO_2 reference and less intense pixels (blue) signify that the pixel absorbance spectrum more closely resembles the Hb reference.

Spectral Sweep illumination is slow for two fundamental reasons: acquisition of 126 frames takes 126 times longer than acquisition of a single frame, and processing of such large data cubes takes time. One suggested solution to this speed issue has been selecting only a few narrow illumination bands to significantly reduce the number of slices in the cube, thereby reducing the acquisition time and processing time.[20,21] This solution has been shown to speed up data acquisition and processing, but does not necessarily gather the same spectral information as a Spectral Sweep.

5.3 3 Shot

To gather spectral information equivalent to the Spectral Sweep with fewer images, the 3 Shot method sequences through three complex broadband illumination spectra in the 527 nm to 638 nm wavelength range. A hyperspectral image cube acquired with this method consists of 3 slices and is used to calculate the percent HbO_2 for each spatial pixel without explicitly measuring the absorbance spectra. Formally, the following illuminations are programmed into the OL 490 by loading a configuration file with 'SpectrumDefType=Arbitrary':

$$L_{1,3shot} = \sum_{n=8}^{119} L_{OL490}(\lambda_n) V_1(\lambda_n) \qquad \text{eq 5.5}$$

$$L_{2,3shot} = \sum_{n=8}^{119} L_{OL490}(\lambda_n) V_2(\lambda_n) \qquad \text{eq 5.6}$$

$$L_{3,3shot} = \sum_{n=8}^{119} L_{OL490}(\lambda_n) \qquad \text{eq 5.7}$$

for the wavelengths described by eq 5.4, where $V_1(\lambda_n)$ represents the positive subtraction of normalized reference spectra and $V_2(\lambda_n)$ represents the negative subtraction of normalized reference spectra as in Figure 5.1. The limits of summation are intentionally n = 8 and n = 119, because the reference spectra have been filtered by a moving average filter that trims seven discrete values from the beginning and end of each spectrum.

After proportioning out the background, each slice in the cube represents the absorbance of the broadband illumination at which the image is acquired. Absorbance spectra are not explicitly measured, but a mathematic combination the three slices results in a single two-dimensional image where higher pixel values indicate absorbance similar to HbO_2 and lower pixel values indicate absorbance similar to Hb. The data cube is 42 times smaller than the Spectral Sweep data cube and the processing algorithm is considerably simpler, but the resulting visualization of tissue oxygenation is the same. So, a color-coded bitmap image that appears nearly identical to one generated by the Spectral Sweep method can be generated by the 3 Shot method much more quickly.

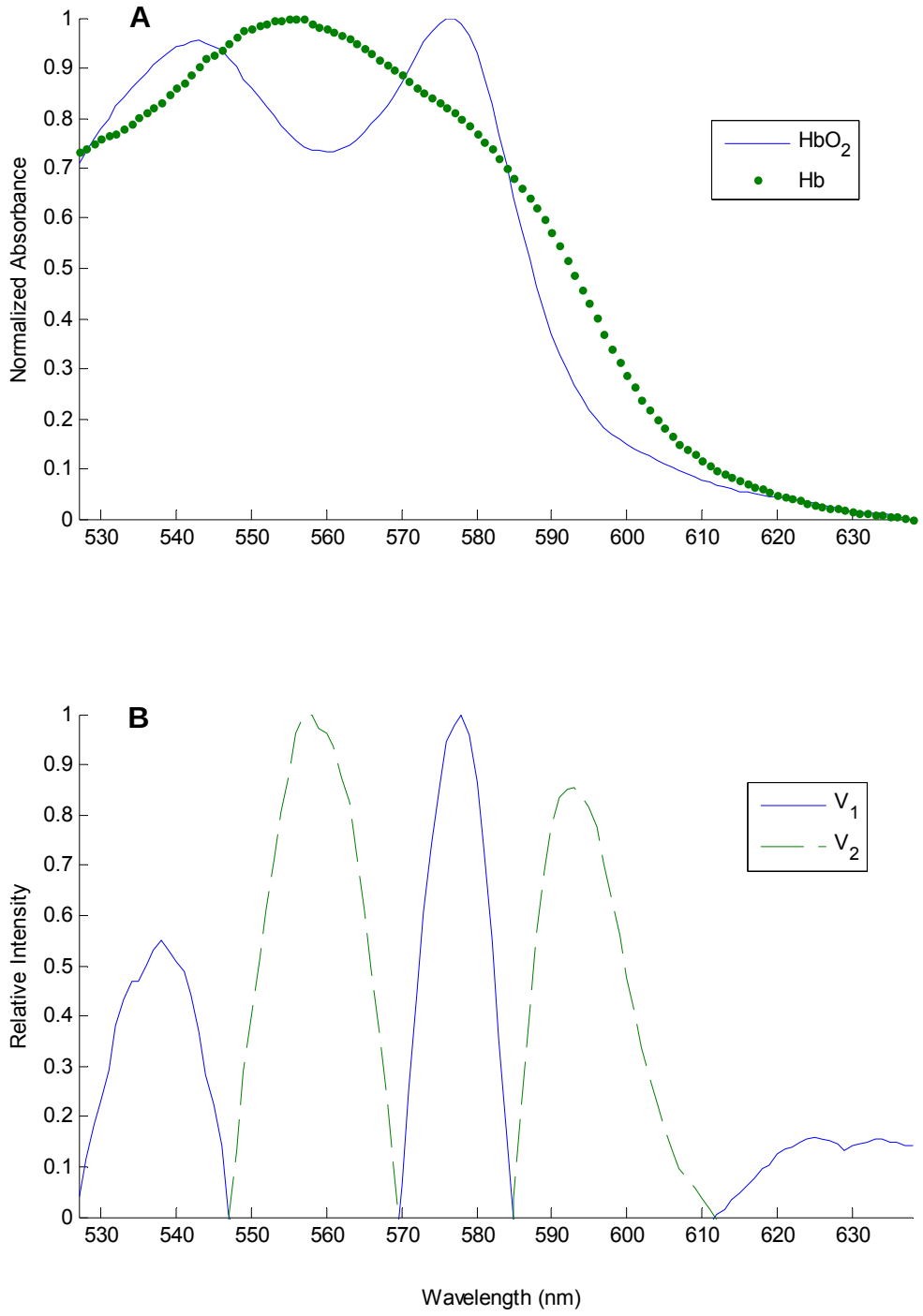

Figure 5.1 (a) Normalized absorbtion spectra of HbO_2 and Hb used as references for multivariate deconvolution of Spectral Sweep absorbance cubes. (b) Positive and negative subtraction of spectra in (a) used for 3 Shot illumination.

CHAPTER 6

SYSTEM CALIBRATION AND OPTIMIZATION

The DLP Hyperspectral Imaging system (DLP HSI) prototype, like all prototypes, requires calibration and optimization before relevant clinical and surgical data can be obtained. This chapter describes preliminary optimization of operating conditions for the system and calibration of the system as a spectrophotometer with standardized color tiles.

6.1 Optimizing Operating Conditions

6.1.1 Flattening Spectral Sweep

Because of the non-uniform spectral emission of the OL 490 Xe lamp and the non-uniform spectral response of the CCD detector, when bandpasses of 100% intensity are swept through a wavelength range from the OL 490, the HQ2 detects each one at a different digital value. This means that within a single hyperspectral cube, the images captured at some wavelengths will be brighter than those captured at other wavelengths. As seen below in the color tile calibration, a spectrally non-uniform response may result in lower quality spectroscopy. Spectral non-uniformity is a known issue in hyperspectral imaging and has been corrected for previously by comparing sample cubes to a reference cube that mimics the spectral response of the imaging system. This reference cube is the “background” cube that was discussed in section 4.3, and the previous correction was to calculate absorbance or reflectance with Beer’s law. However, the programmability of the DMD as a spectral filter allows for correction of the spectral non-uniformity by modulating the intensity of wavelengths that have higher intensities.

6.1.1.1 Modulating Intensities with the OL 490

The response of the detector to the light source when sweeping from 520 nm to 645 nm in 1 nm increments with a bandpass of 10 nm programmed with OL 490 AS is non-uniform

spectrally, and the center wavelength calibration is also offset. To create a calibrated bandpass sweep that is easy to modulate, a MATLAB script is written to automatically create 126 Gwectra files, each one commanding the intensity of four columns of mirrors about a calibrated center wavelength. For example to program a bandpass illumination at 520 nm, the calibrated center wavelength is calculated by the 350 μm slit calibration curve in section 2.2.2.2 to be 519.74 nm. The corresponding Gwectra file, raw_520.gxt, sets the columns of mirrors with wavelength 519.05 nm, 519.44 nm, 519.84 nm, and 520.23 nm to a magnitude of 100, and all other columns to 0. To adjust the intensity of any bandpass, the magnitude of the four 'on' columns is multiplied by an adjustment factor.

In order to quantify the spectral non-uniformity, a plot of detector response versus wavelength is constructed with hyperspectral image cubes acquired with the calibrated Gwectra sweep illuminations. To create the plot, five hyperspectral cubes of the Spectralon 99.9% reflectance target is captured at a focal distance of 45 cm, f/4, gain 1, and 4 x 4 binning. For each image in the cube, the mean of 3,111 pixels from the center of the cube represents the detector's response to the bandpass with that center wavelength. To bring the maximum counts just under saturation, the exposure time is 6 ms. The raw response is shown in Figure 6.1. To quantify the spectral non-uniformity, the standard deviation through the spectral dimension is calculated (see Table 6.1).

From the response in Figure 6.1, an adjustment vector, B, to modulate the higher intensity wavelengths is calculated according to eq 6.1, where C is the average counts from the center of detector array.

$$\mathrm{B}_{\lambda_p} = \frac{\max(C) - C_{\lambda_p} + \min(C)}{\max(C)} \qquad \text{eq 6.1}$$

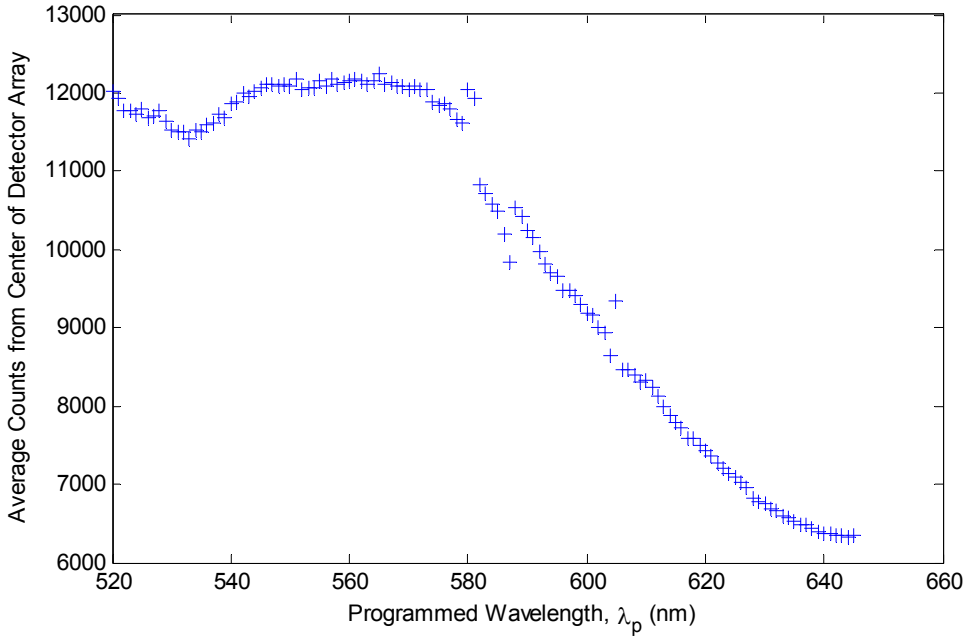

Figure 6.1 Spectral non-uniformity of light source and detector with calibrated bandpass sweep. For each bandpass, all of the mirrors in four columns are turned on.

Since the adjustment vector effectively lowers the illumination intensity at the wavelengths that are closest to saturation in the raw sweep, the exposure time can be increased when illuminating with the 1x adjusted Gwectra files. After one adjustment, the spectral non-uniformity is improved significantly, but a second adjustment vector is calculated from the response of the adjusted 1x Gwectra files to create a sweep of 2x adjusted Gwectra files. The algorithm is iterated a total of seven times, with the quantitative results in Table 6.1 and the qualitative results shown in Figure 6.2.

Table 6.1 Quantitative results of correcting spectral non-uniformity with light source modulation.

Number of Light Source Adjustments	Exposure Time per Image (ms)	Mean (counts per pixel per image)	Standard Deviation	% Deviation
0	6	10,011	2,153	21.51
1	8	9,765	814	8.34
2	10	10,400	245	2.36
3	12	11,675	133	1.14
4	13	12,215	91	0.74
5	13	11,904	61	0.51
6	13	11,878	56	0.47
7	13	11,502	56	0.49

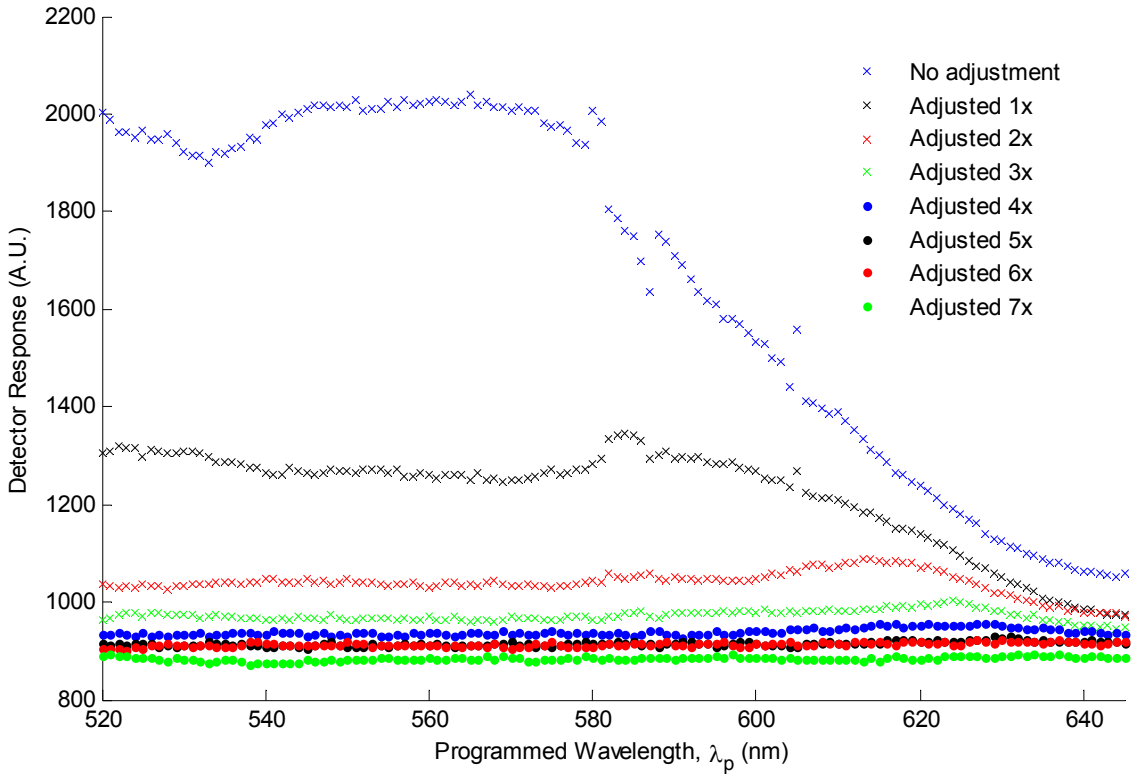

Figure 6.2 Detector response to calibrated and adjusted bandpass sweep illuminations of OL 490. The original values in each curve have been divided by the relative exposure time for a more accurate comparison.

The minimum percent deviation (0.47%) occurs after six adjustments, indicating that the 6x adjusted set of Gwectra bandpass files should be loaded as the configuration file for the "Spectral Sweep" method if the highest quality spectroscopy is desired. However, for a balance of speed and quality, the user may use the Gwectra sweep files with only three or four adjustments. It is important to remember that flattening is achieved by lowering the intensities of the brighter wavelengths, which means that the total amount of light is decreased with each adjustment. Another option for correcting the spectral non-uniformity is by adjusting the exposure time of each image in the hyperspectral cube. This may be a less desirable option since the minimum resolution for exposure time in the HQ2 is 210 μs, which means that overall higher exposure times with a smaller lens aperture may be required for adequate spectral flattening.

6.1.1.2 Modulating Intensities with the HQ2

To test the effectiveness of varying exposure time by bandpass, the detector response in Figure 6.1 is inverted and multiplied by the previous 6 ms exposure time and the maximum number of counts desired, 12,000, resulting in a vector of adjusted exposure times averaging 7.592 ms (see eq 6.2).

$$\mathrm{E}_{\lambda_p,f} = \frac{12000 \cdot \mathrm{E}_{\lambda_p,i}}{C_{\lambda_p}} \qquad \text{eq 6.2}$$

Illuminating with the raw Gwectra sweep files at 100% intensity and varying the detector exposure time results in percent deviation of 1.21%, better than two iterations of light source adjustment. Eq 6.2 is applied to the vector of variable exposure times from the first adjustment to get a second adjusted list of exposure times. The results from both adjustments are shown in Table 6.2. Since the second adjustment barely reduces the percent deviation, the aperture of the lens is constricted to cut off the incoming light, and the list of variable exposure times is multiplied by a correction factor to maintain the level of digital counts near 12,000 without saturating.

Table 6.2 Quantitative results of varying exposure time to correct for spectral non-uniformity

Number of Exposure Time Adjustments	Exposure Time per Image (ms)	Mean (counts per pixel per image)	Std Dev	% Deviation
0	6.000	10,011	2,153	21.51
1	7.592	11,694	141	1.21
2	7.808	11,807	123	1.04
1*	13.666	10,410	96	0.92
2*	14.054	10,701	105	0.98

*Aperture reduced to f/5.6 and exposure time correction factor of 1.80

Reducing the lens aperture to f/5.6 and multiplying all exposure times by 1.80 has little effect of the spectral non-uniformity according to its influence on the percent deviation metric. Also, since the minimum percent deviation in Table 6.1 is lower than the minimum percent deviation in Table 6.2, it appears that modulating light intensity with the mirrors is more effective for flattening the non-uniform spectral response of the detector. However, varying the exposure time by slice in hyperspectral acquisition is more efficient since the percent deviation can be

drastically reduced without greatly increasing the exposure time per image. Since both methods reduce the non-uniformity in the spectral domain somewhat, perhaps a combination of mirror adjustment and variable exposure may be best for flattening detector response.

6.1.2 Adjusting 3 shot illumination spectra

Three complex broadband illumination spectra were derived from the reference absorbance spectra of Hb and HbO_2 for the 3 Shot method described in section 5.3. Initially the OL 490 was programmed to illuminate with these spectra by directly copying the spectra into Gwectra files. The optical output measured by a spectrometer when these spectra were explicitly programmed is seen in Figure 6.3(a). Explicitly using the calculated spectra, the measured optical output was significantly different than the desired illumination. In the plot, the solid line is shifted horizontally from the dotted line, and the measured first peak is not as intense as the desired first peak.

In order to generate an illumination spectrum that more closely matches the desired optical output, a new Gwectra file was written. In the new file, the intensities at each wavelength were shifted horizontally according to the center wavelength calibration curves mentioned earlier and vertically according to the error between the measured and desired intensities. Programming the OL 490 with the new Gwectra file, the optical output is seen in Figure 6.3(b). In the plot, the solid and dashed lines coincide much better than in the previous plot.

Reprogramming the mirrors of the DMD in the OL 490 allows for refinement of illumination spectra for the 3 Shot method. The same wavelength calibration and intensity adjustment was performed for the other two complex broadband illuminations. For most of the wavelength range, the actual optical output matches well with the desired optical output. Due to the minimum bandpass limitation when using the 350 μm slit, it is fundamentally impossible to mimic the two bumps desired between 620 nm and 640 nm. If lower overall light intensity is adequate, the 150 μm slit, which has a smaller minimum bandpass limitation, could be used to further refine the actual optical output.

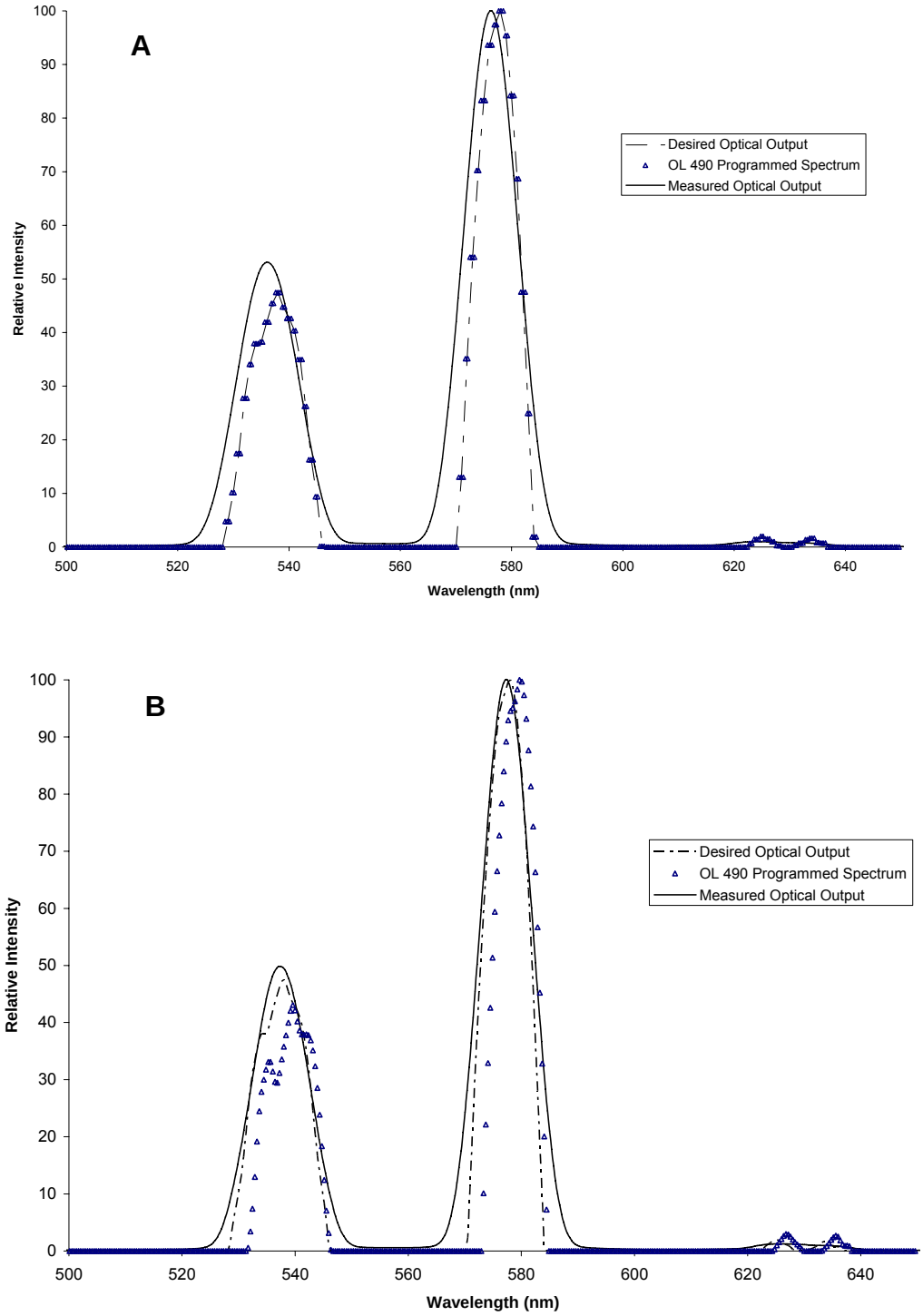

Figure 6.3 Comparison of optical output measured by a spectrometer and desired optical output for first illumination spectrum of 3 Shot method before, (a), and after, (b), applying center wavelength calibration and intensity adjustment.

6.2 System speed

Speed is a key requirement in the DLP Hyperspectral Imaging system design. Camera selection was based primarily on speed, the purpose the 3 Shot method is speed, and one of the main reasons hyperspectral imaging is not a primetime medical imaging modality is its inherent lack of speed. The current DLP HSI prototype is purposefully versatile. The user can adjust exposure times (constant or variable), binning of the CCD array, processing algorithms for chemometric visualization, lens aperture, and OL 490 illumination methods. To address the need for speed, it is important to understand the role each of these parameters play in determining the final frame rate of the system.

Several fundamental bottlenecks limit the maximum speed of the DLP HSI. Minimum exposure time of the OL 490 is 80 μs, minimum exposure time of the HQ2 is 210 μs, maximum transfer rate of camera to computer 20 MHz, and image processing time is significant.

6.2.1 System speed tests

Theoretically, increasing exposure time in each slice will increase acquisition time for each image and increase total acquisition time for the hyperspectral cube. Practically, exposure time is varied to achieve near 12,000 counts at the maximum intensity when capturing a background cube, so exposure time is not considered an independent variable. Rather, exposure time depends on lens aperture, camera binning and gain, illumination intensity, and focal distance. Illumination intensity is dependent on illumination method and is fixed for either the “Spectral Sweep” or “3 shot” illuminations. Focal distance is variable and is adjusted depending on the physical constraints of the clinical or surgical setup. In surgery, the camera must be at least 1 m away from the subject and should be unobtrusive to the surgeon. On the lab bench, the camera is set to a focal distance of 45 cm. Camera gain can be varied according to CoolSNAP HQ2 specifications while the lens aperture can be varied from f/16 to f/1.4. The two parameters in concert affect the exposure time primarily, with side effects of focus range and detector noise. For the following speed tests, ‘high gain’ refers to a camera gain of 3 and a lens aperture of

f/1.4, while 'low gain' refers to a camera gain of 1 and a lens aperture of f/8. Camera binning affects both exposure time and spatial resolution. For the following speed tests, bins of 2 x 2 and 4 x 4 are set. In the clinic, 'low gain' and 4 x 4 binning is typically used to ensure good quality imaging at reasonable speeds.

A final parameter that does not affect exposure time but still affects the speed of the system is the processing algorithm. The most basic processing algorithm reads the hyperspectral image cube into MATLAB and outputs one of the raw images as a Windows bitmap file for display. For visualization of oxygenation, "Oxyz Jet" and "3shot Jet - *," where * can be any pair of thresholds, are the processing algorithms used. In each of the oxygenation algorithms, the hyperspectral image cube and background cube in the same parent directory are read into MATLAB for calculating absorbance. Chemometric analyses transform the absorbance cube into a chemically relevant image which is output as a bitmap for display.

To measure the effect of each parameter on the overall speed of the DLP HSI, the system is set to a focal distance of 45 cm with the Spectralon target filling the detector FOV, and a combination of parameters based on the 2x2x2x2 factorial analysis model presented above are programmed into the GUI. Temporary data cubes are acquired to set the exposure time that allows for a maximum response near 12,000 counts (see Table 6.3). Due to the illumination intensity of the 3 Shot illuminations the exposure time could not be adequately lowered to keep the detector from saturating under 'high gain' conditions.

Table 6.3 Exposure time (μs) required to get maximum response near 12,000 counts for the given combination of parameters.

		Spectral Sweep		3 shot	
		Raw	**Oxy**	**Raw**	**Oxy**
2 x 2	**Low Gain**	980	980	5750	5750
	High Gain	184000	184000	saturates	saturates
4 x 4	**Low Gain**	200	200	1250	1250
	High Gain	40000	40000	saturates	saturates

After the exposure times are determined, the system is set to acquire continuously for a period of 10 min. The number of output bitmaps created within that 10 min is counted, and the time to output one processed image for the set parameters is calculated by eq 6.3.

$$t = \frac{600}{\#bitmaps} \qquad \text{eq 6.3}$$

Table 6.4 shows the results of all 12 runs. As expected from casual observations, the fastest time to output one 3 Shot image visualizing oxygenation is near 1/3 sec, which means that under these conditions, the system is operating a nearly 3 frames per second (fps). Acquiring Spectral Sweep images with 2 x 2 binning causes an exception violation in the software because the resulting image cube is too large for MATLAB to process (696 x 520 x 126). Comparing Oxy to Raw, it appears that processing algorithm has an increased effect on speed when binning is reduced, but no differential effect on speed when gain is increased. From the Spectral Sweep results, it also appears that processing algorithm has a greater effect on speed than does gain level. These observations may be helpful in determining how to make image acquisition and processing most efficient with the DLP HSI.

Table 6.4 Time (sec) to output one processed image for the given combination of parameters.

		Spectral Sweep		**3 shot**	
		Raw	**Oxy**	**Raw**	**Oxy**
2 x 2	**Low Gain**	exception	exception	0.48	0.71
	High Gain	exception	exception	saturates	saturates
4 x 4	**Low Gain**	14.63	23.08	0.32	0.39
	High Gain	9.68	18.75	saturates	saturates

6.2.2 Timing Budget and Diagram

To further illustrate the timing of each process in the hyperspectral image acquisition sequence, the timing diagram in Figure 6.4 follows the flow of data from initializing acquisition to visualization of a processed bitmap. The closed loop describes acquisition of a single slice of a hyperspectral cube, thus the time required to complete that loop must be multiplied by the number of slices or illumination spectra in order to calculate acquisition time. By examining the time log of the GUI during acquisition, processing time for each algorithm is deduced. This processing time is subtracted from the output time in Table 6.4 for 4 x 4 binning and low gain for 3 Shot (high gain for Spectral Sweep) to determine the total acquisition time. Dividing the total acquisition time by the number of slices equals the time to complete one cycle of the closed

loop. For Spectral Sweep, the acquisition time is 116 ms/slice, and for 3 Shot, the acquisition time is 93 ms/slice. This difference, 23 ms/slice, is less than the difference in exposure time for the two methods, 38.75 ms/slice, indicating that initialization of the camera or light source plays a large factor in acquisition time.

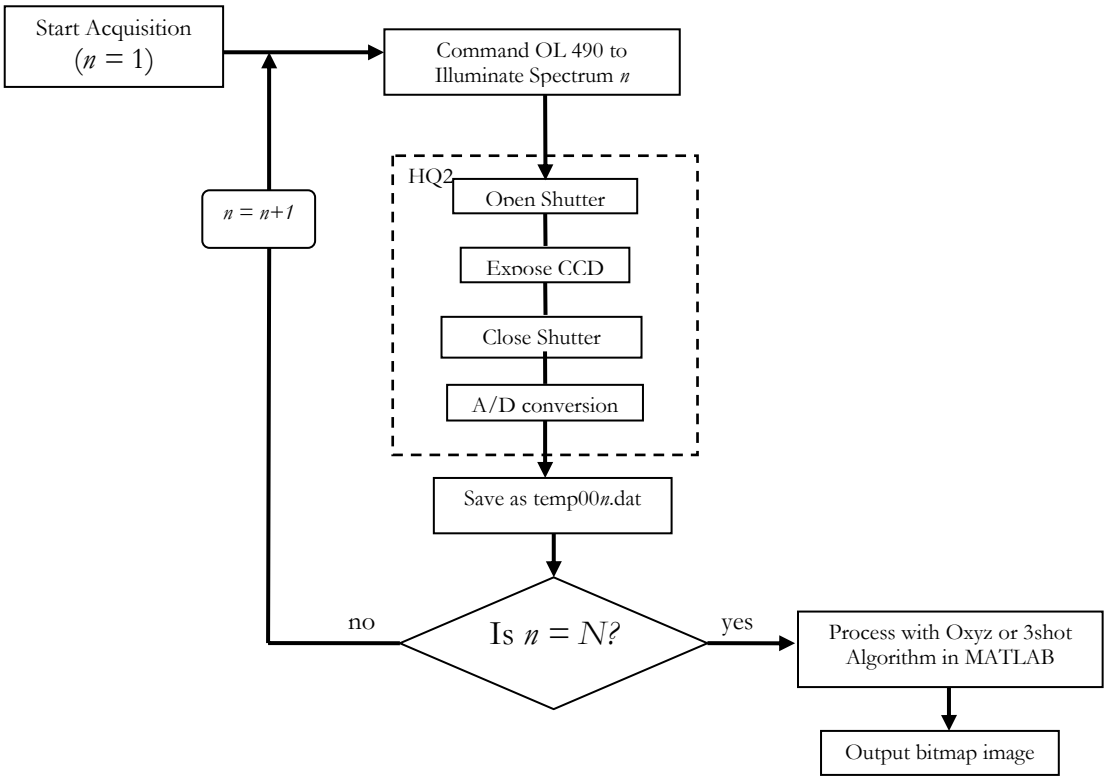

Figure 6.4 Timing diagram of hyperspectral acquisition where N is the total number of slices to be acquired. For Spectral Sweep, N = 126, and for 3 Shot, N = 3.

6.3 Color Tile Tests

The DLP Hyperspectral Imager is calibrated as a spectrophotometer by capturing hyperspectral images of four standard National Institute of Standards and Technology (NIST) color tiles with known reflectance spectra (see Figure 6.5). The system is programmed to perform a Full Spectral Sweep (see section 5.1), and the standard imaging procedure is followed (see section 4.3) with the color tiles in the camera FOV. Five consecutive image cubes of the color tiles are acquired and averaged to calculate reflectance spectra for each tile.

Reflectance is the inverse of absorbance, which can be calculated as described in section 4.4. The wavelength axis of each spatial pixel in the image reflectance cube corresponds to the reflectance spectra for that spatial point. Averaging 225 of these pixel spectra from the middle of each color tile effectively reduces error and gives a good measure of each color tile's reflectance spectrum. The average reflectance spectrum measured by the system for each color tile is compared to its corresponding standard spectrum by calculating the root mean square error (RMSE)[22] between the two spectra using eq 6.4, where R_{DLP} and R_{NIST} are the reflectance measured by the DLP Hyperspectral Imager and NIST, respectively.

$$RMSE = \sqrt{\frac{\sum_{n=1}^{51}(R_{DLP}(\lambda_n) - R_{NIST}(\lambda_n))^2}{51}} \qquad \text{eq 6.4}$$

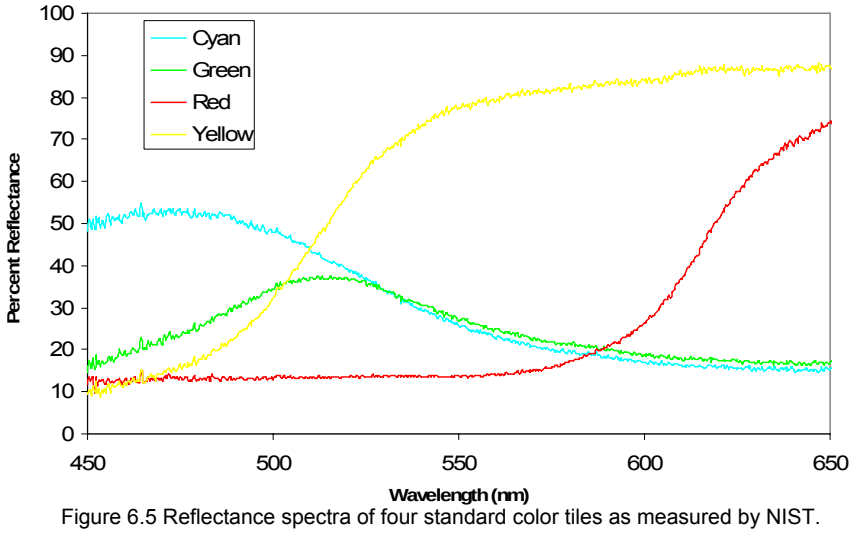

Figure 6.5 Reflectance spectra of four standard color tiles as measured by NIST.

Qualitative results of color tile imaging with Full Spectral Sweep are shown in Figure 6.6. In the sample reflectance image captured at 580 nm, it is evident that tile 2 reflects more light than the other three color tiles at that wavelength because the pixels are more intense (whiter). Cross-referencing the standard reflectance spectra with regards to the single image, it appears that tile 2 must be the yellow tile, because it is the only one of the four tiles that highly reflects 580 nm light. However, the single bandpass image is inadequate for distinguishing between the

other three color tiles, demonstrating the necessity of measured reflectance spectra in Figure 6.6(b). Comparing the DLP-measured spectra in Figure 6.6(b) to the NIST-measured spectra in Figure 6.5, it is evident that tile 1 is Cyan, tile 2 is Yellow, tile 3 is Red, and tile 4 is Green.

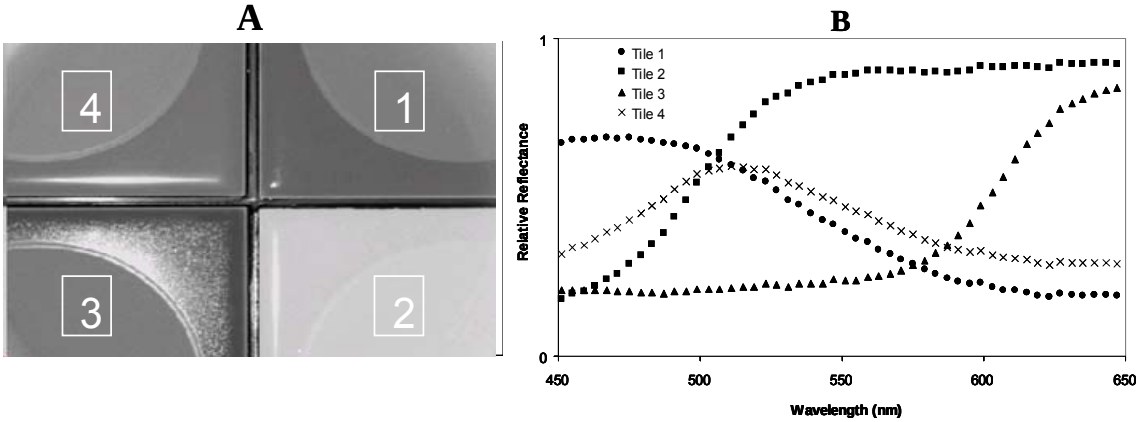

Figure 6.6 Reflectance image in (a) is captured at 580nm. The white boxes outline the 225 pixel areas from which spectra were sampled, averaged and plotted in (b).

Quantitative results of the RMSE analysis are shown in the solid bars of Figure 6.7. Since the RMSE is only useful as a relative metric, the absolute value for each color tile is meaningless. Comparing the RMSE amongst color tiles illustrates that the DLP Hyperspectral Imaging system more accurately measures the reflectance of the red and yellow tiles than the cyan and green tiles. This may indicate that the system is more suited for identifying objects that better reflect longer wavelengths.

Ideally, the RMSE between DLP-measured and NIST-measured spectra should approach zero to prove that the new imaging system is a calibrated spectrophotometer. In an attempt to reduce the RMSE for each color tile, the Full Spectral Sweep is adjusted to remove wavelength dependence of illumination intensity. Background hyperspectral image cubes acquired with the raw Full Spectral Sweep illumination scheme and constant camera exposure time indicate a detector response that is lower at the extremes and higher in the middle of the wavelength range (see Figure 6.8).

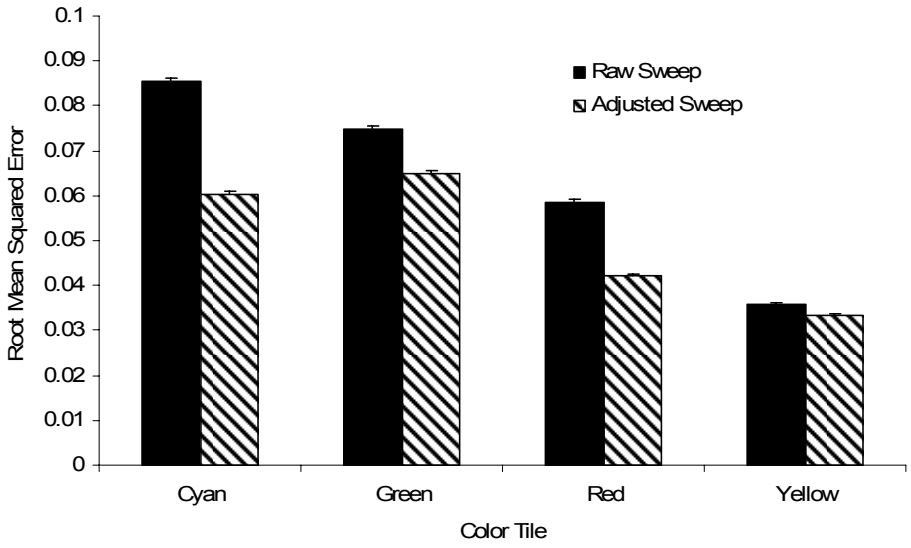

Figure 6.7 Root mean square error (RMSE) between DLP-measured reflectance spectrum and NIST-measured reflectance spectrum for each of the color tiles.

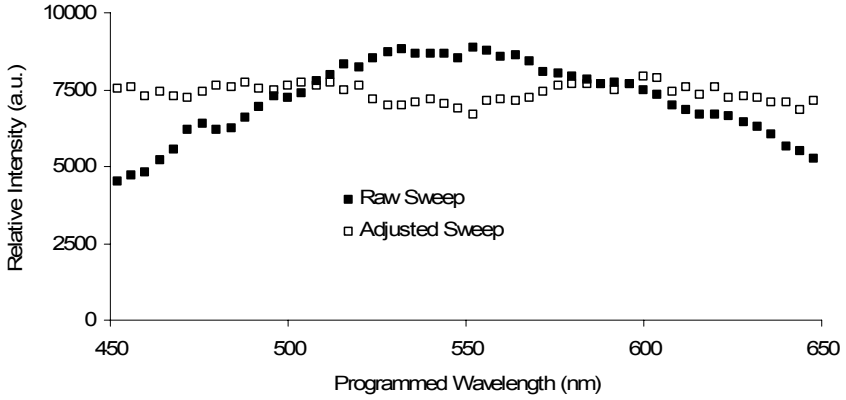

Figure 6.8 Bandpass illumination intensities measured from the Spectralon target during background capture for the raw Full Spectral Sweep and the adjusted Full Spectral Sweep.

By adjusting the intensity of each bandpass in the illumination sequence, as well as varying the exposure time, the detector response for capturing a white background group is significantly flattened. Collecting a new set of hyperspectral image cubes with the adjusted Full Spectral Sweep illumination, the RMSE for each color tile is lowered (see striped bars in Figure 6.7).

CHAPTER 7

CLINICAL AND SURGICAL APPLICATIONS

This chapter verifies the DLP Hyperspectral Imaging system as a multipurpose medical imaging platform by describing the variety of medical situations in which the DLP HSI has already been applied. After characterizing and calibrating the DLP Hyperspectral Imaging system on the lab bench, the system is transported to the University of Texas Southwestern Medical Center (UTSW), the Veterans Affairs North Texas Health Care System (Dallas VA), and the University of Texas at Arlington Animal Care Facility (UTA AF) to collect chemically relevant images of *in vivo* tissue in human and animal subjects. Images of a finger occlusion prove the principle of visualizing tissue oxygenation with the DLP HSI system, images of partial nephrectomies validate the surgical relevance of the system, and clinical images of human feet, rabbit brains, and mouse retinas help understand neuropathy, brain cancer, and diabetic retinopathy.

7.1 Occluded finger proof-of-principle

Tying a rubber band as a tourniquet around the base of a human subject's index finger effectively occludes the blood flow to that finger without directly affecting blood flow in other fingers. Occluding arterial blood flow inhibits fresh oxygenated blood from entering the finger which causes the tissue to become ischemic, so the percent HbO_2 in the finger should decrease while the rubber band is tied around the base of the finger. When the rubber band is removed from the finger, autoregulation forces a transient increase in blood flow to the finger known as reactive hyperemia.[23] In a period of reactive hyperemia the percent HbO_2 in the finger should increase to levels higher than normal. The purpose of this highly controlled proof-of-principle experiment is to visualize ischemia and reactive hyperemia with the prototype DLP Hyperspectral Imaging system.

7.1.1 Methods

To visualize the ischemia induced by occluding blood flow to a finger and the ensuing reactive hyperemia upon removal of the occlusion, a subject's hand is imaged with the DLP HSI in Spectral Sweep and 3 Shot modes. The system is warmed up, focused at a distance of 18 cm, and set to capture a background cube according to the imaging procedure in section 4.3. The subject's hand is placed palm up in the FOV of the camera so that three fingers and part of the palm can be imaged. 'Control' hyperspectral image cubes – five Spectral Sweep and five 3 Shot - are acquired of the non-occluded fingers. Each Spectral Sweep cube is analyzed with 'Oxyz Jet' and each 3 Shot cube is analyzed with '3 shot jet (mid)17' processing algorithm, resulting in five output bitmap images color-coded for percent HbO_2 for each illumination method. After acquiring 'Control' images, a rubber band is wrapped three times around the base of the subject's middle finger and five 'Occluded' hyperspectral image cubes for each method are acquired and processed in the same way as the 'Control' images.

To visualize the real-time progression of reactive hyperemia after removal of the occlusion, 3 Shot images are acquired and processed continuously after acquiring the 'Occluded' images. While the system continues outputting 3 Shot images color-coded for percent HbO_2, the rubber band is cut with a pair of scissors. After a period of three minutes, the system is switched to Spectral Sweep mode to collect five 'Reperfusion' hyperspectral image cubes.

The Spectral Sweep hyperspectral images are averaged for each time point in the experiment (n = 5, for 'Control', 'Occluded', and 'Reperfusion'). The 3 Shot output bitmaps are averaged for 'Control' and 'Occluded' time points (n = 5), and the mean pixel value for a constant 49 pixel area represents percent HbO_2 at each time point. For the real-time progression of reactive hyperemia, the mean pixel value for the 49 pixel area is plotted versus time for several seconds prior to cutting the rubber band and 180 seconds immediately thereafter.

7.1.2 Results

Visual inspection of the processed Spectral Sweep images (see Figure 7.1) shows that the DLP Hyperspectral Imaging system can differentiate between oxygenated and deoxygenated tissue. In Figure 7.1(a), all three fingers are colored shades of red, orange, and yellow, which correspond to a percent HbO_2 between 60 and 80%, as indicated on the colorbar at the right. As expected under 'Control' conditions, there is no difference in the surface oxygenation amongst the three fingers. In Figure 7.1(b), the middle finger is colored blue-green, which corresponds to a percent HbO_2 between 40 and 50%, while the other two fingers appear the same as they did in the 'Control' image. As expected under 'Occluded' conditions, the rubber band tourniquet inhibits blood flow to the finger and effectively de-oxygenates the tissue. In Figure 7.1(c), the middle finger is colored red-orange, corresponding to a percent HbO_2 higher than 75%. As expected under 'Reperfusion' conditions, the DLP HSI visualizes an overshoot in tissue oxygenation related to reactive hyperemia most likely caused by vascular autoregulation of the previously occluded finger.

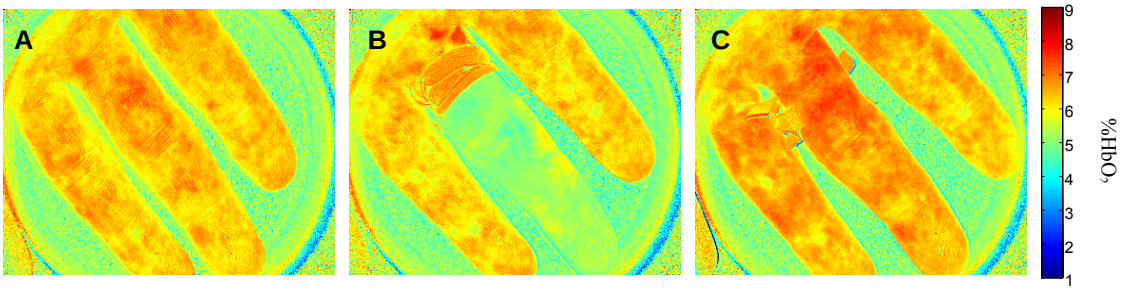

Figure 7.1 Average of five Spectral Sweep Oxyz output images captured (a) as 'Control', (b) while 'Occluded', and (c) for 'Reperfusion'.

To quantify this overshoot related to reactive hyperemia, inspection of the 3 Shot output images is necessary. In Figure 7.2(a), the processed 3 Shot output image under 'Occluded' conditions matches its counterpart Spectral Sweep image (Figure 7.1(b)). The non-occluded fingers appear redder than those in the Spectral Sweep image, indicating a higher percent HbO_2 than measured by the Spectral Sweep method. The two methods must be calibrated further to determine the truer method of measuring absolute oxygenation. Because of this

discrepancy in absolute measures, all results must be considered in relative terms rather than in absolute oxygen percentages.

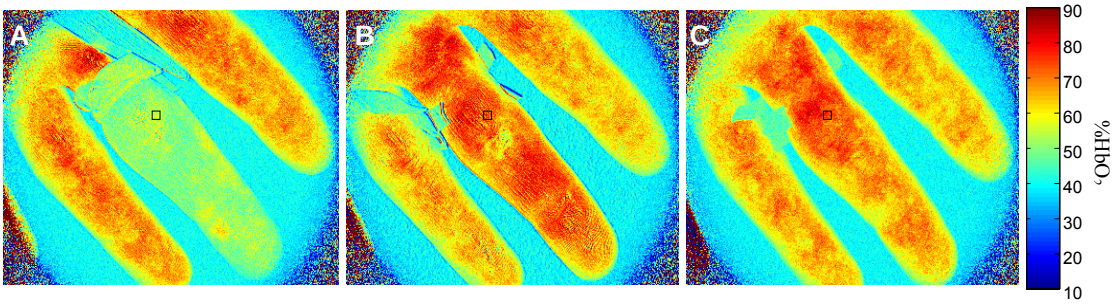

Figure 7.2 Color-coded 3 Shot output images captured (a) immediately before cutting the rubber band, (b) 10 seconds after cutting the rubber band, and (c) 2 minutes after cutting the rubber band. The black square in each image indicates the 49 pixel area sampled for averaging.

Inspecting the 3 Shot images immediately after the occlusion is removed and several minutes later (see Figure 7.2(b) and (c)), it appears that there is an immediate overshoot of percent HbO_2 in the previously occluded middle finger and a subsequent return to normal tissue oxygenation levels. This overshoot is quantified by calculating the mean of the pixel values in the black sample area of each image divided by the average 'Control' values for the same pixel area. With this calculation, the transient response of reactive hyperemia in the middle finger is examined. In Figure 7.3, the average percent HbO_2 relative to control for the black sample area is plotted for every 3 Shot output image acquired between occlusion and reperfusion. While occluded, the surface oxygenation is less than 70% of the control oxygenation, but in the first 10 seconds after removing the tourniquet the surface oxygenation raises to 112% of control.

Variability in consecutive images is apparent when viewing the output images in real-time and is also apparent in the wide vertical spread of the data points in Figure 7.3. This image to image variability is not entirely understood, but may be an artifact of the OL 490 output variability (see Section 2.2.1). Even with the variability, the overall trend of oxygenation appears to mimic an under-damped 2nd order system response. There is an initial overshoot, then undershoot after about 1.5 minutes, with percent HbO_2 eventually returning to the control level after longer than 3 minutes.

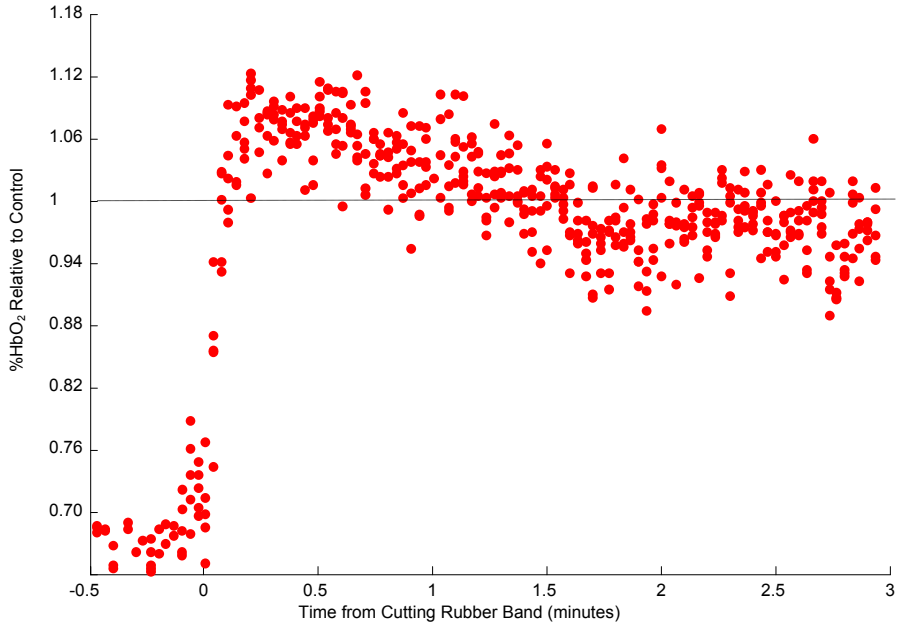

Figure 7.3 Real-time progression of reactive hyperemia after cutting rubber band from finger. Each point represents the average pixel value relative to control from the sampled area of a single output image.

7.1.3 Conclusions

The DLP HSI can be used to visualize ischemia and reactive hyperemia, as evidenced by the proof-of-principle finger occlusion test. Processed Spectral Sweep output images show high contrast between oxygenated and de-oxygenated tissue and indicate gross physiological changes. Processed 3 Shot output images show the same contrast between oxygenated and de-oxygenated tissue, but the two illumination and processing methods do not give identical absolute measurements of percent HbO_2.

Images acquired and processed by the 3 Shot method are generated at about 3 frames per second, while Spectral Sweep images are generated at about 3 frames per minute. Both are useful methods for visualizing the spatial distribution of surface tissue oxygenation, but the 3 Shot method is preferable when visualizing short duration physiological changes. Analyzing several minutes of continuous 3 Shot outputs shows reactive hyperemia of the surface tissue in a previously occluded middle finger.

7.2 Partial nephrectomies

Partial nephrectromy is a surgical procedure in which a section of a patient's kidney is removed, usually to eliminate a tumor. Sparing the remainder of the kidney often requires vascular occlusion in order to temporarily interrupt renal blood and prevent hemorrhage. Two methods of renal vascular occlusion: artery-only occlusion (AO) and artery and vein occlusion (AV), have demonstrated differential effects on renal tissue viability during 2 to 24 hour long periods of ischemia.[24] To understand the effects of competing clamping methods during shorter periods of ischemia, the DLP HSI is used to image the renal tissue oxygenation during partial nephrectomies in pigs and then humans for periods of ischemia less than one hour long.

7.2.1 Porcine Study

7.2.1.1 Methods

Following approval by the UTSW Institutional Animal Care and Use Committee (IACUC), four female Yorkshire pigs, weighing between 60-80 kg, underwent AO or AV occlusion of each kidney. At the beginning of the study, one kidney was used to perfect the investigational technique and, therefore, is not included in the analysis. In order to verify the images obtained by the prototype DLP HSI, hyperspectral image cubes are acquired by sweeping 126 contiguous bandpasses, identical to the Spectral Sweep illumination method, with an already characterized LCTF-based hyperspectral imaging system. The primary difference between the two systems is the method of filtering light. In the LCTF system broadband light is reflected from the tissue sample and then filtered by a liquid crystal tunable filter (LCTF) before being detected by a CoolSNAP HQ2 array detector. In the DLP system's Spectral Sweep method, narrowband light from the spectral light engine is reflected from the tissue sample and directly detected by a CoolSNAP HQ2 array detector. There is no LCTF equivalent to the DLP 3 Shot method.

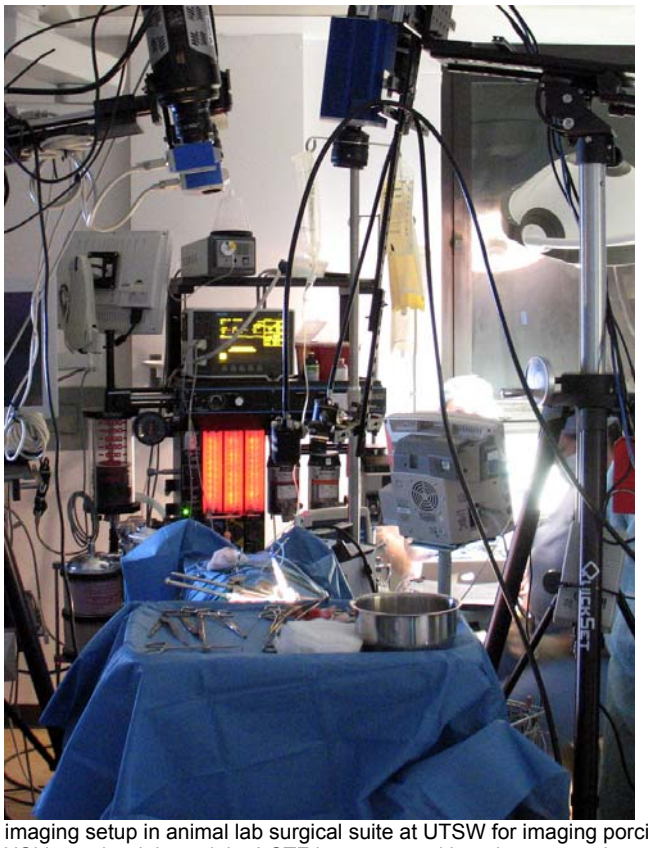

Figure 7.4 Hyperspectral imaging setup in animal lab surgical suite at UTSW for imaging porcine partial nephrectomy. The DLP HSI is on the right and the LCTF hyperspectral imaging system is on the left.

After anesthetizing each subject according to protocol, the surgeon approaches the right kidney through an open midline incision and pulls the peritoneum away from the visible surface of the kidney. While the surgeon exposes the kidney, background cubes for both illumination methods are acquired in a dark corner of the surgical suite. The DLP HSI tripod is then abutted to the surgical bedside (see Figure 7.4) and the friction head is adjusted so that the exposed kidney is fully visible in the camera's FOV. The wheels of the tripod dolly are locked in place so that all images are acquired from the same angle and distance. 'Control' hyperspectral image cubes are acquired and processed by Spectral Sweep and 3 Shot methods as in the finger occlusion test above. The surgeon then dissects the hilem and clamps either the artery only (AO) or the artery and the vein (AV) with a curved Satinsky clamp.

The renal vasculature remains occluded for one hour before removing the clamp. Spectral Sweep 'Occluded' image cubes are acquired and processed in approximately 5 minute intervals throughout the occlusion. 3 Shot image cubes are acquired and processed continuously during application of the clamp, several times during the hour of occlusion, and continuously during removal of the clamp. After one minute of reperfusion, Spectral Sweep 'Reperfusion' image cubes are acquired in 5 minute intervals for 30 minutes. Following ischemia and reperfusion of the right kidney, the identical procedure is carried out on the left kidney using the opposite clamping technique. During the procedure, the subject's rectal temperature is maintained between 37^{o}C and 39^{o}C and its serum oxygenation, as measured by a pulse oximeter on the animal's ear, is kept between 98% and 100%.

Percent HbO_2 is measured over a uniform 81 pixel area chosen from the center of each kidney at each time point during the study. An average of the pixels for each region is calculated along with a standard deviation for each image cube. Images from each 10 minute time frame during ischemia are grouped as a single dataset in order to determine differences between AV and AO clamping conditions at each of six time periods. A regression model is fit to the individual levels using SAS statistical software (SAS Institute, Cary, NC) in order to determine whether there is a statistically significant difference between clamping methods with regard to kidney tissue ischemia over a period of one hour.

Real-time progression of ischemia and reactive hyperemia is measured in a 225 pixel area for all of the 3 Shot output bitmaps acquired during tightening and removal of the Satinsky clamp in one pig subject. The mean pixel value in each image's sample area is plotted as a function of the time the output image was originally processed. This plot should show the transient behavior of the initial decline of percent HbO_2 after occlusion and the extent of reactive hyperemia after the occlusion is removed. It is unknown whether these immediate transient effects will be different between AV and AO clamping.

7.2.1.2 LCTF versus DLP Results

Comparing images acquired by the LCTF system and the DLP system at the same time during the surgery verifies the acuity of the DLP HSI for visualizing oxygenation. The final hyperspectral image cube acquired for one 'Occluded' kidney from each system is processed by the same Oxyz processing algorithm, and the resulting image color-coded for percent HbO_2 is displayed in Figure 7.5. There is no noticeable difference in the processed images generated by cubes from each system. Since the renal vasculature has been clamped for nearly one hour, the renal tissue absorbance spectrum is similar to that for Hb, exhibiting one absorbance peak at 560 nm.

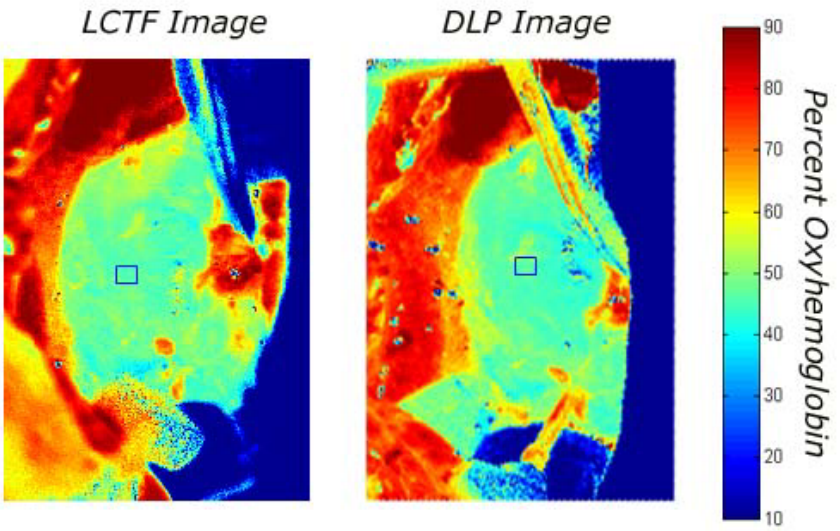

Figure 7.5 Comparison of LCTF image to DLP image for a single pig kidney clamped for approximately sixty minutes. Both hyperspectral data cubes are recorded with the same illumination method of 126 sequential frames at contiguous wavelengths, and processed with the same processing algorithm, producing nearly identical images. The images are color-coded to represent percentage of correlation to the HbO_2 reference spectrum. The boxed areas indicate the areas from which the spectra shown in Figure 7.6 are sampled.

In Figure 7.6, the average absorbance spectrum measured in the sample area for the DLP system's hyperspectral cube matches that of the LCTF system's cube. This close spectral matching between the two systems means that both systems measure the same spectroscopy from de-oxygenated tissue. However, a similar comparison was performed with 'Reperfusion' image cubes (see Figure 7.7). Each system's measured absorbance spectrum includes two

peaks like the HbO_2 reference spectrum, but the peaks from one system are slightly offset horizontally from the peaks from the other system, and the two DLP peaks have the same amplitude whereas the first LCTF peak is lower than the second LCTF peak.

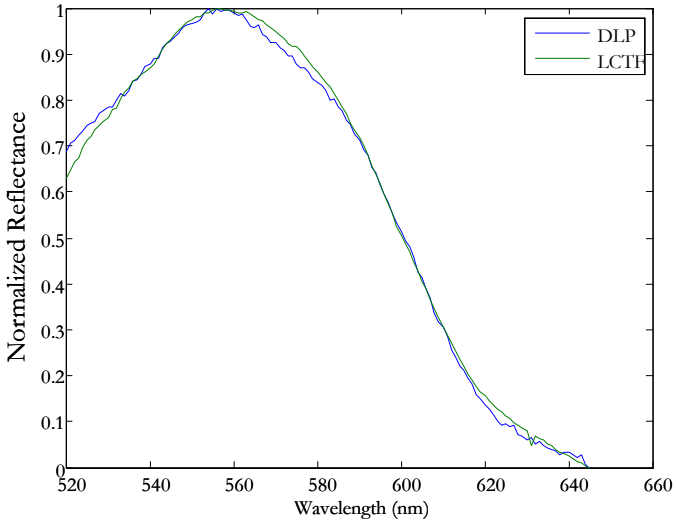

Figure 7.6 Comparison of spectra taken from the center of the pig kidney images from Figure 7.5. The normalized reflectance spectra from the LCTF and DLP systems are nearly identical (RMSE = 0.0180).

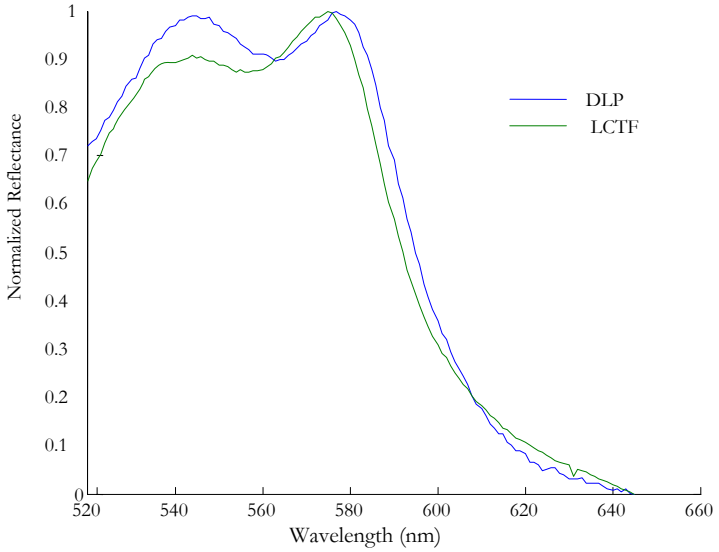

Figure 7.7 Comparison of spectra taken from the center of the pig kidney images from 'Reperfusion' images. The normalized reflectance spectra from the LCTF and DLP systems both indicate high percent HbO2 but they are not identical (RMSE = 0.0553).

Overall, the comparison of spectra measured by the two systems indicates that both systems are adequate for differentiating between Hb and HbO_2 spectra. However, before

measuring complex absorbance spectra both systems should be calibrated to some standard complex reflectance material.

7.2.1.3 Spectral Sweep Results

Spectral Sweep images acquired by the DLP HSI allow the surgeon to visualize slow changes in tissue chemistry, so one representative image color-coded for percent HbO_2 is sufficient to the show gross effects of vascular occlusion to the kidney. In Figure 7.8, spatial maps of the surface tissue oxygenation at 'Control', 'Occluded', and 'Reperfusion' time points show that each kidney overall has a lower percent HbO_2 during AV clamping. This is indicated by the kidneys in (b), (e), (h), and (k) appearing almost uniformly blue green, corresponding to a percent HbO_2 between 40% and 50%. The 'Control' kidneys in (a), (d), (g), and (j) appear nearly uniformly orange, corresponding to a percent HbO_2 of between 66% and 74%. Even after the renal artery and vein was clamped for 60 minutes, once the clamp is removed, the entire kidney appears to recover to a higher percent HbO_2 than before the occlusion. The 'Reperfusion' kidneys in (c), (f), (i), and (l) appear orange-red, corresponding to a percent HbO_2 of between 75% and 83%. 'Reperfusion' images in the figure are the processed Spectral Sweep output images for the hyperspectral data cubes captured one minute after the clamp was removed.

Similarly, kidneys undergoing AO clamping show gross visual changes as seen in the sample images in Figure 7.9. In all of the images, a black box surrounds the 81 pixel area selected as a sample by which to calculate the mean percent HbO_2 for each kidney. This sample value sufficiently predicts the overall oxygenation of the kidney, but the advantage of visualizing a 2D spatial image instead of just a point measurement of oxygenation is to see the spatial profile of tissue oxygenation. In all of the images this is important because it helps distinguish between the kidney, which changes color when occluded, and the surround adipose and muscle tissue, which is a constant red-orange in all three sample images for each kidney.

Since the FOV includes areas surrounding the kidney, some images contain a reflection of the kidney off of the metallic instruments used to hold the cavity open during surgery. Seeing the spatial distribution of oxygenation is even more important in Pig 3 AV, where the lower pole of the kidney is removed between capturing Figure 7.8(h) and Figure 7.8(i). After the surgeon cuts off the lower pole and stitches closed the open end of the kidney, hyperspectral imaging shows that the lower edge is colored dark red indicating very high percent HbO_2.

Subsequent 'Reperfusion' images show oscillations of the percent HbO_2 during each kidney's reperfusion. To better quantify these oscillations and understand the first 30 minutes of reperfusion, the mean of the 81 pixel area of interest for each 'Reperfusion' image is divided by the mean of the 'Control' image for that kidney to determine the percent HbO_2 relative to control. All of the data for AV kidneys is grouped into one dataset (n = 24) and all of the data for AO kidneys is grouped into a second dataset (n = 18). The first image cube is acquired at different times after the clamp is removed in each pig, but the interval between acquisitions is about 5 minutes for all pigs. Since the time points between subjects do not align, the datasets are considered separate XY datasets with the x-variable being acquisition time and the y-variable being percent HbO_2 relative to control. For each dataset, a third-order fit is applied in MATLAB, and the plot with residuals is seen in Figure 7.10. The residuals for both datasets in the first 20 minutes are small, indicating that all kidneys within each dataset exhibited similar reactive hyperemia to the line of fit through that time period. Since the residuals of the AO dataset overlap those of the AV dataset, there is no statistical difference between AO and AV with regard to the 30 minute progression of reperfusion. The most important conclusion from this plot is that in all cases, there is an initial overshoot of percent HbO_2 relative to control measurements followed by decline and some sort of oscillation.

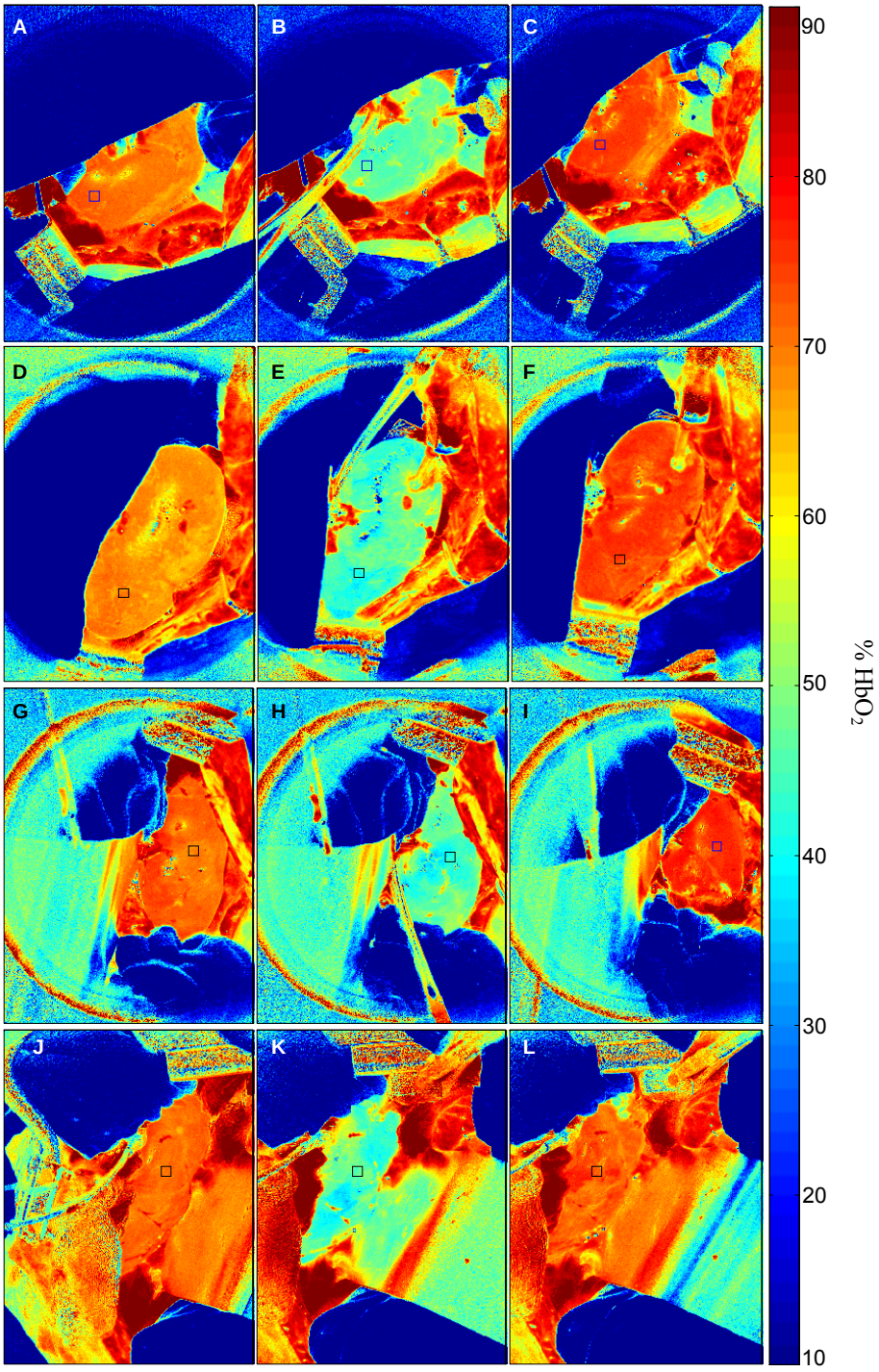

Figure 7.8 Processed Spectral Sweep images of kidneys undergoing AV clamping. Pig 1 (a) control, (b) occluded, (c) reperfusion. Pig 2 (d) control, (e) occluded, (f) reperfusion. Pig 3 (g) control, (h) occluded, (i) reperfusion. Pig 4 (j) control, (k) occluded, (l) reperfusion.

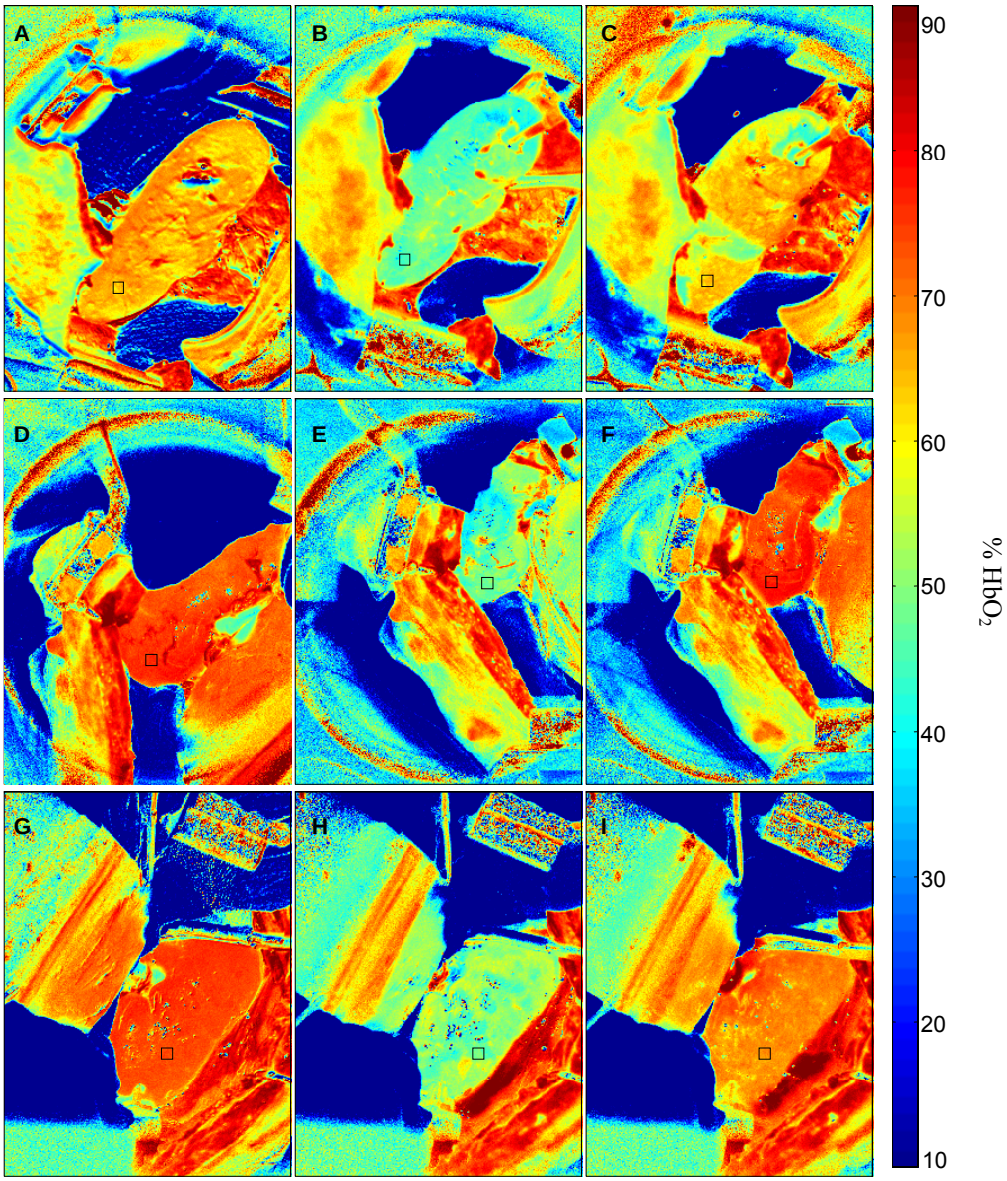

Figure 7.9 Processed Spectral Sweep images of kidneys undergoing AO clamping. Pig 2 (a) control, (b) occluded, (c) reperfusion. Pig 3 (d) control, (e) occluded, (f) reperfusion. Pig 4 (g) control, (h) occluded, (i) reperfusion.

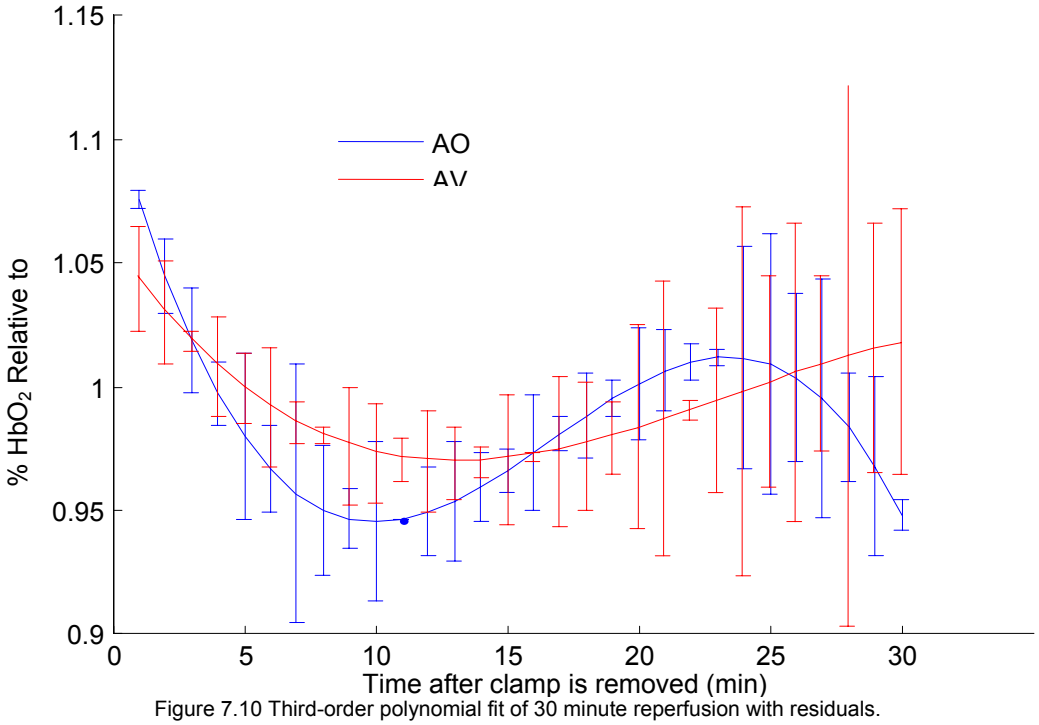

Figure 7.10 Third-order polynomial fit of 30 minute reperfusion with residuals.

Even though there is no noticeable difference in kidney reperfusion between clamping methods, a difference in the percent HbO_2 of occluded kidneys with different clamping methods can be seen from analysis of all Spectral Sweep 'Occlusion' images. All color-coded images captured within each 10 minute period for each clamping method are grouped into a single XY dataset where the x-value is the time duration of the occlusion when the image is captured and the y-value is the average percent HbO_2 from the 81 pixel sample area in the image. Figure 7.11 is a plot of the means and standard errors for each time period and clamping method. A regression model is fit to test the significance of the difference between AV and AO in each time period. The output of the regression model is a p-value indicating the probability that the two sets of sample data are from the same population. If the value of p equals 0.05, there is a 5% probability that the two datasets are the same. For zero to 10 minutes, 40 to 50 minutes, and 50 to 60 minutes, there is no difference in kidney surface tissue HbO_2 percentage between AV and AO clamping ($p>0.2$). For 10 to 20 minutes and 30 to 40 minutes there is a statistically significant difference between AV and AO clamping ($p<0.05$). For 20 to 30 minutes, it appears

that there is a difference between AV and AO (p=0.06), but more sample data showing the same difference is required in order to prove a significant difference. Overall, kidneys with the artery only clamped show higher percent HbO_2 than kidneys with the artery and vein clamped. This difference is statistically significant in two of the six time periods, but percent HbO_2 only varies by a maximum of 3 percentage points which implies that the benefits of lowered ischemia from AO clamping may not outweigh the extra loss of blood unmitigated by not clamping both the artery and vein.

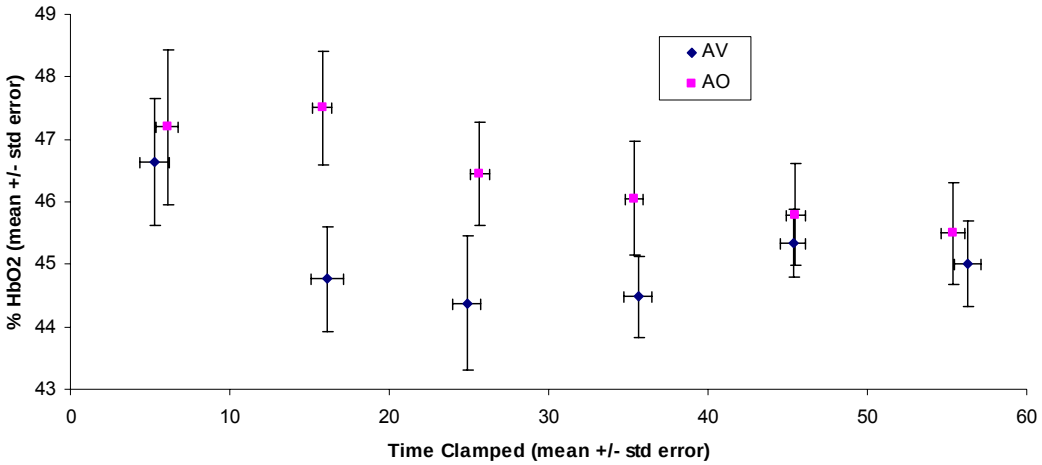

Figure 7.11 Comparison of clamping methods during one hour of occlusion.

Results of the porcine kidney study have thus far only been from the Spectral Sweep method of hyperspectral imaging. These image results are useful because they can be compared to other hyperspectral imaging system results, and it is possible to re-analyze the hyperspectral cubes with regard to other chromophores besides HbO_2 and Hb. The Spectral Sweep images are high quality and show changes in oxygenation over long periods of time. In order to visualize the spatial distribution of oxygenation with finer time resolution, however, the 3 Shot images must be analyzed.

7.2.1.4 3 Shot Results

In the porcine kidney studies, 3 Shot images appear similar to Spectral Sweep images (see Figure 7.12). Comparing (c) and (d) to (e) to (f), the relative tissue oxygenation is the same for both illumination methods. It is obvious that between 'Control' and 'Occluded' states there is a drop in surface oxygenation for the renal unit, but the surrounding muscle and adipose tissue remains highly oxygenated. The major difference between Spectral Sweep and 3 Shot processed images is the threshold vector by which the final image is mapped to percent HbO_2. For the Spectral Sweep method, the spectral information stored in the 126 slice data cube allows a wider range of values, so the background is truly blue, representing virtually no oxygenation. For the 3 Shot method, the range of pixel values in a processed image is much less than that for a Spectral Sweep image, so a tighter threshold must be applied to visualize the same contrast. This tighter threshold causes the mapped percent HbO_2 values to be slightly different than those mapped in the Spectral Sweep images, so the detectable range and resolution of percent HbO_2 may be less with the 3 Shot method than with the Spectral Sweep method.

The overall trend of pixel intensities in 3 Shot output images is identical to the trend of Spectral Sweep images and matches the expected oxygenation trend. Therefore, 3 Shot output images are sufficient for mapping the spatial distribution of tissue oxygenation over time. For the first three pig subjects, continuous acquisition of 3 Shot images during application and removal of the Satinsky clamp is not performed because the primary concern is capturing quality images to test hour long effects of clamping. Before imaging the fourth pig subject, data from the other subjects indicated that a majority of tissue chemistry changes occur during the first minute after clamping and during the first few minutes after removing the clamp. So, for the fourth pig subject, continuous 3 Shot images are acquired during both critical time periods for each kidney.

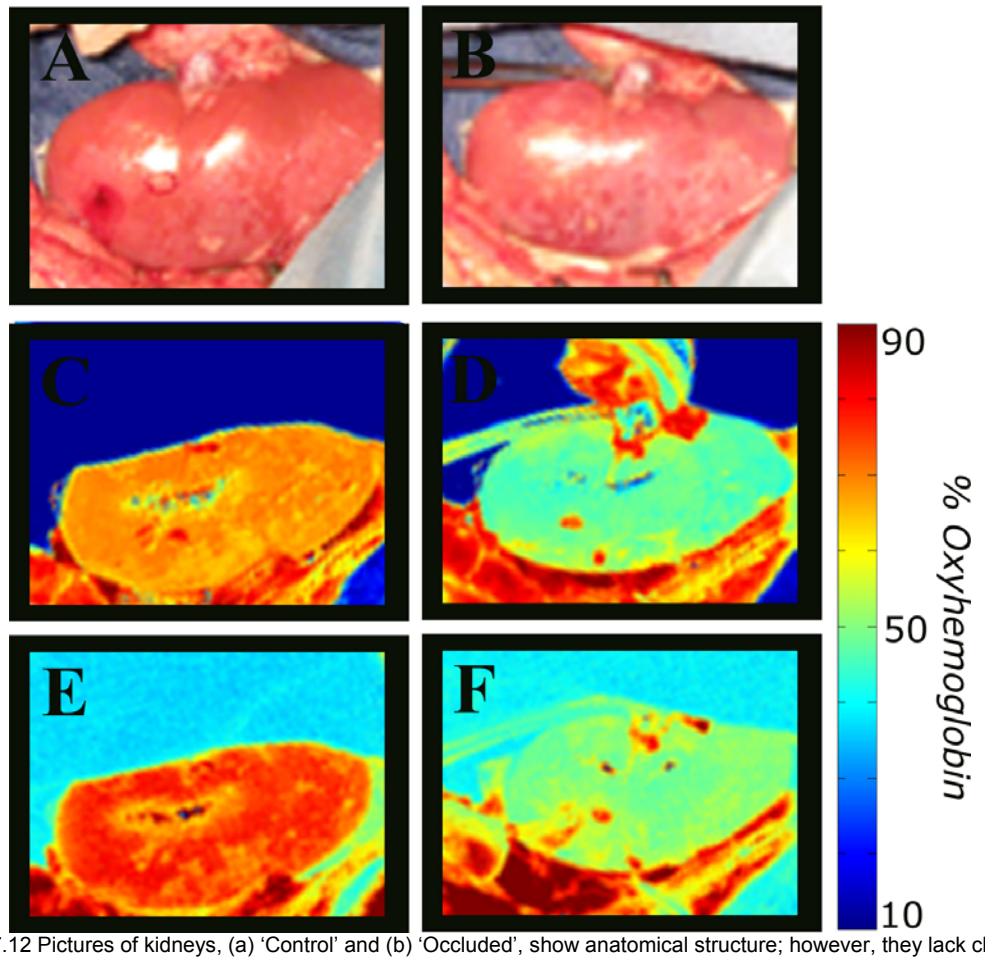

Figure 7.12 Pictures of kidneys, (a) 'Control' and (b) 'Occluded', show anatomical structure; however, they lack chemical information useful for differentiating between normal and ischemic tissue. Spectral Sweep images, (c) 'Control' and (d) 'Occluded', are clear and give values of oxygenation using a supervised multivariate least squares analysis. 3-Shot images, (e) 'Control' and (f) 'Occluded', use chemometrically derived, complex spectral illumination and are quick to acquire, easy to process, and show relative values of oxygenation.

A 225 pixel area from the center of the kidney is averaged in each image and divided by the average of the same area for the first 20 control images to result in the percent HbO_2 relative to control. In Figure 7.13, this value is plotted for the kidney clamped AO (n = 247) and for the kidney clamped AV (n = 217) for 12 seconds prior to tightening of the clamp and about one minute following application of the clamp. For the first 10 seconds of occlusion both methods of clamping result in a linear decline of oxygenation. The transient response then becomes non-linear, and flattens after 30 seconds in both cases. There is a zero-order time delay between the two responses, with the AO decline lagging behind the AV decline. This lag may be due to the flow of blood through the renal vein, which would not occur under AV

clamping. There is also a steady-state difference between the oxygenation levels, with AO being higher than AV, which corroborates the results shown in Figure 7.11.

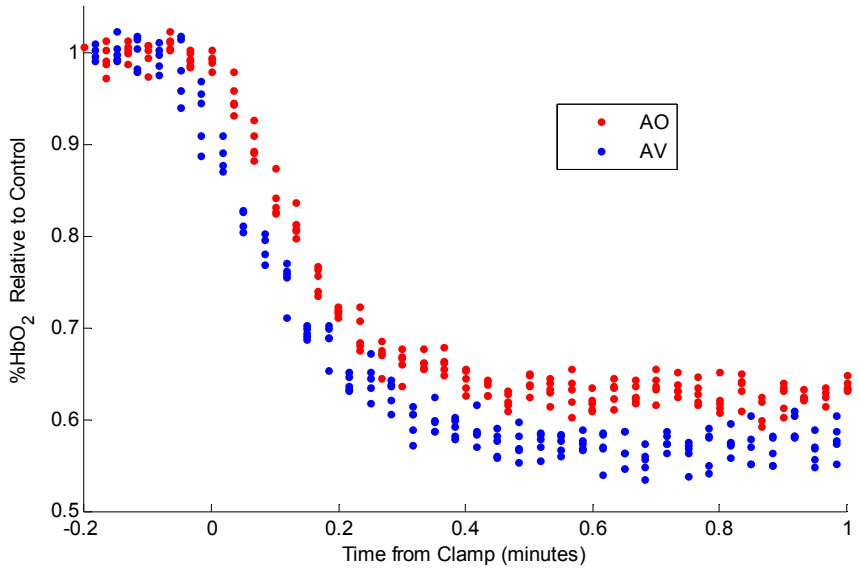

Figure 7.13 Monitoring the time progression percentage of oxyhemoglobin perfusing the kidney before and during renal AO and AV occlusion. Each point represents the mean pixel value of a 225 pixel area divided by a control pixel average.

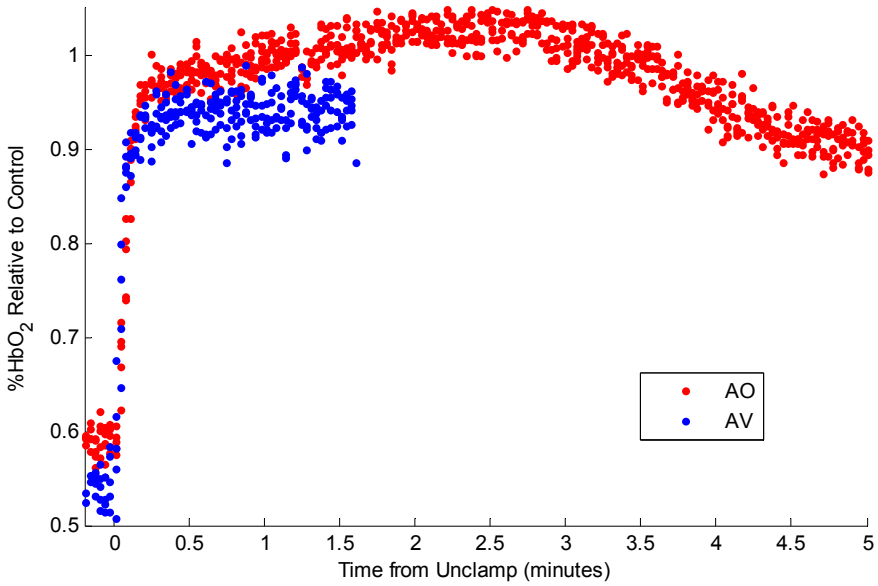

Figure 7.14 Monitoring the time progression percentage of oxyhemoglobin perfusing the kidney during and after renal AO and AV occlusion. Each point represents the mean pixel value of a 225 pixel area divided by a control pixel average.

The 3 Shot outputs acquired during the removal of the Satinsky clamp are analyzed using the same procedure for the AO clamped kidney (n = 1540) and the AV clamped kidney (n = 269). Images are continuously acquired until it visually appears that there is no longer any fluctuation in kidney oxygenation levels. From the number of images in each case, it is apparent that visual fluctuations cease more quickly in the AV case than in the AO case. Another interesting observation is that the AO case has an overshoot of oxygenation associated with reactive hyperemia and then declines to a steady state lower than its control value, and lower than the AV steady state. This may be a potential detriment to clamping the artery only instead of the artery and the vein. Perhaps, there is a longer term oscillation that is not captured due to lack of images in the AV case.

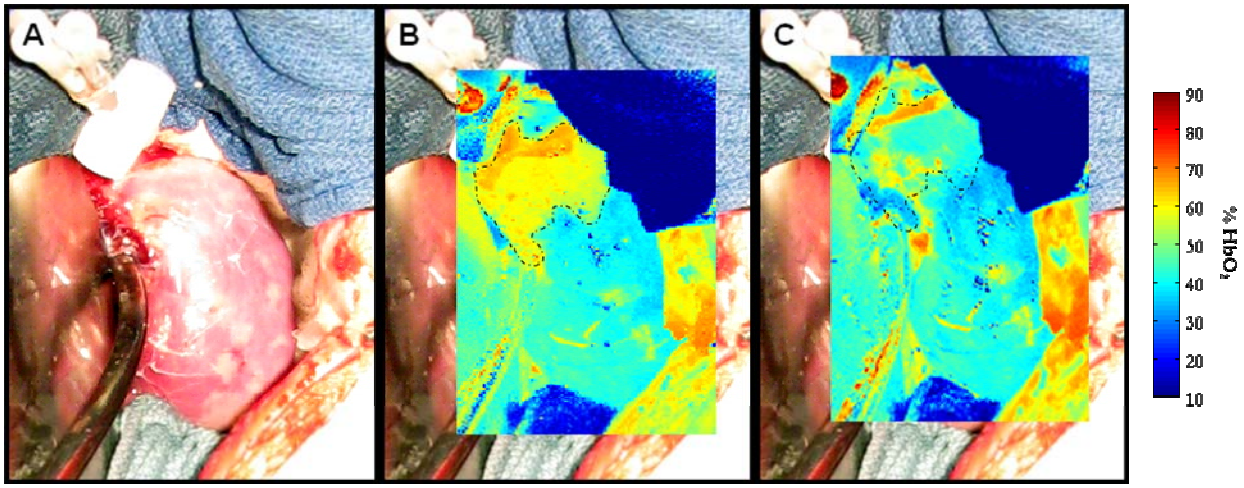

Figure 7.15 Bilateral ischemia exhibited in pig kidney having two renal arteries. The raw image in (a) shows the kidney immediately after clamping one renal artery. 3 Shot images (b) show that the lower pole is ischemic, but the upper pole is still highly oxygenated. After clamping the second artery, 3 shot images (c) show that the upper pole becomes ischemic as well.

An unanticipated advantage of near real-time 3 Shot images showing the surgeon the spatial distribution of tissue oxygenation is illustrated when clamping fails to cause the entire kidney to become ischemic. In pig 3, the surgeon clamps the renal vasculature AO as in previous pig subjects. Raw views of the kidney seem to imply the clamping is successful (see Figure 7.15(a)), but as the surgeon watches the real-time 3 Shot output display in the GUI, he notices that the upper pole is still highly oxygenated but the lower pole has become ischemic

(see Figure 7.15(b)). This prompts a re-examination of the renal vasculature, in which the surgeon finds a second artery supplying oxygenated blood to the renal unit. Apparently, in this case, the clamped artery supplies blood to the lower pole, and an unclamped second artery supplies blood to the upper pole. Upon clamping the second artery, the upper pole also becomes ischemic, but never reaches the same level of ischemia as the initially occluded lower pole (see Figure 7.15(c)). Therefore, the DLP HSI can also be used to determine the precise tissue areas that are supplied by an artery, which helps surgeons to know which arteries to occlude during partial nephrectomies.

7.2.1.5 Conclusions

Hyperspectral imaging with the DLP HSI is useful for comparing competing renal vasculature clamping methods with regard to kidney tissue oxygenation during nephron-sparing surgery. Analyzing Spectral Sweep images indicates that the percent HbO_2 of the kidney is higher when the artery only (AO) is clamped than when the artery and vein (AV) is clamped between 10 and 40 minutes. Images from other time periods indicate no difference in percent HbO_2 between AO and AV clamping. The Spectral Sweep image cubes captured by the prototype system visualize the same spatial oxygenation map as other hyperspectral imaging systems, even though the spectrum measured at each pixel is not always consistent between systems.

Generating 3 Shot output images at 3 frames per second allows the surgeon to visualize real-time physiologic changes in tissue oxygenation. This is useful in determining whether or not blood flow is adequately inhibited from the entire kidney. Analyzing 3 Shot images captured during the process of tightening and releasing the clamp shows the transient response of renal tissue at the onset of ischemia and during reactive hyperemia. Though only one subject was sufficiently imaged during this time period, it appears that AV clamping may be advantageous to AO clamping when immediate ischemia or no hyperfusion is desired.

7.2.2 Human Study

Animal studies are necessary to ensure the safety and utility of prototype medical devices, but the end use of the DLP HSI is for human imaging, so its utility in live human surgeries must also be tested. An Institutional Review Board (IRB) approved protocol at UTSW permits the prototype hyperspectral imaging system to image open cavity partial nephrectomies in human subjects.

7.2.2.1 Methods

The surgical procedure for humans is different than that for the porcine study, because human subject survival is of the utmost importance. The surgeon makes an incision in the side of the subject to expose the kidney. 'Control' hyperspectral data cubes are acquired with the DLP HSI in Spectral Sweep and 3 Shot modes. Then the surgeon clamps the renal vasculature with a predetermined method (AO or AV) to occlude blood flow to the kidney. 'Occluded' hyperspectral data cubes are acquired at non-critical points in the surgery, when the surgeon allows all other room lights to be turned off. After the kidney is sufficiently bereft of blood to prevent hemorrhage, the surgeon removes the tumor and stitches the exposed renal tissue closed. One more 'Occluded' data cube is acquired before clamp is removed. The surgeon removes the clamp, and 'Reperfusion' hyperspectral data cubes are acquired prior to closing the abdominal cavity.

To date, three human subjects have been imaged. The following results section is focused on the first of these human subjects. The subject is an otherwise healthy male, about 60 years old, with a tumor on his right kidney.

7.2.2.2 Results

In human surgery, the room lights and operating lights cannot be switched off for minutes at a time as is possible during animal surgeries. Therefore, only one Spectral Sweep data cube is captured as a control to verify the image results of the 3 Shot illumination method.

Subsequent hyperspectral images are captured with the 3 Shot method so that the room and operating lights only remain off for several seconds.

View Finder pictures of the kidney show the gross anatomy before and after the tumor is removed, and 3 Shot image outputs show the relative oxygenation of the kidney throughout the surgery. In Figure 7.16(a), the blue sample area highlights a uniform region of the kidney tissue. The sample area is used to trace the trend of oxygenation throughout the surgery.

Hyperspectral images are acquired at five different time points during the surgery. One of the images is unreliable due to light pollution from the headlamp worn by the surgeon, and the other four images are shown in Figure 7.16. In the 'Control' image, (b), the kidney is highly oxygenated and the spatial distribution of tissue oxygenation is fairly uniform. In the first 'Occluded' image, (c), most of the kidney exhibits lower oxygenation levels. After the tumor is removed and the clamp is still tightened, (d), the kidney shows decreased oxygenation levels in all areas. When the clamp is finally removed, (e), the kidney oxygenation levels return to near those measured in the 'Control' image.

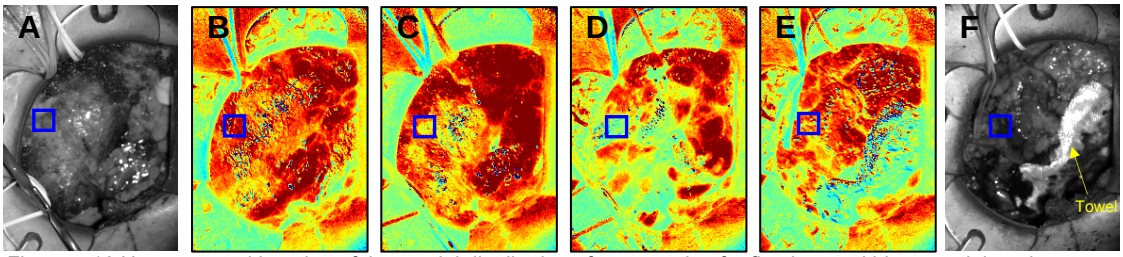

Figure 7.16 Hyperspectral imaging of the spatial distribution of oxygenation for first human kidney partial nephrectomy. View Finder pictures show the anatomy of the kidney (a) before and (f) after dissection, where the blue sample area is a section of normal kidney. The other images are processed 3 Shot outputs captured (b) before clamping, (c) immediately after clamping, (d) after tumor is removed (still clamped), and (e) immediately after unclamping.

In Figure 7.17, the average and standard deviation of the 81 pixel values in each sample area are plotted to show the trend of oxygenation throughout the surgery. The overall trend implies that the kidney becomes most ischemic in image three and then recovers to a level similar to control.

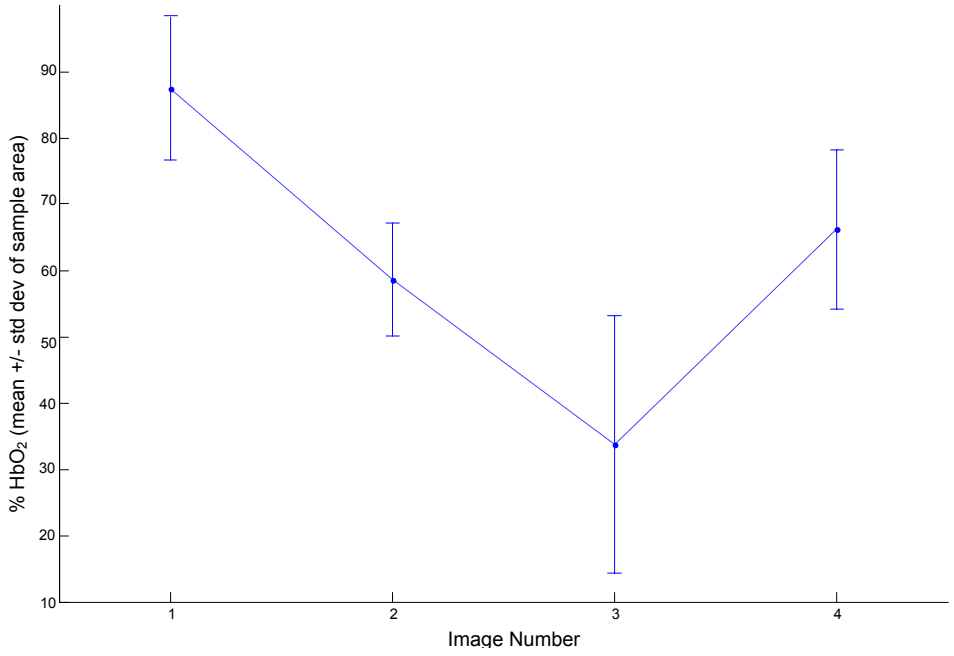

Figure 7.17 Progression of relative oxygenation measured from output images in Figure 7.16. Image number 1 is (b), 2 is (c), 3 is (d), and 4 is (e).

7.2.2.3 Conclusions

The DLP HSI can successfully map the spatial distribution of tissue oxygenation during a human partial nephrectomy. Light pollution from the operating room lights and the surgeons head lamp interferes with hyperspectral imaging, so fewer images can be captured in human cases than in animal cases. However, the 3 Shot output images acquired during the human study are useful for the surgeon to visualize which areas of the kidney are higher and lower oxygenated. Analysis of many more subjects is needed in order to compare AO versus AV clamping in human nephron-sparing surgeries.

7.3 Lower limb neuropathy

Nerve damage may be correlated to the loss of blood flow in the surrounding tissue bed. To diagnose nerve damage in the lower limb of patients, physicians probe the leg with a mechanical or electrical prick and ask the patient if they can feel it. If the patient cannot feel the prick, that area is diagnosed as neuropathic. This process is time consuming, and the spatial

resolution of the diagnosed neuropathy is a function of the number of discrete point measurements made by the physician. With the DLP Hyperspectral Imaging system it may be possible to map the spatial distribution of neuropathy along the entire lower limb by mapping its tissue oxygenation.

7.3.1 Methods

A clinical study is devised to test the utility of hyperspectral imaging for monitoring wound care in amputees and for studying their neuropathy. Amputees and patients exhibiting lower limb neuropathy are voluntarily enrolled in the clinical study at a weekly wound care clinic in the Dallas VA. After signing the consent forms, each subject is seated in a room reserved for hyperspectral imaging, the overhead lights are turned off, and the DLP HSI is used to capture Spectral Sweep and 3 Shot images along the entire limb of interest.

To date, five human subjects have been enrolled in the study. The following results section is focused on the first of these human subjects. The subject is a male over 50 years old who has previously been diagnosed with neuropathy in the lower half of his left leg, as measured by the prick test.

7.3.2 Results

Spectral Sweep and 3 Shot hyperspectral image cubes are acquired from the subject's toes to his knee in the lower limb's frontal plane. The output images color-coded for percent HbO_2 with the 3 Shot method show similar relative oxygenation levels to the color-coded outputs of the Spectral Sweep method. Overlaying the Spectral Sweep images on a picture of the subject's leg creates a surface tissue oxygenation map for the entire leg (see Figure 7.18).

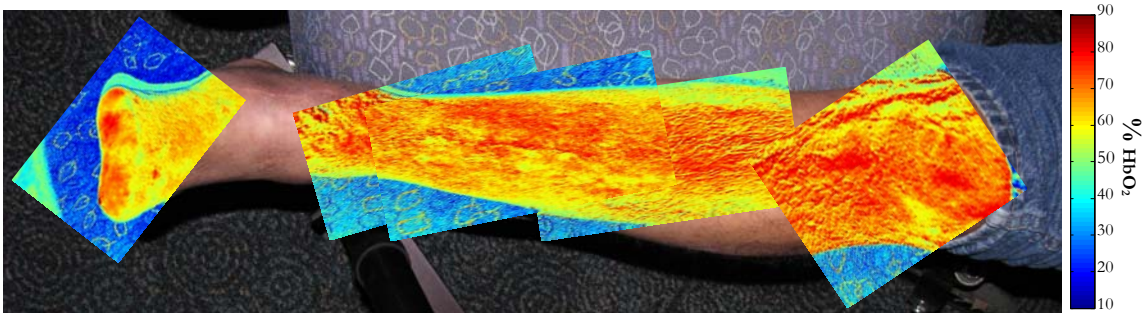

Figure 7.18 Full leg scan of Spectral Sweep images mapping the surface oxygenation of a patient with lower limb neuropathy.

Due to the curvature of the ankle, the detected absorbance images captured between the foot and the shin contain an unreal intensity gradient and are not shown. Those images unsuccessfully predicted the spatial map of tissue oxygenation, emphasizing an important constraint of the prototype: the topography of the tissue being imaged. Tissue planes further from the camera and light source optics may appear less oxygenated than closer tissue planes, when their real oxygenation is the same.

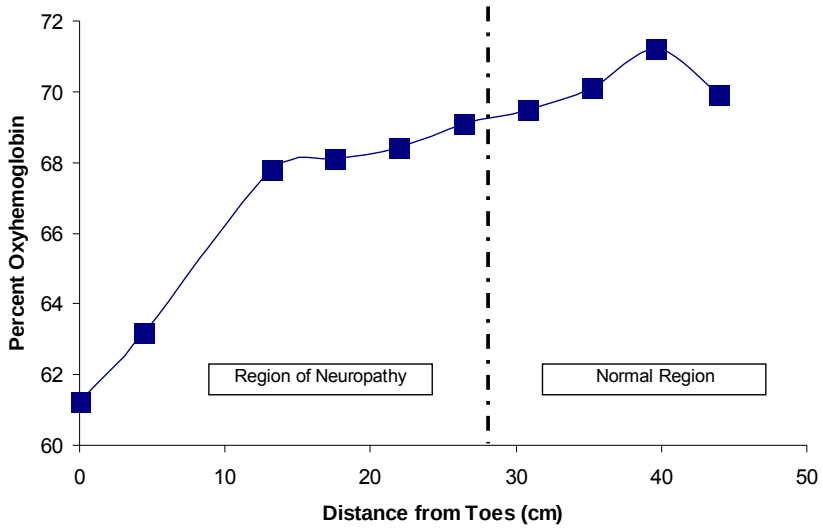

Figure 7.19 Spatial progression of surface oxygenation as measured along the centerline of the leg in the hyperspectral images in Figure 7.18. The dashed line represents the limit of neuropathy as determined by a physician administering a clinical nervous response exam on the leg.

It is difficult to see any difference in oxygenation from the bottom half of the leg to the top half of the leg in the images alone. A sample area of pixel values along the midline of the leg is plotted versus the axial distance from the toes (see Figure 7.19) to quantify this difference. This

plot indicates that there is an increase in surface tissue oxygenation progressing from the toes to the knee. However, this increase does not seem to match the results of the prick test. If surface tissue oxygenation mimics underlying neuropathy, there should be a jump in oxygenation between the region of neuropathy and the normal region, but the hyperspectral images do not show this jump. This emphasizes another important constraint of the prototype: the depth of the tissue being imaged. The DLP HSI relies on measuring the absorbance of light in the visible wavelength range, and visible light does not penetrate deep into the tissue, so the measured percent HbO_2 is only indicative of epithelial tissue oxygenation. Epithelial tissue is highly regulated and its oxygenation levels do not correspond to neuropathy like deeper tissue oxygenation does. Development of a prototype that operates in the near infrared wavelength range may be useful for visualizing deeper tissue oxygenation.

7.3.3 Conclusions

The DLP HSI is useful for mapping the spatial distribution of tissue oxygenation for areas that are larger than the field of view of the camera. Several image cubes are captured in overlapping regions, and the resulting output images are overlain to create a large spatial map.

When acquiring images with the DLP HSI, it is important to know the topography and depth of the tissue of interest. The tissue area should be a uniform distance from the system's detector and light source illumination optics to eliminate unreal effects of distance on measured percent HbO_2. The tissue of interest should also be on the surface of the subject (e.g. epithelium), since visible light does not penetrate past the surface layers of tissue. In the case presented, epithelial oxygenation does not seem to correlate exactly with neuropathy, but a larger sample size is needed to confirm these results.

7.4 Foot reactive hyperemia

Wearing shoes that are too tight or developing diabetic foot ulcers can cause ischemia in localized regions of the foot. As discussed in the finger occlusion test, reactive hyperemia is the

autoregulatory response to recover from ischemia. To better understand the reactive hyperemia in feet, a clinical study using an LCTF-based hyperspectral imaging system is devised. In part of this study, the DLP Hyperspectral Imaging system captures images in parallel with the LCTF system to compare the resulting images and oxygenation measurements of the two systems.

7.4.1 Methods

To introduce ischemia on the anterior surface of a subject's foot, three ¾" bolts are inserted into the subject's shoe and situated atop the foot. A healthy subject undergoes a period of localized ischemia due to the increased pressure from the bolts. After 30 minutes, the bolts are removed, and the subject's shoe and sock are removed. The foot is placed in the field of view of the LCTF and DLP hyperspectral imaging systems, and Spectral Sweep image cubes are captured at 3 minutes, 5 minutes, 10 minutes, 15 minutes, 20 minutes, 25 minutes, and 30 minutes post-occlusion. Both systems cannot collect data simultaneously because their light source illuminations interfere with each other, so the LCTF system acquires an image cube prior to the DLP system at each time point.

The image cubes are all processed by the same 'Oxyz gray' algorithm, which compares each pixel spectrum to reference spectra for Hb and HbO_2 using multivariate least squares analysis. A gray-scale output image where whiter pixels indicate higher percent HbO_2 is the result of the processing data cube with this algorithm. The meaning of the pixel values is identical to the color-coded images in other application examples, only in gray-scale. Sample areas for normal tissue and for previously ischemic tissue are averaged at each time point.

20 subjects are imaged with the LCTF system, and three of them are concurrently imaged with the DLP system. The following results section is focused on the third of those concurrently imaged human subjects. The subject is a male, 20 to 30 years old, with no known adverse health conditions.

7.4.2 Results

Processed images from data cubes acquired with the DLP system match those from data acquired with the LCTF system. In Figure 7.20, the processed images from hyperspectral imaging 10 minutes after injury removal show an identical spatial region of reactive hyperemia as indicated by the shape and distribution of the white pixels in and around the red sample area. The orientation of the foot is slightly different in each image because the optics head of the LCTF system is tilted at a different angle than the DLP system.

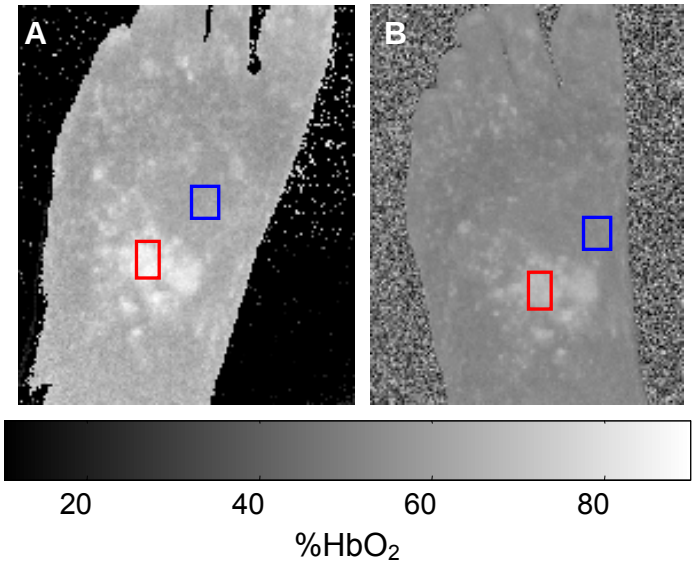

Figure 7.20 Processed hyperspectral images acquired 10 minutes after injury is removed, in which the red sample area is the site of injury and the blue area is a control site. The data for (a) was acquired with LCTF hyperspectral imaging system filtering contiguous bandpasses, and the data for (b) was acquired with DLP HSI Spectral Sweep method. Both hyperspectral cubes were processed with Oxyz processing algorithm.

The mean and standard deviation of the pixel values in the sample areas of the oxygenation maps in Figure 7.20 are calculated in Table 7.1. As previously mentioned in the results of the porcine kidney studies, the absolute percent HbO_2 values differ considerably between the two systems. However, looking at the relative difference between the red sample area and the blue sample area in each system, it appears that both systems calculate nearly the same percent difference between the previously injured region and normal region of the foot. Both systems are visualizing the same spatial maps of relative tissue oxygenation, but in order to correlate those maps with absolute values of percent HbO_2 more calibration is needed.

Table 7.1 Percent HbO_2 measured from sample areas in Figure 7.20. The percent difference relates the amount of HbO_2 at the site of injury (red area) to a normal region of the foot (blue area). Values higher than 100% indicate an overshoot related to reactive hyperemia.

	LCTF		**DLP**	
	Mean % HbO_2	Std Dev of Pixels	Mean % HbO_2	Std Dev of Pixels
Red Area	79.13	4.66	66.22	2.76
Blue Area	61.12	2.27	52.04	2.25
%Difference	129.5%		127.2%	

7.4.3 Conclusions

Images resulting from hyperspectral data cubes acquired by the DLP HSI illustrate the same spatial distribution of relative tissue oxygenation as images resulting from cubes acquired by the LCTF hyperspectral imaging system. This confirms that the DLP system is as useful as the LCTF system for hyperspectral imaging, but the measured absolute percent HbO_2 is not consistent between systems. More calibration is needed to adequately describe absolute oxygenation levels. At this point, it is uncertain which system makes more accurate absolute measurements and a tissue calibration standard is needed with which to correlate the values measured by the DLP HSI.

7.5 Brain surgery

Neurosurgeons investigate brain behavior by dissecting the scalp and viewing the cerebral cortex with surgical microscopes. Current imaging only visualizes the physical anatomy of the cortex, or by introducing dyes as contrast agents some functionality can be visualized. Point measures of cerebral HbO_2 content are possible with near infrared spectroscopic techniques, but they do not show a spatial image of oxygenation.[25] By coupling the DLP Hyperspectral Imaging system to a surgical microscope, neurosurgeons may be able to visualize the spatial profile of cerebral tissue chemistry.

7.5.1 Methods

The CoolSNAP HQ2 is directly mounted to the C-mount of a Zeiss surgical microscope at the UTSW animal laboratory, and the OL 490 liquid light guide is coupled to the microscope's

ring illumination optics. After setting the focal distance of the microscopic system, a background cube is captured with the DLP HSI and the surgeon dissects a small cross-section of an anesthetized rabbit's scalp. Imaging through the optics of the microscope, the DLP HSI is set to continuously acquire 3 Shot images of the exposed cortical tissue. Several seconds of control images are captured while an external pump supplies oxygen to the subject. Continuous 3 Shot images are acquired while the external oxygen supply for the subject is cut off for a period of 20 minutes and turned back on.

7.5.2 Results

Watching the spatial distribution of tissue oxygenation, and drawing from his own experience, the surgeon notices one area of the exposed cortex is damaged at the beginning of the imaging session. In Figure 7.21(a), the central region is the cortical tissue and the three red regions around the circumference are scalp and other tissues. The black sample box surrounds an area of healthy brain tissue and the blue sample box surrounds an area of damaged brain tissue. In the control image, the damaged tissue appears ischemic compared to the normal tissue's level of oxygenation. There are no noticeable changes in the damaged tissue oxygen levels shown in the hyperspectral images during the period of external oxygen cutoff. However, after the oxygen is cut off for several minutes, the normal brain tissue begins to show ischemia as indicated by the lower percent HbO_2 in the black sample area of Figure 7.21(b).

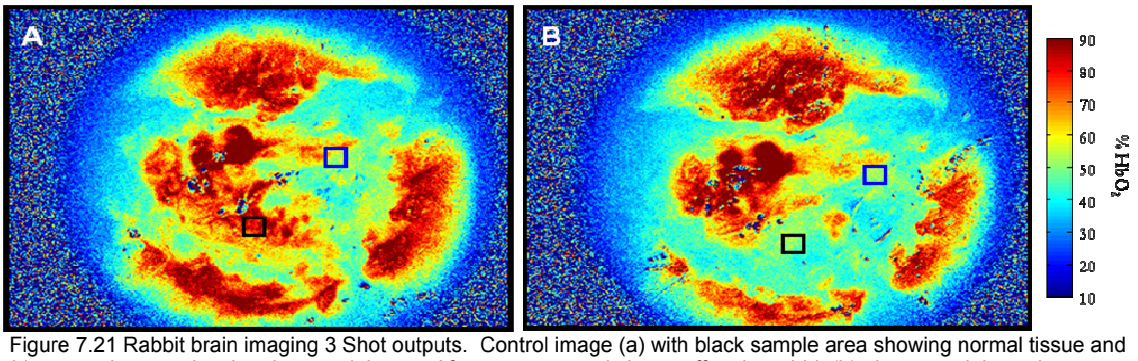

Figure 7.21 Rabbit brain imaging 3 Shot outputs. Control image (a) with black sample area showing normal tissue and blue sample area showing damaged tissue. After oxygen supply is cut off to the rabbit (b), the normal tissue becomes ischemic and there is no change in the damaged tissue.

7.5.3 Conclusions

Initial brain imaging with the DLP HSI coupled to a Zeiss surgical microscope suggests neurosurgery is another viable application for this novel medical imaging platform. The digital visualizations of oxygenation generated by hyperspectral imaging correspond with what the surgeon expects to see. Even though conclusive medical results cannot be derived from the initial imaging session, the results indicate that DLP HSI can enable surgeons to visualize cerebral tissue chemistry in near real-time.

7.6 Diabetic retinopathy

An ocular complication associated with both types of diabetes, diabetic retinopathy causes changes in the blood vessels of the eye that can lead to loss of vision if untreated.[26] The progression of diabetic retinopathy is typically monitored by an ophthalmoscope, which shows the anatomical structure of the retina, or by fluorescein angiography, which highlights the blood perfusion by introducing a fluorescing contrast agent. Hyperspectral imaging may be a means of imaging the retinal blood perfusion without injecting a contrast agent, and thereby would be useful for monitoring diabetic retinopathy.

7.6.1 Methods

A double knockout apoE-/- db/db mouse model for diabetic retinopathy is bred by The Jackson Laboratory (Bar Harbor, ME) for a study on imaging the progression of the disease in mice. Previous studies have shown that these special mice have a genetic predisposition for developing diabetes, so the National Institutes of Health (NIH) funded a study to image 30 of the mice (10 double knockouts, and 20 single knockouts) over a six month period with a microscopic LCTF-based Hyperspectral Imaging system. As an addition to the study, the DLP-based Hyperspectral Imaging system is used to image several of the mice. The CoolSNAP HQ2 is attached to the C-mount of an Olympus SZ-6145TR dissection microscope (Leeds

Instruments, Irving, TX) with variable zoom between 6.7x and 45x, and the OL 490 output LLG is coupled to a ring illuminator around the microscope objective.

In each imaging session, the mouse is anesthetized according to study protocol and placed beneath the microscope objective. The mouse is adjusted so that its eye is within the FOV of the microscopic DLP HSI, and the focus of the microscope is varied until the mouse retina is in the same focal plane that is being imaged. A View Finder image is captured with white light illumination, and then a Spectral Sweep image cube is captured and processed for percent contribution of HbO_2 by multivariate least squares comparison to reference spectra. After the imaging session, the mouse is removed from the microscope stage and placed in an incubator to regain consciousness.

7.6.2 Results

Retinal vasculature is successfully visualized by the microscopic DLP Hyperspectral Imaging system in both View Finder and Spectral Sweep modes. In View Finder mode, white light illumination created by turning all of the DMD mirrors on in the OL 490 is detected by the HQ_2 through the optics of the Olympus microscope at 45x magnification. This mode effectively visualizes the physical anatomy of the mouse eye, and Figure 7.22(a) illustrates when the focal plane of the imaging system is aligned with the retina. The grayscale image indicates a radial pattern of dark lines projecting outward from a hub in the lower right of the eye. It is assumed that these dark lines map the retinal vasculature and the hub is the mouse equivalent of the human fovea. To prove this assumption, the processed Spectral Sweep image in Figure 7.22(b) shows the retinal vasculature is mapped the same when visualizing oxygen concentration.

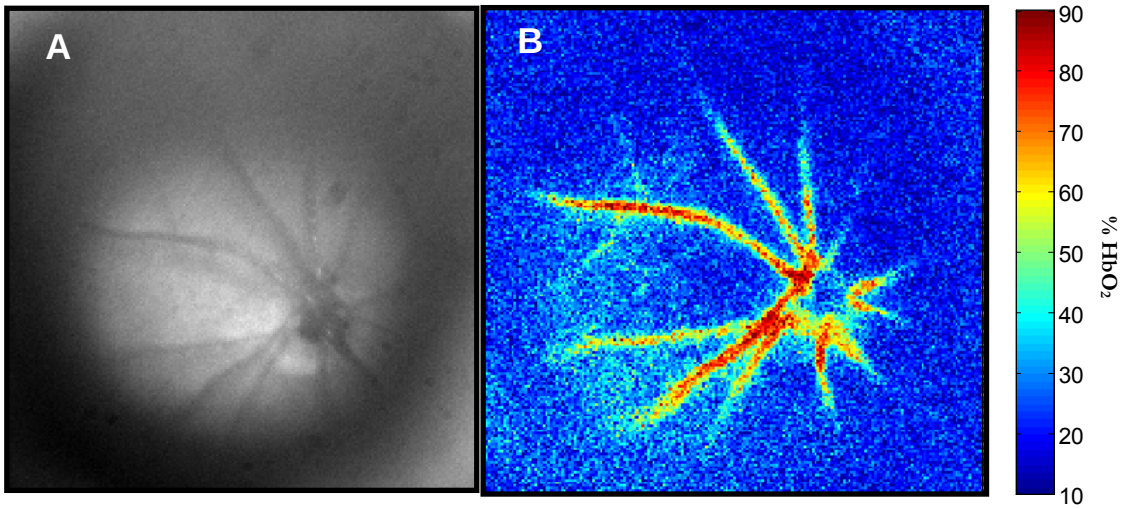

Figure 7.22 Mouse retinal images. The View Finder image in (a) shows the anatomical structure of the retina, while the processed Spectral Sweep image in (b) shows the percent HbO_2 of the retina, highlighting the highly oxygenated vasculature.

One key difference between the View Finder and Spectral Sweep retinal images is that the hub in (a) appears as dark as all of the other vessels, but in (b) the mouse equivalent of the human fovea is shown to exhibit low oxygen perfusion. This ability to distinguish between anatomically similar structures based on their differing tissue chemistry supports the usefulness of hyperspectral imaging as opposed to white light imaging.

7.6.3 Conclusions

Blood perfusion of retinal vasculature can be mapped with the DLP Hyperspectral Imaging system. By attaching the illumination and detection components of the DLP HSI to a microscope designed for looking at a mouse's retina, raw and hyperspectral images of a diabetic mouse retina were successfully captured and analyzed. These images are part of an ongoing study to monitor the progression of diabetic retinopathy over time in a mouse model predisposed for diabetes. The study hopes to find early markers, such as increased vascular perfusion, for diagnosing cases of diabetic retinopathy that lead to vision loss. Once these markers are found, ophthalmologists can use the microscopic DLP HSI system to monitor the disease in over 15,000,000 human diabetics.

CHAPTER 8

CONCLUSIONS AND FUTURE WORK

A novel hyperspectral imaging system has been developed for real-time, non-invasive, *in vivo* imaging of tissue chemistry in surgical and clinical applications, so the hypothesis can be accepted.

8.1 DLP Hyperspectral Imaging system

Using a spectral light engine to illuminate with simple narrow bandpasses or complex broadband spectra and a CCD FPA to detect the reflectance image from a tissue sample, the DLP Hyperspectral Imaging system remotely visualizes tissue oxygenation in live human and animal subjects. Illuminating with many narrow bandpasses in the Spectral Sweep mode results in large data cubes with full spectral information for each pixel in the image, but requires 20 to 30 seconds to generate a single chemically-encoded image. Spectral Sweep data cubes acquired with the DLP HSI match those captured by LCTF-based hyperspectral imagers, which, along with color tile calibration results, validates the DLP HSI prototype as an imaging spectrophotometer. Illuminating with only three complex broadband illuminations in the 3 Shot mode results in small data cubes with adequate spectral information to generate chemically-encoded images identical to the Spectral Sweep images at a much faster rate: 3 processed images per second.

The DLP HSI is comprised of an OL 490 Agile Light Source for spectral illumination and a CoolSNAP HQ2 CCD FPA for image detection. The OL 490 is fully characterized as a spectral light engine and operates according to the optical specifications written by the manufacturer. Laboratory experiments are performed to verify light source stability, center wavelength accuracy, wavelength range, and minimum spectral bandwidth. From the results of the

experiments, the entrance slit and ideal operating conditions for the OL 490 are determined. Due to small discrepancies between programmed and actual optical output spectra, a feedback spectrometer should be used to monitor and adjust the illumination spectra emitted from the OL490. The CoolSNAP HQ2 is fully characterized as a scientific grade imaging detector and is tested for speed and timing. Limitations in exposure time and initializing image capture and readout slow down the camera, but its ideal frame rate is still higher than a similar grade camera also tested.

The OL 490 and HQ2 are synchronized by a Windows software application which commands the light source to step through a sequence of illumination spectra and commands the camera to acquire an image at each illumination spectrum. This reliance on software triggering may slow down the acquisition time of a hyperspectral image cube, and hardware triggering of the light source and camera may improve future systems. Another bottleneck for speed is the processing done in MATLAB. MATLAB is useful because processing algorithms can be easily updated and modified, but an integrated circuit board or digital signal processor may be faster than using a PC with MATLAB. The OL 490 and HQ2 also have large footprints which should be made more compact before commercialization of the DLP HSI.

Image to image variability in the real-time display of 3 Shot output images leads to uncertainty in measuring the time progression of tissue oxygenation. This flashiness may be due to the processing algorithm, the light source intensity fluctuations, or noise in the detector. Without knowing the exact cause of the variability it is difficult to eliminate this flashiness. However, placing a known reflectance object in the system's FOV during all imaging sessions may serve as a reference to normalize all output images.

8.2 Surgical and Clinical Applications

The DLP HSI prototype can be used as a non-invasive detector of the real-time spatial distribution of *in vivo* tissue oxygenation in a wide variety of surgical and clinical applications. Urologists can use the novel medical imager to visualize ischemia during animal and human

partial nephrectomies. Neurosurgeons can use the system to spatially map the relative cerebral oxygenation levels in brain surgery. Ophthalmologists can use the system monitor diabetic retinopathy. Clinicians can use the DLP HSI to create large spatial maps of full limb oxygenation and watch the real-time progression of reactive hyperemia.

Successful results of hyperspectral imaging sessions already performed at UTSW, the Dallas VA, and UTA pave the way for DLP HSI to be part of full medical studies. Hyperspectral imaging of a porcine partial nephrectomy study showed repeatable results among subjects, and there is an ongoing human study to compare renal vasculature clamping methods. The primary limitation of the DLP HSI in a surgical environment is that all lights must be turned off except for the OL 490 in order for accurate hyperspectral images to be acquired. This limitation may be resolved by switching from open cavity surgeries to endoscopic surgeries.

Another surgical limitation of the DLP HSI is that it only operates in the visible wavelength range. Visible light is mostly absorbed by surface layers of tissue, so information from the underlying tissue layers cannot be detected with the current prototype system. A similar system that can operate in the near infrared (NIR) to far infrared wavelength range may be more useful for visualizing the chemistry of deeper tissue layers. Optronic Labs manufactures an OL 490 NIR that has a published wavelength range of 760 nm to 1600 nm, which is integrated with a FLIR SC 4000 InGaAs array detector (FLIR Systems, Boston, MA) for a prototype NIR DLP HSI. The NIR system has been synchronized with software and mechanically integrated in the same manner as the visible DLP HSI, but the illumination methods and processing algorithms have not been fine tuned for the NIR wavelength range.

The future of DLP Hyperspectral Imaging encompasses both visible and NIR wavelength ranges, and may be extended into the far infrared and thermal ranges. Calibration and industrial design of the current prototypes will help create a robust medical imaging platform for the real-time visualization of *in vivo* tissue chemistry.

REFERENCES

1. Fong A, Bronson B, Wachman E. Advanced photonic tools for hyperspectral imaging in the life sciences. SPIE Newsroom 2008:2008.

2. Hornbeck LJ. Digital Light Processing™ for High-Brightness, High-Resolution Applications. 1997;141:1-16.

3. Hornbeck LJ. Digital Light Processing™: A New MEMS-Based Display Technology. 1996;117:1-23.

4. Bowmaker JK, Dartnell HJA. Visual pigments of rods and cones in a human retina. Journal of Physiology 1980;298:501-511.

5. Sellar RG,3, Boreman GD2. Classification of imaging spectrometers for remote sensing applications. 2005;44:1-3.

6. Zuzak KJ, Naik SC, Alexandrakis G, Hawkins D, Behbehani K, Livingston EH. Characterization of a near-infrared laparoscopic hyperspectral imaging system for minimally invasive surgery. Anal Chem 2007;79:4709-4715.

7. Kommera S. Spectroscopic Characterization of Biliary Tract Tissues *In vivo* to Assist Laparoscopic Cholecystectomy. UTA Masters Thesis 2006.

8. Nitzan M,2, Taitelbaum H. The measurement of oxygen saturation in arterial and venous blood. 2008;11:9-15.

9. Zuzak KJ, Schaeberle MD, Lewis EN, Levin IW. Visible spectroscopic imaging studies of normal and ischemic dermal tissue. Proc SPIE Int Soc Opt Eng 2000;3918:17-26.

10. Zuzak KJ, Schaeberle MD, Levin IW, Neil LE, Freeman J, McNeil JD, Cancio LC. Visible and infrared hyperspectral visualization of normal and ischemic tissue. Annu Int Conf IEEE Eng Med Biol Proc 1999;2:1118.

11. Zuzak KJ, Schaeberle MD, Levin IW, Neil Lewis E. Visible reflectance hyperspectral imaging: Characterization of a noninvasive, in vivo system for determining tissue perfusion. Anal Chem 2002;74:2021-2028.

12. Shah BB, Cavanagh HD, Petroll WM, Kothare AD, Gundabhat P, Behbehani K, Zuzak KJ. *In vivo* microvasculature visualization using hyperspectral imaging. Proc SPIE Int Soc Opt Eng 2006;6080:60800U.

13. MacKinnon N, Stange U, Lane P, MacAulay C, Quatrevalet M. Spectrally programmable light engine for in vitro or in vivo molecular imaging and spectroscopy. 2005;44:2033-2040.

14. Texas Instruments. DLP Discovery 3000 Development Kits - DMD - DLP Technology. 2009;2009:1.

15. Saleh BEA, Teich MC. Fundamentals of photonics. Hoboken, NJ: John Wiley & Sons, Inc., 1991.

16. Smith SW. Ch. 25: Special imaging techniques. The Scientist and Engineer's Guide to Digital Signal Processingwww.dspguide.com, 1997. p. 423-450.

17. Naik SC. Characterization of a Novel, *In Vivo*, Laparoscopic Hyperspectral Imaging System for Minimally Invasive Surgery. UTA Masters Thesis 2006.

18. Kothare AD. Visible Hyperspectral Imaging System With Improved Capabilities for Translational Medicince Projects. UTA Masters Thesis 2005.

19. Webster JG, editor. Medical instrumentation: Application and design. 3rd ed. Hoboken, NJ: John Wiley & Sons, Inc., 1998.

20. Guo B, Gunn SR1, Damper RI1,2, Nelson JDB2. Band selection for hyperspectral image classification using mutual information. 2006;3:522-526.

21. Du Z, Jeong MK1,3, Kong SG1,2. Band selection of hyperspectral images for automatic detection of poultry skin tumors. 2007;4:332-339.

22. Roberts DA1, Gardner M1, Church R1, Ustin S2, Scheer G2, Green RO1,3. Mapping chaparral in the Santa Monica Mountains using multiple endmember spectral mixture models. 1998;65:267-279.

23. Klabunde RE. Cardiovascular physiology concepts. : Lippincott Williams & Wilkins, 2004.

24. Gong EM, Zorn KC, Orvieto MA, Lucioni A, Msezane LP, Shalhav AL. Artery-only occlusion may provide superior renal preservation during laparoscopic partial nephrectomy. Urology 2008;72:843-846.

25. Quaresima V,3, Sacco S, Totaro R, Ferrari M. Noninvasive measurement of cerebral hemoglobin oxygen saturation using two near infrared spectroscopy approaches. 2000;5:201-205.

26. Frank RN. Diabetic Retinopathy. N Engl J Med 2004;350:48-58.

BIOGRAPHICAL INFORMATION

Robert Paul Francis has always been interested in applying learned knowledge to engineer solutions and help people. In pursuit of a BS in Engineering Science from Trinity University, he developed a broad understanding of mechanical, chemical and electrical engineering and applied that understanding to the testing and design of new engineering prototypes. As an upperclassman, he helped smooth the transition for incoming freshman through mentoring. After graduating from Trinity in May 2005, he taught high school students and athletes in rural New Mexico how to do math and play football and learned to work hard, communicate clearly, and manage people. At the University of Texas in Arlington, he has learned the fundamentals of medical imaging and explored the link between research and commercialization through the development of a novel medical imaging system for clinical and surgical applications. After graduating from UTA in May 2009, Robert hopes to continue learning in a company or organization where he can improve technology, especially for medical applications.